REGULATION OF NEURONAL CALCIUM HOMEOSTASIS IN HUNTINGTON'S DISEASE

Jessica J. Pellman

Submitted to the faculty of the University Graduate School
in partial fulfillment of the requirements
for the degree
Doctor of Philosophy
in the Department of Pharmacology and Toxicology,
Indiana University

August 2016

Accepted by the Graduate Faculty, of Indiana University, in partial fulfillment of the requirements for the degree of Doctor of Philosophy.

_____
Nickolay Brustovesky, Ph.D., Chair

_____
Theodore R. Cummins, Ph.D.

Doctoral Committee

_____
Travis J. Jerde, Ph.D.

July 28, 2015

_____
Rajesh Khanna, Ph.D.

_____
Michael R. Vasko, Ph.D.

DEDICATION

To my parents, Wade and Claire, and my husband, Joe, for their love and support.

ACKNOWLEDGEMENTS

First and foremost, I would like to thank my mentor, Dr. Nickolay Brustovetsky, for his support and mentorship. Words cannot express my gratitude for everything he has done for me. He has always been available to discuss anything and offer his guidance. I am grateful that he allowed me the opportunity to work with him. I truly appreciate the time he devoted to making me a better scientist, writer, and presenter. I would also like to thank the current and former members of Dr. Brustovetsky's laboratory, primarily Tatiana Brustovetsky. Tatiana's instruction and assistance with every aspect of my research was invaluable. I learned so much from Tatiana, and for that I am so appreciative. Without her patience, expertise, and many skills, this project would not have been possible. I would also like to thank my current and former lab mates, James Hamilton and Rania Sulaiman, for their help and friendship in the lab. James and Rania contributed to some of the work in this thesis through discussion and technical assistance. I am particularly grateful for their help with isolated mitochondria experiments. Their collaboration and technical abilities facilitated my successful completion of that portion of the thesis.

I would like to express my appreciation to other mentors who have allowed me to do research in their laboratories, Drs. Gerry Oxford, Joyce Hurley, Bill Sullivan, and Zachary Rodd. These experiences helped to shape my graduate training. Each mentor taught me important lessons about science and life. I sincerely thank Dr. Rajesh Khanna and the members of his laboratory group for

their collaboration on a portion of this dissertation work. Xiao-Fang Yang contributed the electrophysiological recordings found in Figure 25. It was a pleasure to work together on this exciting project.

My deepest thanks to my thesis committee members, Drs. Ted Cummins, Travis Jerde, Rajesh Khanna, and Michael Vasko for the time that they have taken to meet with me and for all of the instruction, suggestions, and support that they have provided me. Their questions and feedback helped to shape and improve my research. Thank you to all of the professors and researchers in the Department of Pharmacology and Toxicology who have attended my seminars, and who have provided feedback and constructive critiques that have helped better my research and presentation skills. Thank you to the PharmTox administrative staff, in particular Amy Lawson and Lisa King, for keeping track of all of us.

I would like to thank the Department of Pharmacology and Toxicology Paradise Travel Award and IUSM Graduate Student Travel Award Committees for granting me awards to attend the Society for Neuroscience Meetings in 2013 and 2014. Many thanks to the Indiana Biomedical Gateway program for providing an excellent training program and environment. I am especially appreciative to the members of the Leadership Development Book Club for their encouragement, advice, and friendship.

Lastly, I would like to thank my friends and family for all of their support and encouragement throughout my time in graduate school. To all of the students in the PharmTox department, thank you for sharing this experience with

me. I greatly appreciate the laughter, support, and friendship of Dr. Valerie Fako Miller, Dr. Sarah Wilson, Dr. Nicole Ashpole, Dr. Sherry Pittman, Dr. Vicki Jeffers, Leah Padgett, and Betsy Lungwitz. Thank you for celebrating the little things with me along the way. To my parents, Wade and Claire Jennings, thank you for always believing in me and raising me to live without limitations. Finally, to my husband Joe, thank you for standing with me and enduring all of the ups and downs of graduate school. Mostly, thank you for enjoying life along the way and for making Indy home.

Jessica J. Pellman

REGULATION OF NEURONAL CALCIUM HOMEOSTASIS IN HUNTINGTON'S DISEASE

Huntington's Disease (HD) is an inherited, autosomal dominant, neurodegenerative disorder. There is no cure for HD and the existing therapies only alleviate HD symptoms without eliminating the cause of this neuropathology. HD is linked to a mutation in the huntingtin gene, which results in an elongation of the poly-glutamine stretch in the huntingtin protein (Htt). A major hypothesis is that mutant Htt (mHtt) leads to aberrant Ca^{2+} homeostasis in affected neurons. This may be caused by increased Ca^{2+} influx into the cell via the N-methyl-D-aspartate (NMDA)-subtype of glutamate receptors. The contribution of two major Ca^{2+} removal mechanisms, mitochondria and plasmalemmal Na^{+}/Ca^{2+} exchangers (NCX), in neuronal injury in HD remains unclear.

We investigated Ca^{2+} uptake capacity in isolated synaptic (neuronal) and nonsynaptic mitochondria from the YAC128 mouse model of HD. We found that both Htt and mHtt bind to brain mitochondria and the amount of mitochondria-bound mHtt correlates with increased mitochondrial Ca^{2+} uptake capacity. Mitochondrial Ca^{2+} accumulation was not impaired in striatal neurons from YAC128 mice. We also found that expression of the NCX1 isoform is increased with age in striatum from YAC128 mice compared to striatum from wild-type mice. Interestingly, mHtt and Htt bind to the NCX3 isoform but not to NCX1. NCX3 expression remains unchanged.

To further investigate Ca^{2+} homeostasis modulation, we examined the role of collapsin response mediator protein 2 (CRMP2) in wild-type neurons. CRMP2 is viewed as an axon guidance protein, but has been found to be involved in Ca^{2+} signaling. We found that CRMP2 interacts with NMDA receptors (NMDAR) and disrupting this interaction decreases NMDAR activity. CRMP2 also interacts with and regulates NCX3, resulting in NCX3 internalization and decreased activity.

Augmented mitochondrial Ca^{2+} uptake capacity and an increased expression of NCX1 in the presence of mHtt suggest a compensatory reaction in response to increased Ca^{2+} influx into the cell. The role of NCX warrants further investigation in HD. The novel interactions of CRMP2 with NMDAR and NCX3 provide additional insight into the complexity of Ca^{2+} homeostasis regulation in neurons and may also be important in HD neuropathology.

Nickolay Brustovetsky, Ph.D., Chair

TABLE OF CONTENTS

LIST OF TABLES

LIST OF FIGURES

LIST OF ABBREVIATIONS

2,4-DNP:	2,4-dinitrophenol
ADP:	adenosine 5′-diphosphate
AIF:	apoptosis inducing factor
AL:	alamethicin
AM:	acetoxymethyl
AMPA:	α-amino-3-hydroxy-5-methyl-4-isoxazolepropionic acid
AP-5:	(2*R*)-amino-5-phosphonopentanoate
ATP:	adenosine-5'-triphosphate
a.u.:	arbitrary units
AUC:	area under the curve
BDNF:	brain derived neurotropic factor
BSA:	bovine serum albumin
$[Ca^{2+}]_c$:	cytosolic calcium concentration
CaV2.2:	N-Type voltage-dependent Ca^{2+} channel
CBD3:	Ca^{2+} channel-binding domain 3 peptide
co-IP:	co-immunoprecipitation
CRMP2:	collapsin response mediator protein 2
CsA:	cyclosporine A
CyD:	cyclophilin-D
CNS:	central nervous system
DAPI:	2-(4-amidinophenyl)-1H-indole-6-carboxamidine
DARPP-32:	dopamine and cyclic AMP-regulated phosphoprotein relative molecular mass 32,000
DCD:	delayed Ca^{2+} dysregulation
DIV:	days *in vitro*
DMSO:	dimethyl sulfoxide
EGTA:	ethylene glycol tetraacetic acid
FCCP:	carbonyl cyanide-p-trifluoromethoxyphenylhydrazone
FVB/NJ:	background mouse strain for YAC
GABA:	gamma-aminobutyric acid
GAPDH:	glyceraldehyde 3-phosphate dehydrogenase
GFAP:	glial fibrillary acidic protein
GFP:	green fluorescent protein
Glu:	glutamate
GluN1:	NMDA receptor subunit family 1
GluN2:	NMDA receptor subunit family 2
GluN3:	NMDA receptor subunit family 3
GluR:	glutamate receptor
GSK3β:	glycogen synthase kinase-3β
HD:	Huntington’s Disease
HEPES:	4-(2-hydroxyethyl)-1-piperazineethanesulfonic acid
HTT:	huntingtin gene
Htt:	huntingtin protein
IgG:	Immunoglobulin G

iGluR:	ionotropic glutamate receptor
K_d:	dissociation constant
LDS:	lithium dodecyl sulfate
MAP-2:	microtubule associated protein
MEK:	mitogen-activated protein kinase kinase
mGluR:	metabotropic glutamate receptor
mHtt:	mutant huntingtin protein
MK-801:	(+)-5-methyl-10,11-dihydro-5H-dibenzo[a,d]cyclohepten-5,10-imine maleate
Mtc:	mitochondria
MRI:	magnetic resonance imaging
mRNA:	messenger ribonucleic acid
$[Na^+]_c$:	cytosolic sodium concentration
NCX:	plasmalemmal sodium calcium exchanger
NCX_{fwd}:	NCX in the forward mode
NCX_{rev}:	NCX in the reverse mode
NMDG:	N-methyl-D-glucamine
NMDA:	N-methyl-D-aspartate
NMDAR:	N-methyl-D-aspartate receptor
NR1:	NMDA receptor subunit family 1
NR2:	NMDA receptor subunit family 2
NR2B:	subunit of NMDA receptor
NR3:	NMDA receptor subunit family 3
PAGE:	polyacrylamide gel electrophoresis
PCR:	polymerase chain reaction
PBS:	phosphate-buffered saline
PN1:	postnatal day 1
polyQ:	poly-glutamine
PSD-95:	postsynaptic density protein 95
PTP:	mitochondrial permeability transition pore
ROS:	reactive oxygen species
SDS:	sodium dodecyl sulfate
SEM:	standard error of mean
siRNA:	small interfering ribonucleic acid
Tat:	transactivator of transcription
$\mathbf{t}_{dys}$:	time until Ca^{2+} dysregulation
TPP^+:	tetraphenylphosphonium
TTX:	tetrodotoxin
VDAC:	voltage-dependent anion channel
WT:	wild-type
YAC:	yeast artificial choromosome

I. INTRODUCTION

A. Huntington's Disease

George Huntington, a 22-year old physician working in Long Island, New York, first described the disease that bears his name in 1872 (Harper, 2002). In his report, entitled "On Chorea," Huntington noted that the disease was hereditary and manifested in adulthood (Huntington, 1872). Indeed, the hallmark symptom of Huntington's Disease (HD) is chorea, a movement disorder characterized by abrupt, irregular, and spontaneous movements. In addition to chorea, HD patients also experience personality changes, anxiety, and depression. These symptoms can precede the motor symptoms. A decline in cognitive abilities such as abstract thinking and planning is also associated with HD. In later stages, memory function also can decline (Govert & Schneider, 2013). Patients with advanced HD may lose the ability to walk, talk, swallow, and care for themselves. Complications from HD can be life-threatening and the most common cause of death in HD patients is aspiration pneumonia, most likely due to difficulty swallowing (Haines & Conneally, 1986; Bates *et al.*, 2002; Heemskerk & Roos, 2012).

Huntington's Disease is an autosomal dominant neurodegenerative disorder affecting approximately 1 in 10,000 people, with many more people at risk of developing the disease, but not yet diagnosed (Shannon *et al.*, 2009; Roze *et al.*, 2010). HD is found throughout the world but is most common in populations with European heritage (Warby *et al.*, 2011). Symptoms typically present in midlife, with an average age of onset of thirty-eight years. There is a

large patient to patient variation, however, and symptoms of HD may begin at any age (Bates *et al.*, 2002; Govert & Schneider, 2013; Kumar *et al.*, 2015). Less than 10% of people with HD develop symptoms prior to age 21. Onset of HD at a younger age is called Juvenile HD and differs from adult-onset HD (Nance & Myers, 2001).

Because HD is a genetic disorder and symptoms occur later in life, there is a potential for pre-symptomatic therapy. However, there is currently no cure for HD because the mechanisms of the pathology are not clear, and the existing therapies only decrease HD symptoms without eliminating the cause of this neuropathology. Risk-benefit must be evaluated regarding the current therapies to alleviate symptoms, as the standard therapeutics lose efficacy and have a high incidence of side effects (Anderson, 2011). Thus, understanding of the molecular mechanisms underlying HD is crucial for development of new therapies aimed at treating and curing HD.

The pathology of HD is localized to the brain. Atrophy of the striatum (caudate nucleus and putamen) followed by eventual atrophy of cortical structures has been shown to be consistent with the primary symptoms of HD (Vonsattel & DiFiglia, 1998; Bates *et al.*, 2002; Walker & Raymond, 2004; Li *et al.*, 2014). Striatal volume decreases prior to HD diagnosis and symptoms, but this decrease is not significant until around 10 years before onset of symptoms (Aylward *et al.*, 2004). The trigger of striatal atrophy and neuronal loss is not yet known. The striatum is primarily composed of medium spiny neurons (95% of striatal neurons) (Han *et al.*, 2010). Medium spiny neurons are gamma-

aminobutyric acid (GABA)ergic and are the most vulnerable and first affected in HD (Reiner *et al.*, 1988; Vonsattel & DiFiglia, 1998; Walker & Raymond, 2004; Ehrlich, 2012; Li *et al.*, 2014). The mechanisms underlying increased vulnerability of striatal neurons are not understood.

In 1993, the Huntington's Disease Collaborative Research Group found that HD is causally linked to a mutation in *IT15,* now known as the huntingtin gene (*HTT*). *HTT* is located on chromosome 4 at position 16.3 (MacDonald *et al.*, 1993). In healthy individuals *HTT* contains a stretch of 16-20 CAG repeats encoding a poly-glutamine (polyQ) stretch near the NH_2 terminus in the huntingtin protein (Htt). A mutation causing an expansion in the HTT CAG repeat domain to greater than 35 repeats is diagnosed as HD (Myers, 2004; Paulson & Albin, 2011). Individuals with Htt containing intermediate polyQ repeat lengths of ~27-35 may not develop symptoms but are at risk of passing HD to their children (Ashizawa *et al.*, 1994). Genetic anticipation, i.e. further expanse in the polyQ repeat from generation to generation, has been shown to occur in HD (Harper & Jones, 2002). Greater number of repeats increases the severity of the disease and is correlated with earlier onset of the disease (Harper & Jones, 2002; Roze *et al.*, 2010; Zuccato *et al.*, 2010)

a. Huntingtin Protein Function

HTT encodes the huntingtin protein, a large (348 kDa) cytoplasmic protein with a polyQ stretch of variable length near the N-terminus. In the wild-type (WT) Htt protein, this stretch is less than 35 glutamines long (MacDonald *et al.*, 1993; La Spada *et al.*, 2011). Htt is ubiquitously expressed in various tissues, with

highest expression found in neurons of the central nervous system (CNS). Expression of Htt, however, is not different between medium spiny neurons, and other neuronal types. Furthermore, the expression level of Htt does not correlate with vulnerability to HD (Trottier *et al.*, 1995; Fusco *et al.*, 1999).

Htt is essential in development because the Htt knock-out is embryonic lethal (DiFiglia *et al.*, 1995). Subsequent studies found that the addition of human mutant Htt (mHtt) can compensate for endogenous Htt knock-out to rescue the embryonic lethality in mice, meaning that mHtt is a functional protein (Leavitt *et al.*, 2001). Furthermore, use of a Cre/loxP site specific strategy to conditionally inactivate Htt in mice resulted in a clasping phenotype similar to HD models, as well as cortical atrophy (Reddy *et al.*, 1999; Dragatsis *et al.*, 2000). These data show that Htt is essential, not only in development, but also in neuronal health later in life. Most importantly, these studies suggest that the expanded polyQ stretch of mHtt does not result in a complete loss of function.

Htt is involved in many processes and functions in adults. A few include, regulation of brain derived neurotropic factor (BDNF) production (Zuccato *et al.*, 2001; Gauthier *et al.*, 2004), vesicle transport (Brandstaetter *et al.*, 2014), endocytosis (Velier *et al.*, 1998), transcriptional regulation (Li & Li, 2004), anti-apoptotic function (Rigamonti *et al.*, 2000), and N-type voltage-gated Ca^{2+} channel modulation (Swayne *et al.*, 2005). Introduction of mHtt can result in irregular gene transcription (Sugars & Rubinsztein, 2003), defective autophagy (Martinez-Vicente *et al.*, 2010), abnormal mitochondrial biogenesis (Shirendeb *et al.*, 2012), mitochondrial dynamics (Costa *et al.*, 2010; Song *et al.*, 2011;

Shirendeb *et al.*, 2011) mitochondrial trafficking (Trushina *et al.*, 2004; Shirendeb *et al.*, 2012), and mitochondrial Ca^{2+} handling defects (Beal *et al.*, 1993; Panov *et al.*, 2002).

Htt also interacts with over 100 proteins involved in various pathways, including pre- and post-synaptic signaling, cytoskeletal organization, calcium signaling, and mitochondrial function (Shirasaki *et al.*, 2012). Some Htt-protein interactions are dependent on the length of the polyQ stretch, meaning that some proteins interact more strongly with mHtt than Htt. The converse has also been observed (Harjes & Wanker, 2003; Li & Li, 2004). It is unknown if the polyQ stretch mutation results in a loss-of-function of Htt or a gain-of-function of mHtt. Some groups report that both gain- and loss-of-function are involved in HD pathology (Zuccato *et al.*, 2010).

Protein interactions with Htt and mHtt have been reported to be important in Ca^{2+} channel modulation. Two examples of note are postsynaptic density protein 95 (PSD-95) and $Ca_V2.2$. PSD-95 is a scaffold protein that binds to signaling proteins including the N-methyl-D-aspartate (NMDA) subtype of glutamate receptors. The polyQ expansion in mHtt increases interaction between NMDA receptors and PSD-95 leading to increased Ca^{2+} influx and neuronal damage (Sun *et al.*, 2001; Harjes & Wanker, 2003; Fan *et al.*, 2009). Htt interacts with $Ca_V2.2$, an N-type voltage gated Ca^{2+} channel, and enhancing Ca^{2+} influx (Swayne *et al.*, 2005). These findings suggest that both Htt and mHtt are involved in Ca^{2+} signaling.

b. Models of HD

Prior to the identification of the mutation linked to HD, chemical models of HD were used to study the disease. For these models, excitotoxic chemicals such as quinolinic acid or kainic acid were injected into the striatum of rats. The models produced lesions similar to the striatal atrophy seen in HD (McGeer & McGeer, 1976; Beal *et al.*, 1986). Mitochondrial toxins such as 3-nitropropionic acid and malonic acid also have been shown to produce striatal lesions and HD-like behavior in rats (Borlongan *et al.*, 1995; Brouillet *et al.*, 1999). Although these models produce similar behavioral results, they do not correctly recapitulate HD pathology due to the lack of genetic alterations. While these models provide some insight into potential causes of HD pathology, the mechanisms responsible for similar behavior and lesions may be distinct from the mechanism or mechanisms actually responsible for HD pathology. Therefore, chemical models of HD should be used with caution.

Rodent models of HD have been developed based on the expanded polyQ stretch mutation found in mHtt in human HD patients (Ramaswamy *et al.*, 2007; Pouladi *et al.*, 2013). These models are summarized in Table 1. There are three main categories of genetic HD models, expressing expanded polyQ in (1) truncated N-terminal mutant human Htt protein; (2) full-length mutant human Htt protein; and (3) full-length mouse Htt protein.

HD mouse models expressing a portion of N-terminal mHtt with expanded polyQ, most notably the mouse line R6/2, result in a more severe phenotype than full-length mHtt models (Ramaswamy *et al.*, 2007). Furthermore, the R6/2 also

presents other complications, such as diabetes (Bjorkqvist *et al.*, 2005). It is important to note that both truncated and full-length transgenic models maintain endogenous Htt in addition to expressing human mutant Htt. This does not accurately represent the genetics in human HD patients, who typically have one normal copy of HTT and one mutant copy. To address this limitation, we use a control transgenic mouse model in these studies. YAC18 mice express full length human Htt containing 18 glutamines in the polyQ region (Hodgson *et al.*, 1999; Hodgson *et al.*, 1996). The use of this mouse model controls for the presence of both human and mouse Htt. This control does not, however, address if mouse Htt alters the effect of human mHtt.

Knock-in models of HD are the most genetically faithful but phenotypes are very mild and in some models (e.g. HdhQ92 and HdhQ111) striatal atrophy does not occur (Wheeler *et al.*, 1999; Wheeler *et al.*, 2000). For these reasons it is important to acknowledge that animal models are a useful tool in the study of HD but may not recapitulate the human disease in its entirety. Rodent HD models have both limitations and advantages; therefore a carefully selected HD model has to be used to investigate certain aspects of the disease.

In the studies described in this thesis, we used isolated mitochondria and primary neurons from the striata of the YAC128 mouse model of HD. This mouse model makes use of a yeast artificial chromosome (YAC) to express the entire human HD gene with a 128 CAG repeat expansion under the control of the human *HTT* promoter (Slow *et al.*, 2003). Full-length mHtt transgenics, such as the YAC model, show an extended development of the HD phenotype and are

better suited for the study of early changes (Fan & Raymond, 2007). YAC128 was the most recently developed of the YAC models. YAC46 and YAC72, with 46 and 72 CAG repeats, respectively, were previously developed by the same group (Hodgson *et al.*, 1999). Increased CAG repeats were added to decrease the time until HD-related phenotypes could be observed. In YAC128, motor phenotypes are visible by 12 weeks and striatal volume is significantly decreased (15%) by 9 months (Bates *et al.*, 2002; Slow *et al.*, 2003; Ramaswamy *et al.*, 2007). HD symptoms are seen in humans across a range of striatal atrophy classifications, from no visible atrophy to 95% in very severe cases (Vonsattel *et al.*, 1985; Douaud *et al.*, 2006). We chose to use this transgenic model because it develops striatal atrophy, unlike knock-in models, and the animals have a longer life with less severe phenotypes than transgenic models with truncated mHtt.

In addition to animal models of HD, conditionally immortalized, mutant $STHdh^{Q111/Q111}$ striatal neuronal progenitor cells have been used in HD research This cell line is derived from knock-in mice with 111 CAG repeats in the endogenous *HTT* gene. The cells stain positive for neuronal markers and recapitulate some phenotypes seen in HdhQ111 knock-in mouse striatum. These cells may be useful in the study of some aspects of HD (Trettel *et al.*, 2000).

Table 1. Genetic Rodent HD Models

Rodent Model	Construct	Notable Features
Transgenic truncated N-terminal fragment models		
Transgenic R6/2 mice (Mangiarini *et al.*, 1996)	N-terminal fragment (67 aa) of human *HTT* with 115-150 or 195 CAG repeats	Neuronal atrophy by 3 months (Stack *et al.*, 2005) Death at 10-13 weeks (Mangiarini *et al.*, 1996) Diabetes (Bjorkqvist *et al.*, 2005) Augmented Ca^{2+} uptake capacity in brain nonsynaptic mitochondria (Oliveira *et al.*, 2007)
Transgenic N171-82Q mice (Schilling *et al.*, 1999)	N-terminal fragment (171, 118, or 586 aa) of human *HTT* with 82 CAG repeats	Neuronal atrophy by 16 weeks (McBride *et al.*, 2006)
Transgenic D9-N171-98Q mice, also known as DE5 mice (Brown *et al.*, 2008)	N-terminal fragment of human *HTT* with 98 CAG repeats expressed only in medium spiny neurons of the striatum	No striatal atrophy (Kim *et al.*, 2011) Motor abnormalities (Brown *et al.*, 2008)
Transgenic Short Stop mice (Slow *et al.*, 2005)	N-terminal fragment (171 aa) of human *HTT* with 128 CAG repeats	Presence of mHtt aggregates No behavioral dysfunction or neuronal loss (Slow *et al.*, 2005)
Transgenic HD rats (von *et al.*, 2003)	Express 727 amino acids of the HTT_{51Q} gene, corresponding to 22% of the full-length gene	Reduced mitochondrial membrane potential stability in response to Ca^{2+}, decreased Ca^{2+} uptake capacity, increased propensity to PTP induction (Gellerich *et al.*, 2008)
Transgenic full-length models		
Transgenic BACHD mice (Gray *et al.*, 2008)	Full-length human *HTT* gene with 97 mixed CAA-CAG repeats	Striatal atrophy by 12 months Symptoms by 6 months (Gray *et al.*, 2008)
Transgenic YAC46 or YAC72 mice (Hodgson *et al.*, 1999)	Full-length human *HTT* gene with 46 or 72 CAG repeats	Decreased Ca^{2+} uptake capacity (Panov *et al.*, 2002)

Rodent Model	Construct	Notable Features
Transgenic YAC128 mice (Slow *et al.*, 2003)	Full-length human *HTT* gene with 128 CAG repeats	Striatal atrophy by 9 months (Slow *et al.*, 2003) Augmented mitochondrial depolarization in response to Ca^{2+} in medium spiny neurons, increased susceptibility to PTP induction (Fernandes *et al.*, 2007) Augmented Ca^{2+} uptake capacity in brain nonsynaptic mitochondria (Oliveira *et al.*, 2007)
Transgenic BACHD rats (Yu-Taeger *et al.*, 2012)	Full-length human *HTT* gene with 97 mixed CAA/CAG repeats	Early onset motor deficits mHtt aggregates (Yu-Taeger *et al.*, 2012)
Knock-in full-length models		
Knock-in HdhQ50, Q92, and Q111 mice (Wheeler *et al.*, 1999)	Mouse *HTT* gene with inserted 50, 92, or 111 CAG repeats in exon 1	No striatal degeneration (Wheeler *et al.*, 1999) No cognitive phenotypes (Wheeler *et al.*, 2000) Gait abnormalities at 24 months in Q111 (Wheeler *et al.*, 2000) No increase in sensitivity to Ca^{2+}-induced damage in striatal and cortical nonsynaptic mitochondria (Brustovetsky *et al.*, 2005)
Knock-in Hdh150Q and Hdhq200 mice (Lin *et al.*, 2001; Yu *et al.*, 2003)	Mouse *HTT* gene with inserted 150 and 200 CAG repeats in exon 1 in a single allele ($Hdh^{150/+}$) or both alleles ($Hdh^{150/150}$)	No cognitive symptoms Liver mitochondria from $Hdh^{150/150}$ mice have increased propensity to Ca^{2+}-induced PTP (Choo *et al.*, 2004). No change in Ca^{2+} uptake capacity in brain nonsynaptic mitochondria (Oliveira *et al.*, 2007)

c. Proposed Mechanisms of Neurodegeneration in Huntington's Disease

Because Htt has multiple functions and interactions, several mechanisms have been postulated to cause neurodegeneration in HD. Furthermore, the possibility of both gain- and loss-of-function of mHtt suggests that it is likely that many pathways may be involved in HD pathology. My research is focused on Ca^{2+} homeostasis but other mechanisms likely participate in neuronal loss and symptom onset in HD. I will briefly describe some of the leading pathways linked to neurodegeneration in HD.

Transcriptional dysregulation has been detected in postmortem HD brains (Arzberger *et al.*, 1997) as well as mouse models of HD (Luthi-Carter *et al.*, 2000; Luthi-Carter *et al.*, 2003). The polyQ stretch of mHtt may lead to this dysregulation by recruiting other polyQ containing proteins, such as transcription factors, and preventing their normal function (Cha, 2007). PolyQ proteins have been shown to interact with transcription factors and mHtt has increased nuclear localization compared to Htt, which is found mostly in the cytosol (Kegel *et al.*, 2002). Increased nuclear localization along with the polyQ tract, suggests that mHtt may be interacting with transcription factors in HD (Sugars & Rubinsztein, 2003). Altered transcription could lead to dysregulation of many molecular functions and, ultimately neurodegeneration.

One, of many, consequences of altered transcription by mHtt could be loss of BDNF, a growth factor. In HD, decreased BDNF has been observed and is linked to neurodegeneration (Cha, 2007). BDNF is produced in the cortex and transported to medium spiny neurons. Studies have shown that medium spiny

neurons depend on BDNF from the cortex, and that BDNF is decreased nearly 50% in HD. (Zuccato & Cattaneo, 2007; Zuccato & Cattaneo, 2009). Further studies have shown that experimentally decreasing BDNF in the cortex leads to neuronal loss in the striatum (Zuccato *et al.*, 2010). In support of this, experimental application of BDNF is neuroprotective in the presence of mHtt (Kells *et al.*, 2004). Studies are ongoing to study delivery of BDNF as a potential therapeutic in HD.

Both Htt and mHtt are subject to cleavage by caspases, specifically caspase-2, caspase-3, caspase-6, and caspase-7 (Wellington *et al.*, 2000; Wellington *et al.*, 2002). The toxic fragment hypothesis proposes that the cleavage of mHtt produces toxic fragments containing expanded polyQ sections. These fragments can, in turn, lead to additional amplification of caspase activity and, subsequently, more fragments. Fragment aggregation is dependent upon polyQ and fragment length (Chen *et al.*, 2002) and accumulation of these fragments may lead to further caspase activity and eventual cell death (Goldberg *et al.*, 1996; Zuccato *et al.*, 2010). In support of the toxic fragment hypothesis, in studies where caspase-6 was inhibited, reducing mHtt cleavage, the phenotype of HD mice improved (Graham *et al.*, 2006). Fragments of mHtt can also be produced by calpains, calcium-dependent proteases (Bizat *et al.*, 2003; Gafni *et al.*, 2004). Calpain activation and increased levels of calpains have been detected in HD patients (Gafni *et al.*, 2004). Calpains are activated by alterations in calcium homeostasis, due to excitotoxicity or mitochondrial dysfunction.

Ca^{2+} signaling has been demonstrated to be altered in neurons from mouse models of HD (Tang *et al.*, 2003; Bezprozvanny & Hayden, 2004). Mutant Htt-induced excitotoxicity has been reported in striatal neurons from mice expressing full-length human mHtt (YAC lines), but not in transgenic mice bearing an NH_2-terminal portion of the protein (R6/2 and N171–82Q lines) that have shown striatal resistance to excitotoxicity. The resistance to excitotoxicity in the truncated models may represent an adaptive measure in response to mHtt expression to generate compensatory mechanisms that reduce some of the toxic effects of the mHtt fragment with expanded polyQ stretch (Fan & Raymond, 2007).

Elevated cytosolic Ca^{2+} has been proposed as a mechanism responsible for increased neuronal cell death in HD (Tang *et al.*, 2005). In support of this hypothesis, aberrant functioning of mechanisms responsible for the increase in intracellular Ca^{2+} (from extracellular and intracellular sources) has been implicated in HD neuropathology (Chen *et al.*, 1999a; Milnerwood *et al.*, 2010; Bezprozvanny, 2011). However, Ca^{2+} influx mechanisms in the cell are counterbalanced by mechanisms that extrude or sequester Ca^{2+} to remove excessive Ca^{2+} from the cytosol (Guerini *et al.*, 2005). These mechanisms have not been previously investigated (Na^+/Ca^{2+} exchanger activity) in HD or previous studies have resulted in varied and conflicting results (mitochondrial Ca^{2+} uptake capacity in HD). These mechanisms will be the focus of this dissertation.

B. Calcium Dysregulation

In non-pathological situations, the concentration of cytosolic Ca^{2+} in neurons is under tight control. The basal cytosolic concentration of Ca^{2+} is maintained at approximately 100 nM and can increase to between 1 and 100μM when neurons are stimulated, while the extracellular Ca^{2+} concentration is approximately 2 mM (Nicholls, 1986). Increased cytosolic Ca^{2+} is rapidly removed by extrusion or by mechanisms that sequester the cation, in an attempt to return to resting (or basal) Ca^{2+} concentrations (Nicholls, 1986; Gleichmann & Mattson, 2010). Ca^{2+} dysregulation can occur when there is an imbalance between Ca^{2+} influx and removal of the cation from the cytosol. Ca^{2+} dysregulation can be divided into phases (as shown in Figure 1); beginning with (1) the entry of Ca^{2+}, predominantly through NMDA receptors (additional explanation in the next section). During (2) the latent period, it is thought that cytosolic Ca^{2+} levels are lowered by mechanisms such as Na^{+}/Ca^{2+} exchanger (NCX) operation in the forward mode and mitochondrial Ca^{2+} uptake (Guerini *et al.*, 2005). In (3) the last phase, a second irreversible increase in cytosolic Ca^{2+} occurs and this constitutes delayed Ca^{2+} dysregulation (DCD), sometimes also called delayed Ca^{2+} deregulation (Nicholls & Budd, 1998).

We believe that “dysregulation” is a more appropriate term because there is still some remaining control over intracellular Ca^{2+} concentrations. During the last phase of Ca^{2+} dysregulation, the cytosolic Ca^{2+} concentration is much greater than basal Ca^{2+} concentration, but does not reach the levels of extracellular Ca^{2+} concentrations. This suggests an impairment (dys-) not a

removal (de-) of regulation. The phases of DCD are shown in an example trace in Figure 1.

DCD is a hallmark of glutamate excitotoxicity (Manev *et al.*, 1989; Thayer & Miller, 1990; Tymianski *et al.*, 1993a; Budd & Nicholls, 1996). Glutamate is a major neurotransmitter in the body and glutamate-induced excitotoxicity is a key factor contributing to neuronal loss in many neurodegenerative diseases, including Parkinson's disease, Alzheimer's disease, multiple sclerosis, and HD. Excitotoxicity also plays a role in damage and neuronal death in stroke and traumatic brain injury (Mattson, 2003; Salinska *et al.*, 2005). Persistent elevation of extracellular glutamate ultimately results in a sustained elevation in cytosolic Ca2+ concentration and activation of Ca2+-dependent degradation enzymes such as phospholipases, DNAases, and proteinases (calpains). A causal link has been established between sustained elevation of cytosolic Ca2+ and cell death (Manev *et al.*, 1989; Choi & Hartley, 1993).

Prolonged increase in cytosolic Ca2+ initiates multiple damaging pathways, both directly and indirectly influenced by elevated Ca2+. Increased free cytosolic Ca2+ activates degradation enzymes such as calpains, Ca2+-dependent proteases (Goll *et al.*, 2003). This results in the degradation of proteins, including cytoskeleton proteins, membrane receptors, and metabolic enzymes (Chan & Mattson, 1999; Nixon, 2003). The activation of calpains also may lead to the activation of caspases, initiating the apoptotic pathway (Waterhouse *et al.*, 1998; Lankiewicz *et al.*, 2000; Smith *et al.*, 2008). Ca2+-dependent phospholipases, such phospholipase A2, are activated as well.

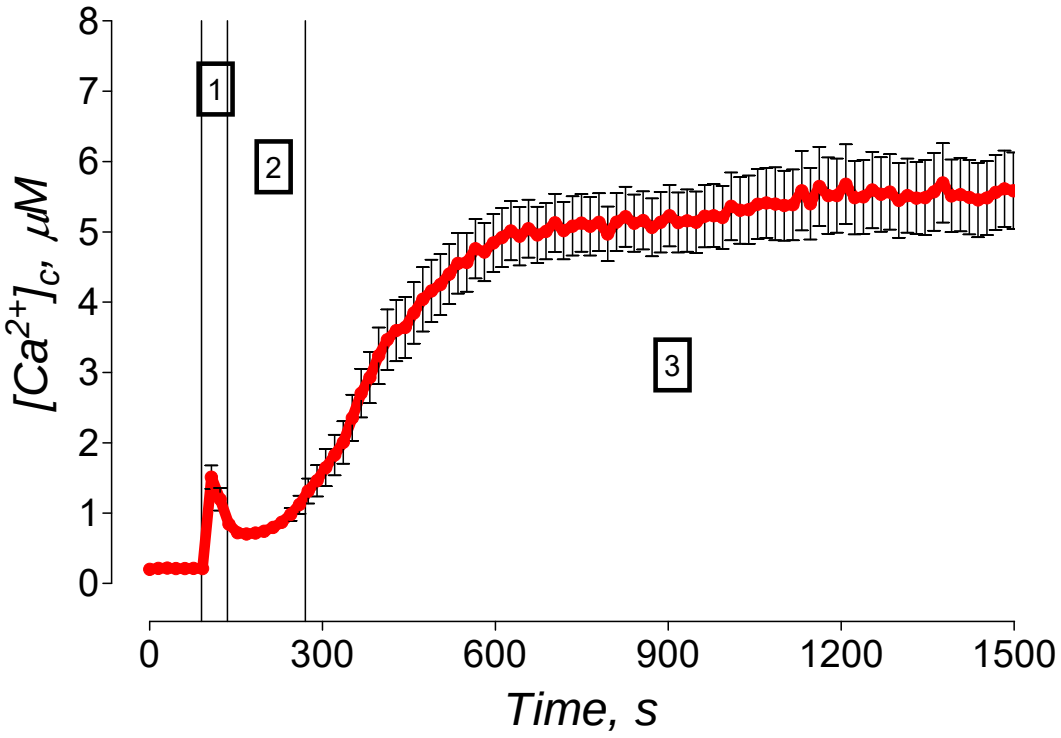

Figure 1. Example of delayed Ca^{2+} dysregulation phases
Neurons were loaded with Ca^{2+}-sensitive dye Fura-2FF-AM to monitor changes in cytosolic Ca^{2+} concentration ($[Ca^{2+}]_c$) over time. The data are mean±SEM. At 90 seconds (the first solid line) glutamate plus glycine was applied. In **(1)** Ca^{2+} influx occurs, likely through NMDA receptors. Next, in **(2)**, is the latent period where Ca^{2+} removal mechanisms work to lower intracellular Ca^{2+} to the basal level. Finally, in **(3)**, delayed Ca^{2+} dysregulation occurs as Ca^{2+} influx overwhelms Ca^{2+} removal mechanisms.

These enzymes degrade important membrane phospholipids, disrupting organelle membranes (Bonventre, 1997). The activation of these degradation enzymes ultimately results in neuronal death.

Mitochondria play an important role in regulation of Ca^{2+} homeostasis in neurons by taking up elevated Ca^{2+} from the cytosol. However, excessive Ca^{2+} uptake by mitochondria during DCD can result in mitochondrial permeability transition, a condition characterized by dramatically increased permeability of the inner mitochondrial membrane, leading to inhibition of oxidative phosphorylation, inhibition of Ca^{2+} uptake, and release of different mitochondrial apoptogenic proteins such as cytochrome *c*, Smac/DIABLO, Apoptosis Inducing Factor (AIF), and Omi/HtrA2 (Fan *et al.*, 2001; Hagberg, 2004; Orrenius *et al.*, 2015). Cytochrome *c* initiates the apoptotic pathway by activating pro-apoptotic proteins, subsequently leading to eventual neuronal death (Slee *et al.*, 1999; Brustovetsky *et al.*, 2002; Goldstein *et al.*, 2005).

a. Glutamate Receptors

Glutamate receptors (GluR) are transmembrane receptors expressed primarily in the CNS. Glutamate, the major excitatory neurotransmitter in the brain, binds to GluRs and mediates fast synaptic transmission (Dingledine *et al.*, 1999; Glasgow *et al.*, 2015). There are two classes of glutamate receptors, metabotropic GluR (mGluR) and ionotropic GluR (iGluR). mGluR are G-protein coupled receptors, whereas iGluR are ion channels (Gregory *et al.*, 2013). It is important to note that mGluR appear to have a minimal role in the onset of

glutamate-induced delayed Ca^{2+} dysregulation (Tymianski *et al.*, 1993a; Kritis *et al.*, 2015). On the other hand, iGluR activation by glutamate binding to the receptor allows the flow of cations into cells, quickly raising intracellular Ca^{2+} and Na^{+} concentrations (Sattler & Tymianski, 2000). Because iGluR activation can so quickly alter ion concentrations and thus contribute to DCD, this research is focused on the iGluR class of GluR.

There are three subtypes of iGluR; they are named for chemical compounds that bind to the receptor more selectively than glutamate. These subtypes are N-methyl-D-aspartate (NMDA) receptors, α-amino-3-hydroxy-5-methyl-4-isoxazolepropionic acid (AMPA) receptors, and kainate receptors (Dingledine *et al.*, 1999; Kohr, 2006). Activation of iGluRs causes the ion channel to open, allowing ions to flow freely down their respective electrochemical gradients. Since glutamate is the major excitatory neurotransmitter, iGluRs play an important role in neuronal synaptic transmission (McEntee & Crook, 1993; Okubo *et al.*, 2010).

Under normal conditions, glutamate is released from glutamatergic nerve terminals and binds to post-synaptic glutamate receptors. Glutamate activates iGluRs, leading to depolarization of the plasma membrane and cation influx into neurons (McEntee & Crook, 1993). It has been hypothesized that continuous presence of glutamate results in prolonged iGluR activation. This allows an uninterrupted influx of Ca^{2+} into the cytosol leading to Ca^{2+} dysregulation (Tymianski *et al.*, 1993a).

i. NMDA Subtype of Ionotropic Glutamate Receptors

The NMDA receptor (NMDAR) is an iGluR, which can be specifically activated by NMDA, an exogenous molecule. When NMDAR is activated, the ion channel opens, allowing Na^+ and Ca^{2+} to flow into the cell. NMDAR are 3-4 times more permeable to Ca^{2+} than AMPA or Kainate receptors (MacDermott *et al.*, 1986; Traynelis *et al.*, 2010). Ca^{2+} influx, along with plasma membrane depolarization, occurs as a result of the activation of NMDARs (McEntee & Crook, 1993; Okubo *et al.*, 2010). NMDARs are expressed in neurons in both the central and peripheral nervous systems, with high expression in the hippocampus, cortex, and striatum (Monyer *et al.*, 1994). Interestingly, these regions of the brain also correspond to those regions most susceptible to a prolonged elevation in glutamate (Nicholls, 2004), suggesting a link between NMDA receptor density and excitotoxic neuronal death. Supporting this, NMDAR antagonists have been shown to be neuroprotective in ischemia-induced excitotoxicity and animal models of traumatic brain injury (Faden *et al.*, 1989; Steinberg *et al.*, 1989) .

NMDARs are heterotetramers composed of four transmembrane subunits (Kohr, 2006). Seven subunits, classified into three families, have been described. These families are NR1, NR2 and NR3 (also called GluN1, GluN2, and GluN3) (Paoletti & Neyton, 2007). NMDARs are typically made up of two NR1 (or GluN1) subunits and either two NR2 (or GluN2) subunits or a mixture of NR2 and NR3 (GluN2 and GluN3) subunits (Masu *et al.*, 1993; Glasgow *et al.*, 2015). These four subunits multimerize to form the functional pore that allows passage of

cations in response to extracellular ligand binding (Dingledine *et al.*, 1999). The composition of subunits can result in great variation of the properties of the receptors (Groc *et al.*, 2006; Paoletti & Neyton, 2007).

There are eight isoforms of the NR1 subunit, the only member of the NR1 family, derived from alternative splicing. These subunits have overlapping expression in neurons and are expressed from the embryonic stage through adulthood (Kohr, 2006). The alternative splicing yields functional isoforms with slight modifications in the N-terminal (N1) and C-terminal (C1, C2) domains of the subunit protein (Janssens & Lesage, 2001).

The NR2 family consists of four members, NR2A, NR2B, NR2C, and NR2D. Unlike NR1, NR2 subunits are not ubiquitously expressed and expression varies. Only NR2B and NR2D subunits are expressed embryonically with NR2D expression dropping to low levels after birth (Paoletti & Neyton, 2007). NR2A expression begins shortly after birth and is abundantly expressed throughout the CNS. As the neurons mature, NR2A expression increases, and eventually the NR2A subunits outnumber the NR2B subunits (Liu *et al.*, 2004; Brewer *et al.*, 2007). NR2C expression begins later in development and is restricted to the cerebellum and olfactory bulb (Dehorter *et al.*, 2012). NR2A and NR2B are seen as the predominant subunits and appear to have greater importance in excitotoxicity due to localization and expression (Nicholls, 2004). NR2B are more highly expressed in striatal medium spiny neurons compared with other NR2 subtypes and other parts of the brain (Li *et al.*, 2003). Importantly, NR2B subunits

are linked to cell death compared with NR2A (Zhou & Baudry, 2006; Liu *et al.*, 2007).

The NR3 family of subunits contains two members, NR3A and NR3B. These subunits also show variable expression patterns. NR3A expression peaks shortly after birth then declines (Kehoe *et al.*, 2013). NR3B subunit expression on the other hand, slowly increases throughout development. NR3B subunit expression in adulthood is primarily in motor neurons (Paoletti & Neyton, 2007).

A distinguishing feature of NMDARs is the requirement of a co-agonist for activation (McBain & Mayer, 1994). The NR1 subunit binds a co-agonist, glycine or D-serine, and the NR2 subunit binds the excitatory neurotransmitter, normally glutamate (Lester *et al.*, 1990). Interestingly, NMDAR composed of only NR1 and NR3 subunits have been shown to be activated by glycine alone. This subunit combination has, to date, only been identified *in vivo* in the myelin surrounding the optic nerve (Balasuriya *et al.*, 2014).

Another feature unique to NMDAR is that the receptor is both ligand-gated and voltage-dependent. The voltage-dependence of NMDAR is due to an endogenous Mg^{2+} block that prevents ion flow through the channel when the plasma membrane is at resting potential (Nowak *et al.*, 1984). When the plasma membrane is depolarized, Mg^{2+} is expelled from the ion channel, and can be activated if the correct ligands are present (Spandou *et al.*, 2007).

Based on the unique properties of NMDAR, they are thought to play an important role in glutamate-induced DCD. It is hypothesized that prolonged glutamate exposure results in plasma membrane depolarization, causing removal

of the endogenous blocker, Mg^{2+}. Then, once both co-agonists, glutamate and glycine, bind to NMDAR, the receptor becomes continuously activated (Nowak *et al.*, 1984; Planells-Cases *et al.*, 2006). Activation of NMDAR allows massive Ca^{2+} influx, overwhelming the homeostatic Ca^{2+} extrusion and accumulation mechanisms, leading to DCD (Nicholls & Budd, 1998; Tymianski *et al.*, 1993b).

ii. NMDAR Activity in HD Models

Activation of NMDARs can increase susceptibility to excitotoxicity resulting in intracellular Ca^{2+} overload. Some of the first indications that this could be a mechanism for HD pathology came from chemically induced rodent models. Injection of excitatory iGluR agonists into the striata of rats caused neurodegeneration and behavioral abnormalities resembling HD. This approach was used to generate an early model for HD (Coyle & Schwarcz, 1976). While this early model was limited in utility to study HD, it did provide potential clues regarding a possible mechanism of HD pathology.

Since activation of NMDARs could induce excitotoxicity in animal models, these receptors became an attractive target to better understand the pathology of HD. NMDA-evoked currents in striatal slices from both symptomatic and pre-symptomatic R6/2 mice were found to be enhanced compared to WT (Cepeda *et al.*, 2001). These results were also supported by experiments in cultured striatal neurons from R6/2 mice (Andre *et al.*, 2006).

In experiments using medium spiny neurons from YAC72 mice, Zeron and colleagues found enhanced cell death subsequent to exposure to 3mM

NMDA compared with neurons from WT animals (Zeron *et al.*, 2002). They also showed enhanced current in dissociated YAC72 medium spiny neurons in response to 1mM NMDA. Interestingly, this laboratory later showed no difference in current in medium spiny neurons from YAC128 mice compared with neurons from WT animals (Fernandes *et al.*, 2007).

Increased function of NMDAR in the presence of mHtt was first shown using transiently transfected NMDAR subunits and full-length human Htt with either 15 polyQ (normal, Htt-15Q) or 138 polyQ (expanded, mHtt-138Q) (Chen *et al.*, 1999b). Co-expression of the NR1/NR2B-type of NMDARs with mHtt-138Q led to larger NMDAR-mediated currents than with Htt-15Q. Importantly, cells transfected with NR1/NR2A-type NMDARs had similar currents when co-expressed with either Htt-15Q or mHtt-138Q (Chen *et al.*, 1999b). Further evidence suggesting the importance of NR2B in increased NMDAR sensitivity in HD models is a correlation between decreased mRNA levels of NR2A and no change in NR1 or NR2B in neurons with larger NMDAR currents than in medium spiny neurons from WT littermates (Ali & Levine, 2006). These data, together with the high expression of NR2B in the striatum as compared to other parts of the forebrain (Landwehrmeyer *et al.*, 1995; Li *et al.*, 2003), suggest that the NR2B subunit may be a key mediator of the excitotoxic damage elicited by mHtt expression.

iii. NMDAR Agonists and Antagonists

NMDARs are endogenously activated by glutamate as well as L-aspartate (Dingledine *et al.*, 1999). They are additionally activated by NMDA (for which NMDARs are named), an exogenous molecule, which does not activate other iGlurRs. NMDARs are endogenously blocked at resting membrane potentials by Mg^{2+}, but the block can be removed with plasma membrane depolarization (Nowak *et al.*, 1984).

Several NMDAR inhibitors have been developed as laboratory research tools and potential therapeutics. In my research, I used D-(-)-2-Amino-5-phosphonopentanoic acid (AP-5). AP-5 is a competitive antagonist that acts by reversibly binding to the glutamate site on the NR2 subunit and competing with glutamate binding (Morris *et al.*, 1986; Clements & Westbrook, 1994). AP-5 inhibition is reversible with a short half-life. These qualities make AP-5 a useful tool in studying NMDAR because it can be applied and washed off.

Another inhibitor of NMDAR used in my research is (+)-5-methyl-10,11-dihydro-5H-dibenzo[a,d]cyclohepten-5,10-imine maleate (MK-801). MK-801 inhibits NMDARs by binding to and irreversibly blocking the open pore of the NMDAR (Foster & Wong, 1987; Huettner & Bean, 1988). However, our laboratory recently showed that MK-801 also inhibits the activity of NCX operating in the reverse mode (full description in following sections) (Brittain *et al.*, 2012b). For this reason, MK-801 is only used in these studies as an inhibitor of reverse NCX in experiments independent of NMDAR agonists. There are

numerous additional NMDAR antagonists act as competitive, uncompetitive, and non-competitive antagonists that were not used in this research.

iv. NMDAR Regulation

Along with the modulation of NMDAR by mHtt described above, other proteins have been shown to interact with, and regulate the activity of NMDARs. One of these interactions is with PSD-95, a scaffold protein that has been shown to also be regulated by mHtt (Fan *et al.*, 2009). In WT neurons, PSD-95 expression has been shown to enhance NMDAR opening rate. Futhermore, PSD-95 increases NMDAR membrane localization by promoting membrane insertion and inhibiting internalization (Lin *et al.*, 2006).

In collaboration with Dr. Khanna's laboratory, we recently showed that NMDAR may be regulated by collapsin response mediator protein 2 (CRMP2). We showed that a peptide derived from CRMP2 decreased NMDA-induced Ca^{2+} influx into cultured neurons, diminished ion current, and decreased surface expression of NMDAR in dendritic spines (Brittain *et al.*, 2011a). Interaction between NR1 and NR2 subunits with CRMP2 has also been shown (Al-Hallaq *et al.*, 2007). These results suggest that CRMP2 may be involved in modulating NMDAR activity in healthy and possibly HD patients, but the mechanism is not yet understood and involvement in HD pathology is not yet established.

b. Collapsin Response Mediator Protein 2

CRMP2 is a 62 kDa phosphoprotein in the CNS (Charrier *et al.*, 2003). Due to many groups identifying CRMP2 in parallel, it has also been known by the names CRMP-62 (named for its molecular weight), Dihydropyrimidinase-like protein-2 (DPYSL2), Dihydropyrimidinase Related Protein 2 (DRP-2), Turned On After Division 64-kDa (TOAD-64), and *Unc-33* LIke Phosphoprotein 2 (ULIP-2) (Hensley *et al.*, 2011; Charrier *et al.*, 2003). There are five members of the CRMP family of proteins. All of the CRMP genes are highly homologous and are evolutionarily conserved (about 95% between mouse and human) (Byk *et al.*, 1998; Ricard *et al.*, 2001).

CRMP2 is the most studied member of the CRMP family and is traditionally regarded as a regulator of axon guidance and neurite outgrowth (Schmidt & Strittmatter, 2007; Hensley *et al.*, 2011). CRMP2 is the most abundantly expressed member of the CRMP family and is maintained at high levels in adults, unlike other CRMPs that are maintained at low levels in adult CNS (Wang & Strittmatter, 1997). Due to alternative splicing in the N-terminus there are two CRMP2 isoforms, a short form and a long form. The isoforms are identical from residues 1-572, the long form has an additional 112 amino acids in the N-terminus (Quinn *et al.*, 2003).

CRMP2 forms homotetramers and heterotetramers with other members of the CRMP family (Wang & Strittmatter, 1997). CRMP2 interacts with many diverse proteins including cytoskeletal proteins tubulin and actin (Fukata *et al.*, 2002; Arimura *et al.*, 2005), NMDARs (Al-Hallaq *et al.*, 2007), and N-type Ca^{2+}

channel CaV2.2 (Brittain *et al.*, 2009). Recent research on the diverse and unique interactions of CRMP2 showed its involvement in many more processes than originally thought (Brittain *et al.*, 2011a; Wilson *et al.*, 2012).

i. Molecular Tools for the Study of CRMP2

A 15-amino acid peptide, CBD3, from the Ca^{2+} channel binding domain of CRMP2 has been shown to disrupt the interaction between CRMP2 and CaV2.2 (Brittain *et al.*, 2009). The peptide cannot cross the plasma membrane, so the tat cell penetrating motif of the HIV-1 protein was added to facilitate peptide entry into neurons (Tat-CBD3) (Brittain *et al.*, 2011a). In addition to disrupting the interaction between CRMP2 and CaV2.2, tat-CBD3 has previously been shown to decrease NMDAR activity. The mechanism leading to this decrease is not yet understood, but we hypothesize that tat-CBD3 disrupts an interaction between NMDAR and CRMP2. We use this peptide as a tool to understand the interaction of CRMP2 with potential interacting partners.

ii. Potential Involvement of CRMP2 in HD Pathology

At the time of writing this dissertation, only one paper has discussed CRMP2 in relation to HD. Lim and colleagues recently studied glycogen synthase kinase-3β (GSK3β), a regulator of CRMP2 phosphorylation, in HD models and postmortem human brain tissue. This group showed an increase in GSK3β phosphorylation and corresponding decrease in CRMP2 phosphorylation in cortical tissue from the R6/1 mouse model of HD. Interestingly, they saw

increased phosphorylated GSK3β in the striatum but no change in phosphorylated CRMP2. This group did not assess total CRMP2 expression in HD models or investigate interaction between mHtt and CRMP2 (Lim *et al.*, 2014).

C. Mitochondria

Normal Ca^{2+} signaling utilizes fine tuning of cytosolic Ca^{2+} concentrations by different mechanisms (Carafoli, 1988; Erecinska & Silver, 1996). Prolonged glutamate exposure leading to high levels of Ca^{2+} requires high capacity mechanisms of Ca^{2+} clearance (Brini *et al.*, 2002; White & Reynolds, 1995). Two major mechanisms of Ca^{2+} removal and uptake are via mitochondria and plasmalemmal Na^{+}/Ca^{2+} exchanger. Each of these mechanisms, however, can be overwhelmed and contribute to glutamate-induced elevation in cytosolic Ca^{2+} concentrations (Kiedrowski *et al.*, 1994; Kiedrowski, 1999; Chalmers & Nicholls, 2003).

Accumulation of Ca^{2+} in mitochondria is a major mechanism contributing to clearance of elevated cytosolic Ca^{2+} (Kiedrowski & Costa, 1995). A Ca^{2+} channel called the Ca^{2+} uniporter in the inner mitochondrial membrane allows Ca^{2+} influx into mitochondria (Baughman *et al.*, 2011; De *et al.*, 2011) and Ca^{2+} accumulation in the mitochondrial matrix (Bernardi, 1999). The influx is driven by a large negative membrane potential inside of mitochondria. The magnitude of mitochondrial Ca^{2+} uptake capacity is limited by mitochondrial sensitivity to the detrimental effect of Ca^{2+} manifested in induction of the mitochondrial

permeability transition pore (PTP) (Chalmers & Nicholls, 2003). The Ca^{2+} accumulated by mitochondria can be released via mitochondrial Na^{+}/Ca^{2+} exchangers or due to induction of the PTP (Carafoli & Lehninger, 1971).

The affinity of the uniporter to Ca^{2+} is low, and under physiological conditions, the concentration of Ca^{2+} within mitochondria is relatively low (0.2-10μM) (McCormack *et al.*, 1990). Mitochondria can accumulate much larger amounts of Ca^{2+} in response to high cytosolic Ca^{2+} concentration (Thor *et al.*, 1984). Therefore, mitochondrial Ca^{2+} uptake has been regarded as a safety mechanism in situations of temporary intracellular Ca^{2+} overload.

i. Permeability Transition Pore

A large Ca^{2+} load in mitochondria induces mitochondrial damage through induction of the PTP that, in turn causes mitochondrial depolarization (Bernardi, 1999). During PTP induction, the inner mitochondrial membrane becomes permeable to solutes up to 1500 Da (Green & Kroemer, 2004). PTP opening is followed by mitochondrial swelling and eventual rupture of the mitochondrial membrane. This limits the ability of mitochondria to accumulate Ca^{2+}, produce ATP, and retain pro-apoptotic proteins like cytochrome *c* (Rasola & Bernardi, 2011). These factors significantly decrease the cell's ability to maintain calcium homeostasis and often lead to neuronal death (Bernardi & Petronilli, 1996).

The molecular structure and composition of the PTP remains elusive although many proteins have been hypothesized to be part of the PTP complex. The level of expression of Cyclophilin D (CyD), a mitochondrial matrix protein,

correlates with PTP induction in brain mitochondria (Brustovetsky *et al.*, 2003) and is the only protein shown by pharmacological and knock-out studies to sensitize the PTP to Ca^{2+} (Baines *et al.*, 2005; Malouitre *et al.*, 2010). Brain mitochondria isolated from homozygous CyD knockout mice ($Ppif^{-/-}$ mice) were much less susceptible to opening of PTP (Baines *et al.*, 2005). These data support that CyD is an important component of the PTP (Javadov & Kuznetsov, 2013).

ii. Permeability Transition Pore Modulation

The PTP is Ca^{2+} dependent but opening can be facilitated by other factors such as ATP depletion, low pH, and reactive oxygen species (ROS) (Bernardi, 1999; Crompton, 1999). Cyclosporine A (CsA) is an inhibitor of PTP (Broekemeier *et al.*, 1989). CsA inhibits the PTP by binding to mitochondrial CyD (Halestrap & Davidson, 1990). In experiments with isolated mitochondria, CsA makes mitochondria resistant to Ca^{2+} and suppresses the PTP activation (Kushnareva *et al.*, 2005). ADP can also be used as an inhibitor of the PTP and can act synergistically with CsA (Novgorodov *et al.*, 1992; Chalmers & Nicholls, 2003).

iii. Mitochondrial Ca^{2+} Uptake in HD Models

One of the major hypotheses for neurodegeneration in HD posits that mHtt leads to aberrant Ca^{2+} handling in affected neurons (Bezprozvanny & Hayden, 2004). As it was discussed in previous sections, this could be due to augmented

activity of NMDA-subtype of glutamate receptors (Zhang *et al.*, 2008). Defects in mitochondrial Ca^{2+} handling have also been suggested as a potential mechanism leading to DCD and excitotoxic neuronal death (Panov *et al.*, 2002).

In early studies, investigators found decreased Ca^{2+} uptake capacity in brain mitochondria from YAC72 mice and a rat HD model (Panov *et al.*, 2002; Gellerich *et al.*, 2008) and in mitochondria of a conditionally immortalized striatal progenitor cell line $STH^{Q111/Q111}$ expressing mHtt with 111 glutamines (Milakovic *et al.*, 2006; Lim *et al.*, 2008). The facilitated induction of the PTP in mitochondria associated with mHtt was proposed to explain Ca^{2+} handling defects in mitochondria from HD animal and cell models (Milakovic *et al.*, 2006; Gellerich *et al.*, 2008). Indeed, increased propensity to Ca^{2+}-stimulated PTP induction was found in mitochondria in neurons from HD mice and immortalized striatal cells (Choo *et al.*, 2004; Fernandes *et al.*, 2007; Lim *et al.*, 2008; Quintanilla *et al.*, 2013a).

Previous studies in our laboratory did not confirm an increase in likelihood of PTP induction in striatal and cortical mitochondria isolated from HD mice compared with mitochondria from WT mice (Brustovetsky *et al.*, 2005). Another group demonstrated increased Ca^{2+} uptake capacity in brain nonsynaptic mitochondria isolated from R6/2 and YAC128 mice compared to mitochondria from WT littermates (Oliveira *et al.*, 2007). In experiments with cultured cortical neurons expressing N-terminal or full-length mHtt, investigators failed to find a significant effect of mHtt on mitochondrial Ca^{2+} accumulation following exposure of neurons to excitotoxic glutamate (Chang *et al.*, 2006). Thus, the question

whether mHtt increases sensitivity of brain mitochondria and, particularly, neuronal mitochondria to Ca^{2+}-induced damage remains open.

Since the discovery of the Htt mutation, numerous studies have been conducted to elucidate the mHtt effect on mitochondrial Ca^{2+} handling. However, after much investigation, the question whether mHtt impairs mitochondrial functions remains controversial. Some investigators report mHtt-induced defects in mitochondrial Ca^{2+} uptake and increased susceptibility to PTP induction, whereas others do not find evidence for the deleterious alterations associated with mHtt. The reason for this is not clear, but it could be related to the use of different HD models and variations in methodological approaches.

Studies have demonstrated mHtt-induced defects in mitochondrial Ca^{2+} uptake (defects in mitochondrial Ca^{2+} handling) and reduction in Ca^{2+} uptake capacity by mitochondria isolated from cells and tissues expressing mHtt (Panov *et al.*, 2002). Mitochondria from lymphoblasts of patients with HD as well as brain nonsynaptic mitochondria from YAC72 mice had a diminished membrane potential and were depolarized at smaller Ca^{2+} loads compared with mitochondria from healthy YAC18 mice. These defects persisted even in the presence of inhibitors (Panov *et al.*, 2002). Based on the fact that ADP and CsA failed to eliminate the difference between mitochondria from mutant and WT animals, PTP involvement could be excluded. Intriguingly, the effect of mHtt on mitochondrial Ca^{2+} uptake capacity appeared to be elusive, and in the next study Panov et al. found that “the defect in Ca^{2+} handling in brain mitochondria was consistently observed only if brain mitochondria were isolated without BSA”

(Panov *et al.*, 2003). The authors proposed that BSA could replace mHtt in its binding sites on mitochondria, but did not provide experimental evidence supporting this hypothesis.

In addition to isolated mitochondria, neurons in culture were used to study detrimental effects of mHtt on Ca^{2+} signaling and mitochondrial Ca^{2+} handling. Fernandes et al. reported that Ca^{2+} influx into cells mediated by the NMDA-subtype of ionotropic glutamate receptors resulted in augmented mitochondrial depolarization in medium spiny neurons from YAC128 mice (Fernandes *et al.*, 2007). This effect was paralleled by reduced clearance of elevated cytosolic Ca^{2+} following NMDA withdrawal. Suppression of the PTP resulted in a decrease in cytosolic Ca^{2+} and diminished mitochondrial depolarization induced by NMDA in neurons from YAC128 mice, but not from WT mice. Based on these observations, the authors concluded that mitochondria in medium spiny neurons from YAC128 mice have increased susceptibility to PTP induction by Ca^{2+} (Fernandes *et al.*, 2007).

Despite reported defects in mitochondrial Ca^{2+} handling, some investigators did not find evidence for mHtt-induced mitochondrial Ca^{2+} handling deficiency and increased propensity to PTP induction in the presence of mHtt. A previous study by our laboratory did not find an increased susceptibility to Ca^{2+}-induced PTP induction in striatal nonsynaptic mitochondria from HD mice (Q50, Q92, Q111 and R6/2) compared with mitochondria from WT animals (Brustovetsky *et al.*, 2005). In these studies, our laboratory found increased resistance to Ca^{2+} in striatal mitochondria isolated from HD mice. In line with

these findings, Oliveira et al. demonstrated that nonsynaptic mitochondria from R6/2 and YAC128 mice had augmented Ca^{2+} uptake capacity compared with mitochondria from WT mice, whereas mitochondria from $Hdh^{150/+}$ and $Hdh^{150/150}$ mice had similar Ca^{2+} uptake capacity compared with mitochondria from WT animals (Oliveira *et al.*, 2007). The reason for the increased Ca^{2+} uptake capacity is not clear, but it may reflect compensatory adaptation to augmented Ca^{2+} influx via activated NMDA receptors (Bezprozvanny & Hayden, 2004). Both the previous findings by our laboratory (Brustovetsky *et al.*, 2005) and the study by Oliveira et al. (Oliveira *et al.*, 2007) suggested that the lack of mHtt-induced impairment of mitochondrial Ca^{2+} handling argues against facilitated PTP induction in the presence of mHtt, and consequently does not support involvement of the PTP in HD pathogenesis.

Furthermore, it was demonstrated that crossing R6/2 mice with cyclophilin D-knockout mice (cyclophilin D sensitizes the PTP to Ca^{2+} (Tanveer *et al.*, 1996; Basso *et al.*, 2005)) augmented neuronal mitochondrial Ca^{2+} uptake capacity without any improvement in either behavioral or neuropathological characteristics (Perry *et al.*, 2010). The authors reasoned that increased Ca^{2+} capacity of neuronal mitochondria is not advantageous for R6/2 mice. Altogether, these results cast doubt on the ability of mHtt to increase susceptibility to PTP induction and decrease mitochondrial Ca^{2+} uptake capacity as well as the role of mitochondrial Ca^{2+} handling defects in HD pathogenesis.

d. Plasmalemmal Sodium Calcium Exchangers

In neurons, the plasmalemmal Na^+/Ca^{2+} exchanger (NCX) has the highest transport capacity for Ca^{2+} extrusion and therefore plays a key role in the maintenance of Ca^{2+} homeostasis (Yu & Choi, 1997; Carafoli *et al.*, 2001; DiPolo & Beauge, 2006). There is also a mitochondrial Na^+/Ca^{2+} exchanger involved in the regulation of mitochondrial Ca^{2+} homeostasis and oxidative phosphorylation that will not be further discussed in this dissertation. There has been little research on the role of mitochondrial Na^+/Ca^{2+} exchanger in Ca^{2+} in HD, and future studies may help better understand both the mitochondrial Na^+/Ca^{2+} exchanger and Ca^{2+} regulation. All instances of the abbreviation NCX will be in reference to the plasmalemmal NCX. NCX is a nine transmembrane antiporter. This antiporter is driven by the electrochemical gradient of sodium to exchange one Ca^{2+} ion from the cytosol for three external Na^+ ions (Blaustein & Lederer, 1999; Blaustein *et al.*, 2002).

There are three major isoforms of NCX in the brain: NCX1, NCX2, and NCX3 (Sakaue *et al.*, 2000; Kiedrowski *et al.*, 2004). All three isoforms are functionally similar but have differing expression. All of the isoforms are expressed in both the striatum and cortex (Canitano *et al.*, 2002; Papa *et al.*, 2003). In cultured cortical neurons, NCX1 is a dominant isoform (Sakaue *et al.*, 2000; Kiedrowski *et al.*, 2004). NCX2 is predominantly expressed in glial cells (Thurneysen *et al.*, 2002a; Thurneysen *et al.*, 2002b), although other investigators have found minimal neuronal localization of NCX2 (Minelli *et al.*, 2007). While less expressed in neurons than NCX1, NCX3 was found to be

essential for the maintenance of Ca^{2+} homeostasis in ischemia (Jeffs *et al.*, 2007; Secondo *et al.*, 2007). Previous research suggests that NCX1 and NCX3 both may be involved in glutamate-induced DCD (Luo *et al.*, 2007).

NCX is an effective mechanism of Ca^{2+} removal, operating in the forward mode (or Ca^{2+} exit mode) in instances of large cytosolic Ca^{2+} increases because it has a low affinity for Ca^{2+}, suggesting that this mechanism is effective only at relatively high cytosolic Ca^{2+} concentrations. The high capacity and low affinity of NCX make it effective for removal of Ca^{2+} under conditions of elevated cytosolic Ca^{2+} concentration (Tymianski *et al.*, 1993b; Carafoli *et al.*, 2001). Correspondingly, NCX is the dominant mechanism of Ca^{2+} extrusion in instances of cytosolic Ca^{2+} concentrations greater than 500 nM (Blaustein & Lederer, 1999).

Normally, NCX operates in the forward mode (NCX_{for}) to extrude Ca^{2+} from the cytosol in exchange for external Na^{+} (Blaustein *et al.*, 2002). An ischemic episode leading to elevated glutamate in the extracellular milieu and activation of glutamate receptors can cause an increase in cytosolic Na^{+} and depolarization of the plasma membrane, resulting in NCX operation in the reverse mode (NCX_{rev}), or Ca^{2+} entry mode (Kiedrowski *et al.*, 1994; Brittain *et al.*, 2012b). In this case, NCX_{rev} brings Ca^{2+} into the cell in exchange for cytosolic Na^{+}. Consequently, instead of decreasing the concentration of cytosolic Ca^{2+}, NCX_{rev} increases it. Thus, NCX_{rev} is critical for Ca^{2+} dysregulation induced by prolonged exposure to glutamate. We and others have previously shown that both NCX_{rev} and NMDAR are required for DCD (Hoyt *et al.*, 1998; Kiedrowski,

1999; Brittain *et al.*, 2012b). NCX has not been previously studied in the context of HD.

i. Pharmacological Tools to Study NCX

Multiple inhibitors of NCX_{rev} have been developed. In this work we use MK801 (described previously), an NMDAR antagonist that shows potent inhibition of NCX_{rev} (Brittain *et al.*, 2012b). Ni^{2+} is another inhibitor of NCX_{rev} operation. Ni^{2+} competes with Ca^{2+} in every NCX isoform although with varying affinity among isoforms (Annunziato *et al.*, 2004).

In cultured neurons, the modulation of extracellular Na^+ concentrations can be utilized to regulate NCX activity. Replacement of Na^+ from the extracellular bath solution with equimolar N-methyl-D-glucamine (NMDG) can be used to prevent NCX operation in the forward mode. NMDG cannot be exchanged for Ca^{2+} by NCX, and therefore under these conditions NCX_{for} is inhibited (Annunziato *et al.*, 2004).

Additionally, replacing external Na^+ for NMDG can induce NCX reversal. Prior to Na^+/NMDG replacement, neurons have to be incubated with ouabain (1 mM), an inhibitor of Na^+/K^+-ATPase, to increase cytosolic Na^+ and thus facilitate NCX reversal. These manipulations set up conditions favorable to NCX operation in the reverse mode (Brittain *et al.*, 2012a).

C. Hypothesis and Specific Aims

The evidence presented in this introduction suggests that Ca^{2+} handing may be altered in HD contributing to neurodegeneration (Tang *et al.*, 2003; Bezprozvanny & Hayden, 2004). There is evidence for an increased activation of NMDAR in striatal neurons expressing mHtt, particularly NMDARs containing NR2B subunits (Chen *et al.*, 1999b) (Zeron *et al.*, 2002). Ca^{2+} influx through ion channels is counterbalanced by Ca^{2+} removal mechanisms such as mitochondria (Carafoli, 1988; Erecinska & Silver, 1996) and NCX operating in the forward mode (Yu & Choi, 1997; Carafoli *et al.*, 2001; DiPolo & Beauge, 2006). The ability of mitochondria to sequester Ca^{2+} from the cytosol in HD is currently not clear. Mitochondria have been shown to be dysfunctional in HD models by some research groups model (Panov *et al.*, 2002; Gellerich *et al.*, 2008), while others find no defect or even increased Ca^{2+}uptake capacity (Brustovetsky *et al.*, 2005; Oliveira *et al.*, 2007). NCX is a high-capacity mechanism important in the removal of Ca^{2+} but this mechanism has not been previously studied in HD models. I hypothesize that in neurons expressing mHtt, Ca^{2+} removal mechanisms compensate for increased NMDAR activation. This compensation could explain the late-onset of neurodegeneration and subsequent symptoms in HD.

The glutamate-induced Ca^{2+} dysregulation in neurons is mediated by both activation of NMDAR and reversal of NCX (Brittain *et al.*, 2012b). CRMP2, traditionally viewed as an axonal growth protein involved in axon/dendrite specification, has been shown to be involved in regulation of cytosolic Ca^{2+} in

neurons exposed to glutamate. Use of a 15 amino acid fragment of CRMP2 decreased surface expression of NMDAR in dendritic spines and antagonized glutamate-induced Ca^{2+} dysregulation (Brittain *et al.*, 2011a). The mechanism behind this modulation is not fully understood. I hypothesize that CRMP2 interacts with both NMDAR and NCX modulating their activity and that this mechanism might be involved in regulation of Ca^{2+} homeostasis in neurons expressing mHtt.

Specific Aim 1: Determine if mitochondrial Ca^{2+} uptake capacity is decreased in a mouse model of HD.

Specific Aim 2: Examine if NCX is altered in a mouse model of HD.

Specific Aim 3: Determine the mechanism by which CRMP2 modulates NMDAR and NCX_{rev} activities and whether this mechanism is involved in regulation of Ca^{2+} homeostasis in neurons expressing mHtt.

II. MATERIALS AND METHODS

A. Materials

Pyruvate, malate, succinate, glutamate, glycine, N-methyl-D-aspertate (NMDA), EGTA, ADP, gramicidin, oligomycin, rotenone, antimycin A, 2,4-dinitrophenol, N-methyl-D-glucamine (NMDG), tetrodotoxin, ouabain, and, carbonylcyanide-p-trifluoromethoxyphenylhydra-zone (FCCP) were purchased from Sigma (St. Louis, MO). Tetraphenylphosphonium chloride was from Fluka (Buchs, Switzerland). Fura-2AM, Fura-2FF-AM, Fluo-4FF-AM, and SBFI-AM were from Teflabs (Austin, TX). D-(-)-2-Amino-5-phosphonopentanoic acid (AP-5) was from Tocris (Ellisville, MO). Ionomycin was from LKT Laboratories (St. Paul, MN). MK801 ((5R,10S)-(+)-5-methyl-10,11-dihydro-5H-dibenzo[a,d]-cyclohepten-5-10-imine maleate) was purchased from Calbiochem (San Diego, CA). Bovine serum albumin (BSA), free from free fatty acids, was from MP Biomedicals (Irvine, CA). Anti-NCX1 and anti-NCX3 antibodies were kindly provided by Drs. Kenneth Philipson and Michela Ottolia (UCLA). Monoclonal anti-NR2B antibody was from BD Biosciences. Polyclonal anti-CRMP2 antibody was purchased from Sigma. TAT (YGRKKRRQRRR), tat-scramble (YGRKKRRQRRRWEAKEMLYFEALVIE, a random sequence with no homology to any known sequence), tat-CBD3 (YGRKKRRQRRRARSRLAELRGVPRGL), and tat-CBD3A6K (YGRKKRRQRRRARSRLKELRGVPRGL) were synthesized (>95% purity) by Genscript Inc. (Piscataway, NJ). All peptides were verified in house by mass spectrometry (Department of Chemistry, Indiana University School of Medicine).

B. Animals

All procedures with animals were performed in accordance with the Institutional Animal Care and Use Committee approved protocol. Transgenic YAC128, YAC18, and WT (FVB/NJ) mice were purchased from Jackson Laboratories (Bar Harbor, ME) and breeding colonies were established in the Laboratory Animal Resource Center at Indiana University School of Medicine, Indianapolis, IN. YAC128 mice express full-length human mHtt containing 128 glutamines in the polyglutamine stretch in addition to WT mouse Htt whereas YAC18 mice express full-length human Htt containing 18 glutamines (Slow *et al.*, 2003). Male YAC128 or YAC18 mice were bred with female FVB/NJ mice (background strain). All offspring were genotyped with a PCR assay on tail DNA. The mice were housed under standard conditions with free access to water and food. In our experiments, we used early symptomatic 2-month-old and mature 12-month-old YAC128 mice and their age-matched WT littermates (background: FVB/NJ) for isolated mitochondria. Postnatal day 1 (PN1) pups were used for primary cell culture because neurons from older animals do not survive well in culture.

C. Isolation and Purification of Brain Mitochondria

Brain mitochondria were isolated in mannitol-sucrose medium and purified on a discontinuous Percoll gradient as described previously (Brustovetsky *et al.*, 2002) and outlined in Figure 2. Two mouse brains per genotype were rapidly removed according to an IACUC-approved protocol and immediately put into ice-

cold isolation medium containing 225 mM mannitol, 75 mM sucrose, 0.1% bovine serum albumin (BSA, free fatty acid-free), 1 mM EGTA, and 10 mM HEPES, pH 7.4. The tissue was washed with the isolation medium, dissected and homogenized following brain tissue homogenization in 15 ml glass Dounce homogenizer (10 strokes with pestle A, 30 strokes with pestle B) on ice, homogenate was diluted with 30 ml of Isolation Buffer 1 (described below) and centrifuged for 10 minutes at 2,400 rpm in the Beckman Centrifuge Avanti J-26XP, rotor JA-25.50 (650×g for 10 min) (1st centrifugation). This and all other procedures and centrifugations were performed at 2-4ºC. Then, supernate was centrifuged for 10 minutes at 12,500 rpm (18,850×g for 10 min) in the Beckman Centrifuge Avanti J-26XP, rotor JA-25.50 (2nd centrifugation). Supernate was discarded and pellet was re-suspended in 35 ml of Isolation Buffer 2 (described below) and centrifuged for 10 minutes at 12,500 rpm (18,850×g for 10 min) Beckman Centrifuge Avanti J-26XP, rotor JA-25.50 (3rd centrifugation). Next, the pellet was re-suspended in 5 ml of Isolation Buffer 3 (described below). The suspension was layered onto the top of Percoll gradient (26%/40%) in Beckman Ultra-Clear centrifuge tubes and centrifuged for 28 minutes at 15,500 rpm (41,100×g for 28 min) in the Beckman Ultracentrifuge Optima L100K, bucket rotor SW41Ti (4th centrifugation). After the centrifugation, there were 5 layers (Figure 3): 1 – clear (top); 2 – thick white-yellowish, this layer contains synaptosomes; 3 – slightly cloudy thick layer; 4 – thin turbid layer, this layer contains nonsynaptic mitochondria; 5 – clear (bottom). At this stage, synaptosomes were collected for isolation of synaptic mitochondria. Nonsynaptic

mitochondria were resuspended in Isolation Buffer 3 and centrifuged for 20 minutes at 15,500 rpm (41,100×g for 20 min) in Beckman Ultracentrifuge Optima L100K, bucket rotor SW41Ti (5^{th} centrifugation). The pellet was re-suspend in Isolation Buffer 3 and centrifuged again for 20 minutes at 15,500 rpm (41,100×g for 20 min) in Beckman Ultracentrifuge Optima L100K, bucket rotor SW41Ti (6th centrifugation). The pellet was collected, re-suspended in 0.25-0.3 ml of Isolation Buffer 3, and stored on ice. This is a stock suspension of nonsynaptic mitochondria.

Synaptic mitochondria were isolated from synaptosomes by the nitrogen cavitation method using a nitrogen cell disruption bomb, model 4639 (Parr Instrument Company, Moline, IL, USA), cooled on ice as described by Brown et al. (Brown *et al.*, 2004) with some modifications. Briefly, synaptosomes were transferred into an ice-cold 10 ml glass beaker and placed into the nitrogen bomb on ice under 1,100 psi for 13 minutes. Then, the ruptured synaptosomes were layered on top of the discontinuous Percoll gradient (24%/40%) and centrifuged for 28 minutes at 15,500 rpm (41,100×g for 28 min) in Beckman Ultracentrifuge Optima L100K, bucket rotor SW41Ti, (4' centrifugation). The next two centrifugations (5th and 6th centrifugations) were performed together with nonsynaptic mitochondria. The pellet of synaptic mitochondria was resuspended in 0.1 ml of Isolation Buffer 3 and stored on ice. Isolation Buffer 1: 225 mM mannitol, 75 mM sucrose, 10 mM HEPES, pH 7.4 adjusted with KOH, 0.1% BSA, free from fatty acids, and 1 mM EGTA. Isolation Buffer 2: 225 mM mannitol, 75 mM sucrose, 10 mM HEPES, pH 7.4 adjusted with KOH, 0.1 mM EGTA. Isolation

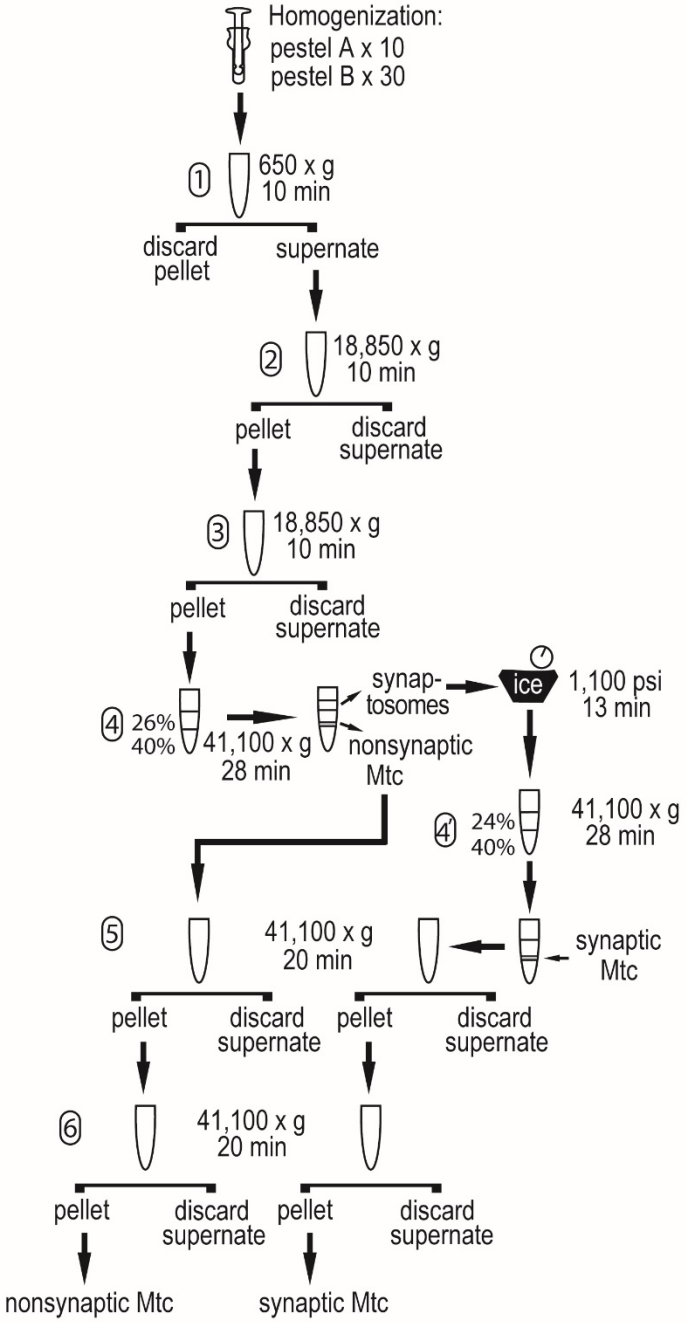

Figure 2. Scheme of Isolation and purification of brain nonsynaptic and synaptic mitochondria.

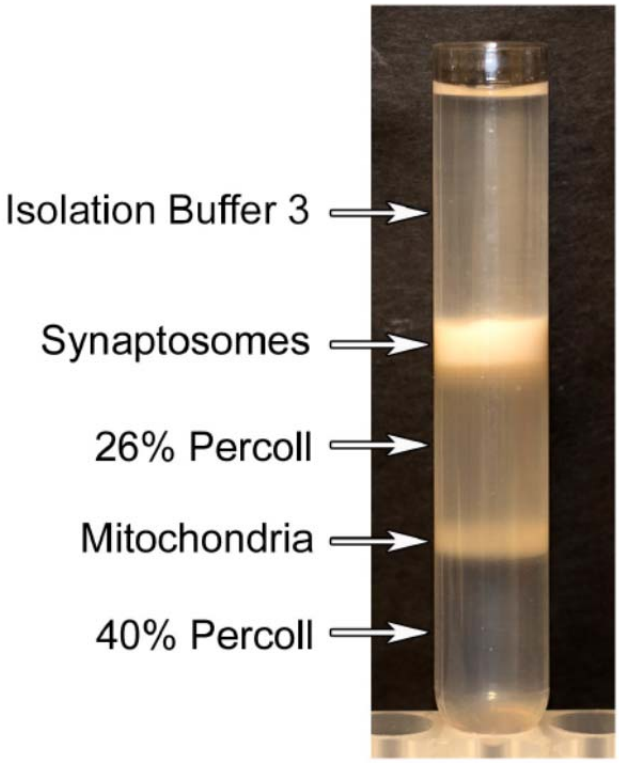

Figure 3. Separation of nonsynaptic mitochondria and synaptosomes on discontinuous Percoll gradient. Layers after centrifugation. 1 – clear (top); 2 – thick white-yellowish, (synaptosomes); 3 – slightly cloudy thick layer; 4 – thin turbid layer, (nonsynaptic mitochondria); 5 – clear (bottom).

Buffer 3: 395 mM sucrose, 0.1 mM EGTA, 10 mM HEPES, pH 7.4. Percoll Buffer: 320 mM sucrose, 1 mM EGTA, 10 mM HEPES, pH 7.4.

D. Western Blotting

Isolated mitochondria, cultured striatal neurons, cultured glia, or whole striata were pretreated with Protease Inhibitor Cocktail (Roche) and solubilized by incubation in NuPAGE LDS sample buffer (Invitrogen, Carlsbad, CA, USA) supplemented with a reducing agent at 70ºC for 15 minutes. Bis-Tris Mops gels (12%; Invitrogen) and Tris-Acetate gels (3-8%; Invitrogen) were used for electrophoresis (20µg protein per lane). After electrophoresis, proteins were transferred to Hybond-ECL nitrocellulose membrane (Amersham Biosciences). Blots were incubated for 1 hour at room temperature in blocking solution of 5% dry milk, phosphate-buffered saline, pH 7.2, and 0.15% Triton X-100. Then, blots were incubated with one of the following primary antibodies: mouse monoclonal anti-mHtt 1C2 (mAb1574, Millipore; 1:1000), mouse monoclonal anti-cyclophilin D (EMD, San Diego, CA; 1:1000), mouse monoclonal anti-MEK1/2 (Invitrogen; 1:1000), rabbit polyclonal anti-VDAC1 (Calbiochem; 1:1000). Blots were incubated with goat anti-mouse or goat anti-rabbit IgG (1:20000) coupled with horseradish peroxidase (Jackson ImmunoResearch Laboratories, West Grove, PA, USA) and developed with Supersignal West Pico chemiluminescent reagents (Pierce, Rockford, IL, USA). Molecular mass markers See Blue Plus 2 Standards (5µl) and HiMark Pre-stained High Molecular Weight Protein Standards (10µl) (Invitrogen) were used to determine molecular masses of the

bands. NIH ImageJ 1.48v software (http://rsb.info.nih.gov//ij) was used to quantify band densities

E. Mitochondrial Swelling and Membrane Potential

Mitochondrial swelling was evaluated at 37ºC and continuous stirring by following changes in light scattering of mitochondrial suspension at 525 nm with an incident beam under 180º in a 0.3 ml chamber. The incubation medium for light scattering measurements contained 215 mM mannitol, 70 mM sucrose, 0.5 mM $MgCl_2$, 3 mM KH_2PO_4, 10 mM HEPES, pH 7.4, 10μM EGTA, 3 mM succinate, 3 mM glutamate. A decrease in light scattering of mitochondrial suspension indicated mitochondrial swelling. Mitochondrial membrane potential was measured in a standard KCl-based incubation medium at 37ºC with a tetraphenylphosphonium (TPP^+) electrode by following TPP^+ distribution between the incubation medium and mitochondria (Kamo *et al.*, 1979). A decrease in external TPP^+ concentration corresponds to mitochondrial polarization, while an increase of TPP^+ in the incubation medium corresponds to depolarization.

F. Measurements of Mitochondrial Ca^{2+} Uptake.

Mitochondrial Ca^{2+} uptake was measured with a miniature Ca^{2+}-selective electrode in a 0.3 ml chamber at 37ºC under continuous stirring. A decrease in the external Ca^{2+} concentration indicated mitochondrial Ca^{2+} uptake. The standard incubation medium contained 125 mM KCl, 0.5 mM $MgCl_2$, 3 mM KH_2PO_4, 10 mM HEPES, pH 7.4, 10μM EGTA, and was supplemented either

with 3 mM pyruvate plus 1 mM malate or 3 mM succinate plus 3 mM glutamate. Here and in other experiments, succinate was used in combination with glutamate to prevent oxaloacetate inhibition of succinate dehydrogenase. Additionally, the incubation medium was supplemented with 0.1 mM ADP and 1μM oligomycin. Ca^{2+} was added to mitochondria as 10μM $CaCl_2$ pulses. In all experiments with isolated mitochondria, the concentration of mitochondrial protein in the chamber was 0.2 mg/ml. All data traces shown are representative of at least three separate experiments.

G. Mitochondrial ROS Production

ROS production by mitochondria was monitored at 37ºC in the standard KCl-based incubation medium with Amplex Red assay for H_2O_2 (Molecular Probes, Eugene, OR) using a Perkin-Elmer LS 55 luminescence spectrometer and excitation/emission wavelengths 550/590 nm.

H. Cell Culture

Striatal and cortical neuronal cultures were prepared from individual striata and cortices of postnatal day 1 YAC128 mice and their WT littermates as previously described (Dubinsky, 1993; Brittain *et al.*, 2012b), but without pooling cells from different animals together. The striata or cortices were removed, minced, and incubated for 20 minutes at 37°C in L-15 containing 3 mg/mL papain and 3 mg/mL bovine serum albumin (BSA). After gentle trituration in growth medium, the cell suspension was layered on L-44 containing 100 mg/ml BSA and

centrifuged at 500 rpm for 5 min. The pellet was resuspended in growth medium. Neurons were cultured in a 5% CO_2 atmosphere at 37°C in Neurobasal medium with B27 supplement (Life Technologies), and osmolality was adjusted to 280 mOsm. For fluorescence measurements, neurons were plated on glass-bottomed Petri dishes without pre-plated glia. For all platings, 35μg/ml uridine plus 15μg/ml 5-fluoro-2'-deoxyuridine were added 24 hours after plating to inhibit proliferation of non-neuronal cells.

Primary cultures of hippocampal neurons were prepared from postnatal day 1 rat pups according to institutional animal care and use committee-approved protocols and procedures. For fluorescence measurements, neurons were plated on glass bottom Petri dishes without preplated glia. Twenty-four hours after plating, 35 g/ml uridine plus 15 g/ml 5-fluoro-2-deoxyuridine were added to inhibit proliferation of non-neuronal cells. Cultures were maintained in a 5% CO_2 atmosphere at 37 °C in minimum essential medium supplemented with 10% NuSerum (BD Biosciences) and 27 mM glucose.

I. Immunocytochemistry

Cultured neurons were fixed with 4% paraformaldehyde for 15 minutes and then washed with PBS. Cells were incubated with a blocking solution containing 2.5% IgG- and protease free BSA (Jackson ImmunoResearch Laboratories, West Grove, PA), 2.5% goat serum, and 0.1% Triton X-100 in PBS for 1 hour at room temperature. Cells were incubated overnight at 4 °C with primary antibodies anti-MAP2 (neuronal marker, mouse monoclonal,1 : 500;

Millipore), anti-GFAP (astroglial marker, rabbit polyclonal, 1 : 1000; Millipore), anti-DARPP-32 (marker of medium spiny neurons, rabbit monoclonal, 1 : 200; Pierce), and anti-GABA (rabbit polyclonal, 1 : 20 000; Pierce). Nuclei were stained with 2-(4-amidinophenyl)-1H-indole-6-carboxamidine (DAPI) (nuclear marker; Invitrogen). Then, cells were incubated with secondary donkey anti-mouse antibody conjugated with AlexaFluor 488 and donkey anti-rabbit AlexaFluor 568 (1 : 1000; Invitrogen). Brightfield and fluorescence images were acquired using a Nikon Eclipse TE2000-U inverted microscope equipped with a Nikon CFI Super Fluoro 20 x 0.75 NA objective and CCD camera Cool $SNAP_{HQ}$ (Roper Scientific, Tucson, AZ, USA) controlled by MetaMorph 6.3 software (Molecular Devices, Downingtown, PA, USA).

In experiments including treatment, cells were treated for 10 minutes then fixed with 4% paraformaldehyde for 15 minutes and then washed with PBS. Cells were incubated with a blocking solution containing 2.5% IgG- and protease free BSA (Jackson ImmunoResearch Laboratories, West Grove, PA), 2.5% goat serum, and 0.1% Triton X-100 in PBS for 1 hour at room temperature. Cells were incubated overnight at 4 °C with primary rabbit polyclonal anti-NCX3 (NCX3 polyclonal antibody 95209, 1:500), mouse monoclonal anti-NR2B (1:500; BD Biosciences), or rabbit polyclonal anti-CRMP2 (1:500; Sigma). Then cells were incubated with a secondary donkey anti-rabbit antibody or goat anti-mouse antibody conjugated with AlexaFluor 488 for anti-NCX3 and anti-NR2B or AlexaFluor 568 for anti-CRMP2 (1:1000) (Invitrogen). Cells were incubated for 1 hour at room temperature. The images were taken using a laser, spinning-disk

confocal microscope based on a Nikon Eclipse TE2000-U equipped with a Yokogawa spinning disk confocal unit CSU-10, a back-thinned EM-CCD camera Andor iXonEM DU-897 (Andor Technology, South Windsor, CT), and a motorized flat top stage Prior H-117 (Prior Scientific, Rockland, MA). This setup was controlled by Andor iQ version 1.4 software (Andor Technology, South Windsor, CT). To visualize immunostaining, neurons were illuminated at 488 nm using an air-cooled krypton/argon laser T643-RYB-A02 (Melles Griot, Carlsbad, CA). Fluorescence was collected through a 505-nm dichroic mirror and a 535±25-nm emission filter using an objective Nikon CFI Plan Apo 100, 1.4 numerical aperture. The fluorescence intensity profiles were generated through randomly chosen cross-sections using AutoQuant software (MediaCybernetics, Silver Spring, MD).

J. Fluorescence Imaging of Cultured Neurons

In our experiments, cultured striatal or cortical neurons from mice cultured for 10-13 days *in vitro* (10-13 DIV) or hippocampal neurons from rats cultured for 12-14 DIV were used. For all experiments, at the time of the experiments neurons were rinsed twice with standard bath solution: 139 mM NaCl, 3 mM KCl, 0.8 mM $MgCl_2$, 1.8 mM $CaCl_2$, 10 mM NaHEPES, 5 mM glucose, 65 mM sucrose, as used previously in studies of DCD and excitotoxicity (Dubinsky *et al.*, 1995; Wang & Thayer, 1996; Brittain *et al.*, 2012b). The pH was adjusted to 7.36-7.38 using 1 M NaOH. Osmolarity of the bath solution was measured with an osmometer (Osmette II, Precision Systems Inc., Natick, MA). The osmolarity was

280 mOsm for striatal and cortical neurons and 340 mOsm for hippocampal neurons. Fluorescence imaging was performed with a Nikon Eclipse TE2000-U inverted microscope used a Nikon objective Plan Fluor 20X 0.45 NA and a back-thinned EM-CCD Hamamatsu C9100-12 camera (Hamamatsu Photonic Systems, Bridgewater, NJ) controlled by Simple PCI software 6.1 (Compix Inc., Sewickley, PA) or Nikon Eclipse TE2000-U inverted microscope using Nikon objective Super Fluor 20, 0.75 numerical aperture and a Photometrics Cool SNAPHQ camera (Roper Scientific, Tucson, AZ) controlled by MetaFluor software version 6.3 (Molecular Devices, Downingtown, PA). The excitation light was delivered by a Lambda-LS system (Sutter Instruments, Novato, CA). The excitation light was delivered by a Lambda-LS system (Sutter Instruments, Novato, CA) and a Lambda 10-2 optical filter changer (Sutter Instruments, Novato, CA) controlled the excitation filters. To minimize photobleaching and phototoxicity, the images were taken every 15 seconds.

a. Measurements of Cytosolic Calcium Concentration

To follow changes in cytosolic Ca^{2+}, neurons were loaded with fluorescent dye at 37°C in the presence of 0.015% Pluronic F-127. The changes in $[Ca^{2+}]_c$ were monitored by following a ratio of F_{340}/F_{380} for ratiometric dyes, or a single wavelength for non-ratiometric dyes. After at least 1.5 minutes of fluorescence recording in the standard bath solution, various treatments were applied to the neurons. At the end of the experiment quantification of maximum signals was carried out (described in K, below).

i. Fura-2-AM

Fura-2-AM is a high-affinity, ratiometric, calcium-sensitive fluorescent dye with dissociation constant (K_d) near the typical basal calcium levels in mammalian cells (~100 nM) (Grynkiewicz *et al.*, 1985). The fluorescence measurements from a ratiometric dye are based on the use of a ratio between two fluorescence emission signals recorded at two different excitation wavelengths. This method allows removal of artifacts due to bleaching, changes in focus, or other disturbances unrelated to the experiment. Additionally, the ratio calculation amplifies the changes in signal intensity. The K_d for Ca^{2+} of Fura-2 is ~224 nM.

Fura-2-AM is a cell-permeant acetoxymethyl (AM) ester. Once Fura-2-AM crosses the plasma membrane, nonspecific esterases hydrolyze the acetoxymethyl ester, liberating the Ca^{2+}-sensitive indicator and significantly reducing permeability of Fura-2. This traps Fura-2 inside the cells, resulting in an extremely low leakage rate and stabilizes the final intracellular indicator concentration. For calcium imaging with Fura-2, neurons are loaded with 2.6μM Fura-2AM at 37°C for 60 minutes. The excitation filters, 340±5 and 380±7 nm, were controlled by a Lambda 10-2 optical filter changer (Sutter Instruments, Novato, CA). Fluorescence was recorded from individual neurons through a 505 nm dichroic mirror at 535±25 nm. The changes in $[Ca^{2+}]_c$ were monitored by following Fura-2 F_{340}/F_{380} ratio, after the background was subtracted from fluorescence signals.

For all calcium sensitive dyes, the maximum and minimum signals are needed to convert fluorescence signal into calcium concentration. To determine the maximum signal neurons are exposure to 5μM ionomycin plus 5μM FCCP. Following the collection of the maximum signal, the minimum signal was collected by exposing the neurons to a calcium free bath solution containing 10 mM Mn^{2+} plus 10μM digitonin.

ii. Fura-2FF-AM

Fura-2FF-AM is a low-affinity, ratiometric, calcium-sensitive fluorescent dye. This dye is appropriate to assess changes in cytosolic calcium during excitotoxic events. Fura-2FF-AM is a derivative of Fura-2 with a K_d of 5.5μM (dynamic range ~0.5 to 50 μM) (Miyawaki *et al.*, 1997). Because Fura-2FF-AM is a derivative of Fura-2, it has similar properties and has excitation wavelengths that are the same as Fura-2, 340±5 and 380±7 nm. Fluorescence was recorded from individual neurons through a 505 nm dichroic mirror at 535±25 nm. The changes in $[Ca^{2+}]_c$ were monitored by following Fura-2FF F_{340}/F_{380} ratio, after the background was subtracted from the fluorescence signals. For calcium imaging with Fura-2FF, neurons are loaded with 2.6μM Fura-2FF-AM at 37°C for 60 minutes.

iii. Fluo-4FF-AM

Fluo-4FF-AM is a nonratiometric, low-affinity, calcium-sensitive indicator with a K_d of 9.7μM (Grynkiewicz *et al.*, 1985). This allows the assessment of

changes in cytosolic Ca^{2+} from 1 to 100 μM, a similar range to Fura-2FF. Fluo-4FF has a single excitation wavelength maximum at 494 nm with emission wavelength maximum at 518 nm. The advantage of using Fluo-4FF instead of Fura-2FF is that it can be co-loaded with a ratiometric dye sensitive to another ion, Na^+, for example. In experiments where Fluo-4FF is used, neurons were loaded with 2.5μM Fluo-4FF-AM for 30 minutes at 37ºC. A single excitation wavelength at 480±20 nm was used, and fluorescence was recorded from individual neurons through a 505 nm dichroic mirror at 535±25 nm. The changes in fluorescence are expressed as F/F_0, after the background was subtracted from the fluorescence signals. By calculating F/F_0 rather than absolute fluorescence, correcting the arbitrary signal variations is possible. Similar to the other calcium indicators, Fluo-4FF-AM is a cell-permeant acetoxymethyl ester, which becomes trapped inside the cell following ester hydroxylation.

b. Measurements of Cytosolic Sodium Concentration

i. SBFI-AM

SBFI-AM is a ratiometric, sodium-sensitive fluorescent indicator. It is derived from benzofuran isophthalate with an acetoxymethyl ester to increase cell permeability. The selectivity for sodium over potassium for SBFI is relatively high with roughly an 18-fold preference for Na^+. However, the presence of K^+ has an effect on the affinity of SBFI for Na^+. The K_d for SBFI in regard to Na^+ in the absence of K^+ is 3.8 mM, but the K_d for Na^+ in the presence of physiological concentrations of potassium is 11.3 mM. All of the experiments in this thesis

contain K^+, thus the K_d that has been used is 11.3 mM (Diarra *et al.*, 2001). In experiments using SBFI, neurons were loaded with 5.3μM of the Na^+-sensitive fluorescent dye SBFI-AM at 37ºC for 60 minutes. The excitation filters 340±5 and 380±7 nm were used. Fluorescence was recorded through a 505 nm dichroic mirror at 535±25 nm. The changes in $[Na^+]_c$ were calculated as F_{340}/F_{380} after subtracting the background from both channels. SBFI is a ratiometric dye, thus the benefits of the ratio calculation concerning data correction and signal amplification apply to this indicator.

The maximum and minimum signals are needed to convert fluorescence signal into sodium concentration. To determine the minimum and maximum signal neurons are exposure to 5μM gramicidin with known concentrations (0-130 mM) of extracellular Na^+ in the bath solution.

K. Calcium and Sodium Fluorescence Signal Converted to Concentration

Cytosolic Ca^{2+} concentrations ($[Ca^{2+}]_c$) and cytosolic Na^+ concentrations ($[Na^+]_c$) were calculated using the Grynkiewicz method and a modification of the method for Na^+ (Grynkiewicz *et al.*, 1985; Diarra *et al.*, 2001) from the ratio following the background subtraction. To perform this calculation, following the experiment calibration points must have been made. These points consist of the maximum and minimum signal. If these calibration points have been collected, the fluorescence signal can be converted to an approximate ion concentration using the K_d from the specific dye that was used. This conversion is done using this equation: $[ion] = K_d \times ((F - F_{min}) / (F_{max} - F))$ (Grynkiewicz *et al.*, 1985).

This conversion calculation must be taken as an approximation of the cytosolic ion concentration (Stanika *et al.*, 2009). Two assumptions exist concerning this calculation method. The first is that K_d used for the indicator acts the same inside the cellular environment as it does in an experiment, calculating it in a non-cellular environment. The cellular environment is complex, and slight variations in the actual K_d could greatly affect the actual concentration in comparison to the calculated concentration. The second assumption is that minimum and maximum calibration points are accurate. The minimal calibration point is where the ion of interest is completely prevented from interacting with the indicators, however, this results in an incomplete quenching of the signal, and the process of saturating the signal for max fluorescence is also imperfect (Stanika *et al.*, 2009). When using indicators with high K_d values, the amount of ions that is needed to completely saturate the signal sometimes exceeds the content in the bath solution. This makes it difficult to produce a maximum fluorescence signal.

L. Co-immunoprecipitation

Co-immunoprecipitation (co-IP) experiments were performed on freshly prepared cell lysates from rat hippocampal neuronal cultures at 12–14 days in vitro. Lysates were clarified to remove any additional precipitate by incubating with Protein A-agarose beads for experiments with rabbit primary antibodies or Protein G-agarose beads for experiments with mouse primary antibodies (Santa Cruz Biotechnology, Inc.) for 2 hours at 4 °C. Then the lysates were incubated overnight with primary anti-NCX1, anti-NCX3, or anti-CRMP2 antibodies under

gentle agitation at 4 °C followed by incubation with Protein A-agarose beads or Protein G-agarose beads for 2 hours at 4 °C. The immunocaptured complexes were then washed three times with lysis buffer before being heated at 70 °C in equal volumes of SDS loading dye (Invitrogen). Samples were then processed by immunoblotting as described previously (5, 16). Blots were probed with anti-NCX1 (NCX1 mAb R3F1), anti-NCX3 (NCX3 polyclonal antibody 95209), anti-NR2B (BD Biosciences), or anti-CRMP2 (Sigma-Aldrich) (all 1:1000). All blots are representative of at least three experiments.

M. Patch-Clamp Electrophysiology

Whole-cell voltage clamp recordings were performed as described previously (Brittain *et al.*, 2012b). Briefly, patch clamp experiments were conducted at room temperature using a HEKA EPC-10 amplifier. Data were collected using the Pulse program (HEKA Elektronik, Lambrecht/Pfalz, Germany). The electrode solution used for recording voltage ramp currents mediated by NCX_{rev} contained 20 mM KCl, 100 mM potassium aspartate, 20 mM tetraethylammonium-Cl, 10 mM HEPES, 0.01 mM K-EGTA, 4.5 mM $MgCl_2$, and 4 mM Na-ATP, pH 7.3, adjusted with KOH (Smith *et al.*, 2006). The external solution used for recording currents contained 129 mM NaCl, 10 mM CsCl (to block K^+ channels), 3 mM KCl, 0.8 mM $MgCl_2$, 1.8 mM $CaCl_2$, 5mM glucose, 10 mM NaHEPES, pH 7.2, 65 mM sucrose, 10 μM nifedipine (to block voltage-gated Ca^{2+} channels), 20 μM ouabain (to inhibit Na^+/K^+-ATPase), and 1 μM tetrodotoxin (to block Na^+ channels). In our experiments, the first voltage ramp generated ion

current that was used as an internal control. Ni^{2+} (5 mM), tat-CBD3 (10 μM), or CBD3 without tat (10 μM) was applied to neurons 5 minutes before the second voltage ramp.

N. Transfection

To down-regulate CRMP2, hippocampal neurons in culture were transfected in suspension during plating using an electroporator BTX 630 ECM (Harvard Apparatus, Holliston, MA) with a plasmid encoding GFP (green fluorescent protein) (4 μg/100μl of cell suspension, $5x10^6$ cells; Clontech) and siRNA (250 nM; Sigma) against CRMP2. This procedure usually provided 10-15% transfection efficacy, depending on plasmid quality, compared to <1% efficacy with commercial cationic lipid liposomes applied to primary neuronal cultures.

O. Statistics

Data are shown as mean ± standard error of mean (SEM) of at least three independent experiments. Statistical analysis of the experimental results consisted of unpaired *t*-test or one-way ANOVA followed by Bonferroni's *post hoc* test (GraphPad Prism® 4.0, GraphPad Software Inc., SanDiego, CA, USA). Every experiment was performed using at least three different preparations of isolated mitochondria or three separate neuronal-glial platings.

III. RESULTS

A. Mitochondrial Ca^{2+} uptake capacity in a mouse model of HD

A major hypothesis in HD pathology is that mHtt leads to abnormalities in Ca^{2+} signaling (Tang *et al.*, 2003; Bezprozvanny & Hayden, 2004). Defects in mitochondrial Ca^{2+} handling have been proposed as a cause of these abnormalities (Panov *et al.*, 2002; Gellerich *et al.*, 2008). Previous studies have shown defects as well as no effect in mitochondrial Ca^{2+} handling (Brustovetsky *et al.*, 2005; Oliveira *et al.*, 2007). The question of whether mHtt increases sensitivity of brain mitochondria and, particularly, neuronal mitochondria to Ca^{2+}-induced damage remains open.

a. Mutant Htt associates with mitochondria

In our studies, we used both synaptic and non-synaptic mitochondria isolated from the YAC128 mouse model of HD and their WT littermates. Synaptic mitochondria are neuronal, whereas the non-synaptic fraction contains mitochondria from astrocytes as well. Following isolation and discontinuous Percoll-gradient purification, both synaptic and non-synaptic mitochondria from YAC128 mice were tested for purity. The purity of isolated mitochondria was assessed by western blotting with antibodies against calnexin (an endoplasmic reticulum marker), MEK1/2 (a cytosolic marker), and COX IV (a mitochondrial marker). The purity control data are shown in Fig. 4(a). These data show the lack of endoplasmic reticulum and cytosolic contaminations in synaptic and non-synaptic mitochondria isolated and purified from WT (FVB/NJ) and YAC128

mice. Since mHtt is predominantly localized in the cytosol, this data confirms that if mHtt is detected in mitochondrial fractions, it is not because of cytosolic contamination.

We then asked if mHtt associates with mitochondria. To assess this, we used Western blotting to probe for mHtt following isolation. Both synaptic and nonsynaptic mitochondria from YAC128 mice retained attached mHtt that could not be washed out after 30 minutes of incubation at 37ºC in the standard KCl-based incubation medium with or without 0.1% BSA (Fig. 4). BSA was previously hypothesized to displace mHtt from binding to mitochondria (Panov *et al.*, 2003). We next asked if mHtt associates with the outside of mitochondria or if mHtt is inserted into the mitochondrial membrane. We tested this using alkali treatment for 30 minutes at pH 13. This method is used to remove peripheral proteins from membranes (Griparic & van der Bliek, 2005). After this treatment, the mHtt level was decreased below the detection limit of Western blotting (Fig. 4). These data suggest that mHtt is associated with the mitochondria but is not inserted into the mitochondrial membrane, consistent with previous findings in a study using clonal striatal ST*Hdh*Q^{111} cells (Choo *et al.*, 2004).

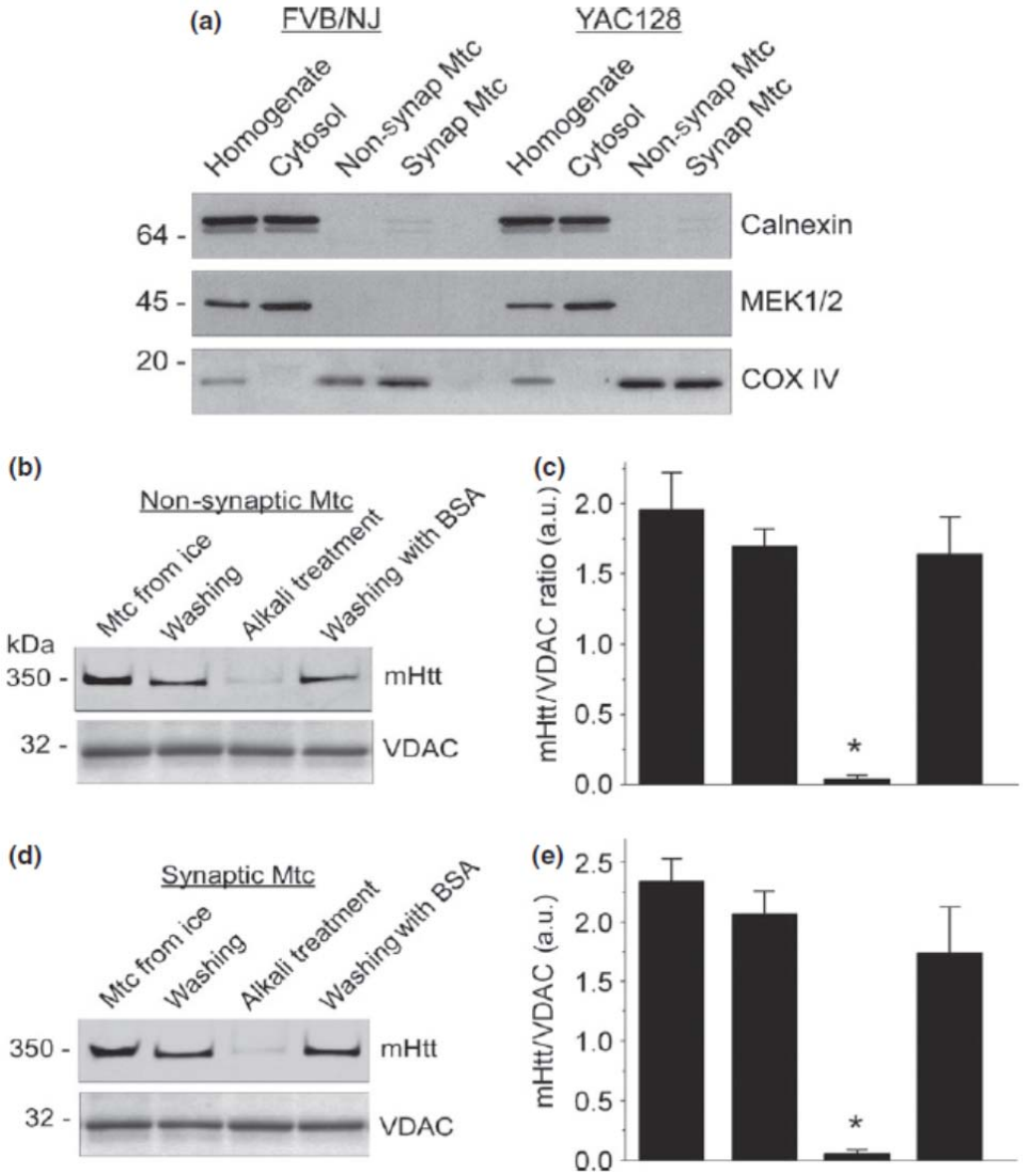
(a)
FVB/NJ
YAC128
Homogenate
Cytosol
Non-synap Mtc
Synap Mtc
Homogenate
Cytosol
Non-synap Mtc
Synap Mtc
64 -
Calnexin
45 -
MEK1/2
20 -
COX IV
(b)
Non-synaptic Mtc
Mtc from ice
Washing
Alkali treatment
Washing with BSA
kDa
350 -
mHtt
32 -
VDAC
(c)
mHtt/VDAC ratio (a.u.)
2.0
1.5
1.0
0.5
0.0
*
(d)
Synaptic Mtc
Mtc from ice
Washing
Alkali treatment
Washing with BSA
350 -
mHtt
32 -
VDAC
(e)
mHtt/VDAC (a.u.)
2.5
2.0
1.5
1.0
0.5
0.0
*

Figure 4.

Figure 4. Detection of mutant human huntingtin (mHtt) in brain nonsynaptic and synaptic mitochondria isolated from YAC128 mice. Purity of synaptic and non-synaptic mitochondria isolated from YAC128 and WT (FVB/NJ) mice (a). Detection of human mutant huntingtin (mHtt) in brain non-synaptic (a) and synaptic (b) mitochondria isolated from YAC128 mice (b–e). In (a), homogenates, cytosolic and mitochondrial fractions were analyzed using western blotting with antibodies against calnexin (ER marker), MEK1/2 (cytosolic marker), and COXIV (mitochondrial marker). Fractions were solubilized and proteins were resolved by sodium dodecyl sulfate–polyacrylamide gel electrophoresis (SDS–PAGE) using 4–12% Bis-Tris gels. In (b and d), mitochondria (Mtc) were analyzed immediately after isolation (Mtc from ice), after 30 minutes of incubation in the standard incubation medium supplemented with 3 mM succinate and 3 mM glutamate without (washing) and with 0.1% bovine serum albumin (BSA), free from fatty acids, (washing with BSA), and after 30 minutes of incubation at pH 13 (alkali treatment). Mitochondrial porin (voltage-dependent anion channel, VDAC) was used as a loading control. In (c and e), the western blotting data were quantified using NIH ImageJ software and presented as a mHtt/VDAC ratio. Data are mean ± SEM, *$p < 0.01$ compared with mitochondria from ice and after washing, $n = 7$.

b. Mutant Htt does not increase propensity to PTP in synaptic mitochondria

An increased propensity to PTP induction in mitochondria exposed to mHtt has been previously reported (Choo *et al.*, 2004; Fernandes *et al.*, 2007; Lim *et al.*, 2008; Quintanilla *et al.*, 2013b). However, in previous studies in our laboratory we did not find evidence for increased susceptibility to PTP induction in striatal and cortical mitochondria from HD mice compared with mitochondria from WT mice (Brustovetsky *et al.*, 2005). In this earlier study, we investigated PTP induction in nonsynaptic mitochondria. In the present study, we asked if PTP susceptibility was altered in synaptic (neuronal) mitochondria from YAC128 (Fig. 5 B,D,F) mice compared with synaptic mitochondria from WT mice (Fig. 5 A,C,E). This has not been previously investigated in synaptic mitochondria. Mitochondrial swelling and depolarization are the major manifestations of PTP induction (Bernardi, 1999). Consequently, we investigated an induction of the PTP by simultaneously monitoring a decrease in light scattering of mitochondrial suspension, indicative of swelling of the organelles, and a release of TPP^+ from mitochondria, indicative of mitochondrial depolarization. Ca^{2+}, in a concentration-dependent manner, induced swelling and depolarization of synaptic mitochondria (Fig. 5). To quantify swelling of mitochondria, data were calculated as a percentage of maximal swelling. Both mitochondrial swelling and depolarization in response to Ca^{2+} were comparable in mitochondria isolated from YAC128 and WT mice (Fig. 5G). These data suggest that synaptic mitochondria from YAC128 mice are not more susceptible to PTP than synaptic mitochondria from WT mice.

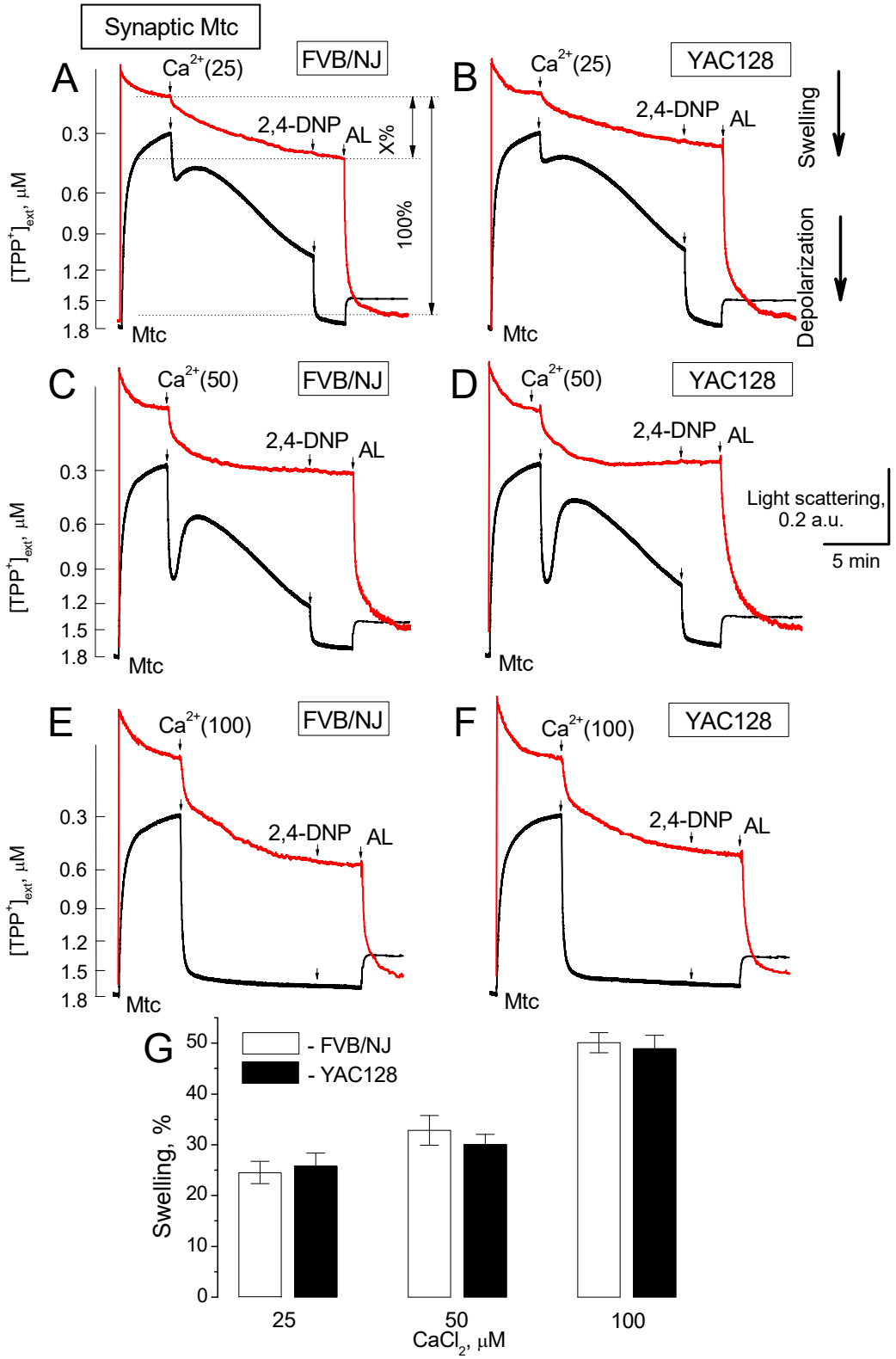
Synaptic Mtc
A
FVB/NJ
Ca2+(25)
2,4-DNP
AL
X%
100%
Mtc
B
YAC128
Ca2+(25)
2,4-DNP
AL
Swelling
Depolarization
Mtc
C
FVB/NJ
Ca2+(50)
2,4-DNP
AL
Mtc
D
YAC128
Ca2+(50)
2,4-DNP
AL
Light scattering,
0.2 a.u.
5 min
Mtc
E
FVB/NJ
Ca2+(100)
2,4-DNP
AL
Mtc
F
YAC128
Ca2+(100)
2,4-DNP
AL
Mtc
[TPP+]ext, μM
0.3
0.6
0.9
1.2
1.5
1.8
G
- FVB/NJ
- YAC128
Swelling, %
0
10
20
30
40
50
25
50
100
CaCl2, μM

Figure 5.

Figure 5. Ca^{2+}-induced mitochondrial swelling and depolarization in synaptic mitochondria from WT (FVB/NJ) and YAC128 mice. Mitochondrial swelling was evaluated in mitochondria from WT (FVB/NJ) (A, C, E) and YAC128 (B, D, F) mice, by following a decline in light scattering of mitochondrial suspension (red traces). A decrease in light scattering indicates mitochondrial swelling. Changes in mitochondrial membrane potential were evaluated following distribution of tetraphenylphosphonium (TPP^+) between incubation medium and mitochondrial matrix (black traces). The decrease in TPP^+ concentration in the incubation medium ($[TPP^+]_{ext}$) indicates TPP^+ accumulation in mitochondria and high membrane potential. The release of TPP^+ from mitochondria indicates a decrease in membrane potential. Mitochondrial swelling and membrane potential were evaluated simultaneously at 37ºC. Where indicated 25, 50, or 100μM Ca^{2+} was applied to mitochondria (Mtc). At the end of the experiments, 60μM 2,4-dinitrophenol (2,4-DNP) was applied to completely depolarize mitochondria and, then, 30μg/ml alamethicin (AL) was added to induce maximal mitochondrial swelling, taken as 100%. The amount of Ca^{2+}-induced swelling was determined as percentage of maximal swelling (shown in **A** as X%). In **G**, percentage of Ca^{2+}-induced mitochondrial swelling. Data are mean±SEM, N=6.

c. Mitochondria from YAC128 mice have increased Ca^{2+} uptake capacity compared with mitochondria from YAC18 and WT mice

Next, we asked if mHtt altered Ca^{2+} uptake capacity of mitochondria isolated from YAC128 mice. In these experiments we assessed Ca^{2+} uptake capacity in mitochondria from YAC128, YAC18 (a control YAC strain, expressing non-pathological full-length human Htt), and WT FVB/NJ mice. We applied pulses of Ca^{2+} until mitochondria fail to take up additional Ca^{2+}. In our hands, Ca^{2+} uptake capacity of nonsynaptic mitochondria from 2- and 12-month-old YAC128 mice was slightly but statistically significantly increased compared with mitochondria from YAC18 and WT mice (Fig. 6). This result is consistent with data previously reported by Oliveira et al. (Oliveira *et al.*, 2007). The slight increase in Ca^{2+} uptake capacity was observed with both Complex I substrates pyruvate/malate (Fig.6B) and Complex II substrate succinate (Fig. 6C) used in combination with glutamate to prevent accumulation of oxaloacetate and inhibition of succinate dehydrogenase (Brustovetsky & Dubinsky, 2000).

Synaptic mitochondria from 2-month-old YAC128 mice also had a slight but statistically significant increase in Ca^{2+} uptake capacity compared with mitochondria from age-matched YAC18 (control) and WT mice regardless of oxidative substrates (Fig. 7A, D). BSA (Fig. 7B) considerably increased Ca^{2+} uptake capacity in synaptic mitochondria from all types of animals. Interestingly, Ca^{2+} uptake capacity of synaptic mitochondria from 12-month-old YAC128 mice was noticeably increased compared with mitochondria from 2-month-old YAC128 mice and age-matched 12-month-old YAC18 and WT mice (Fig. 7C).

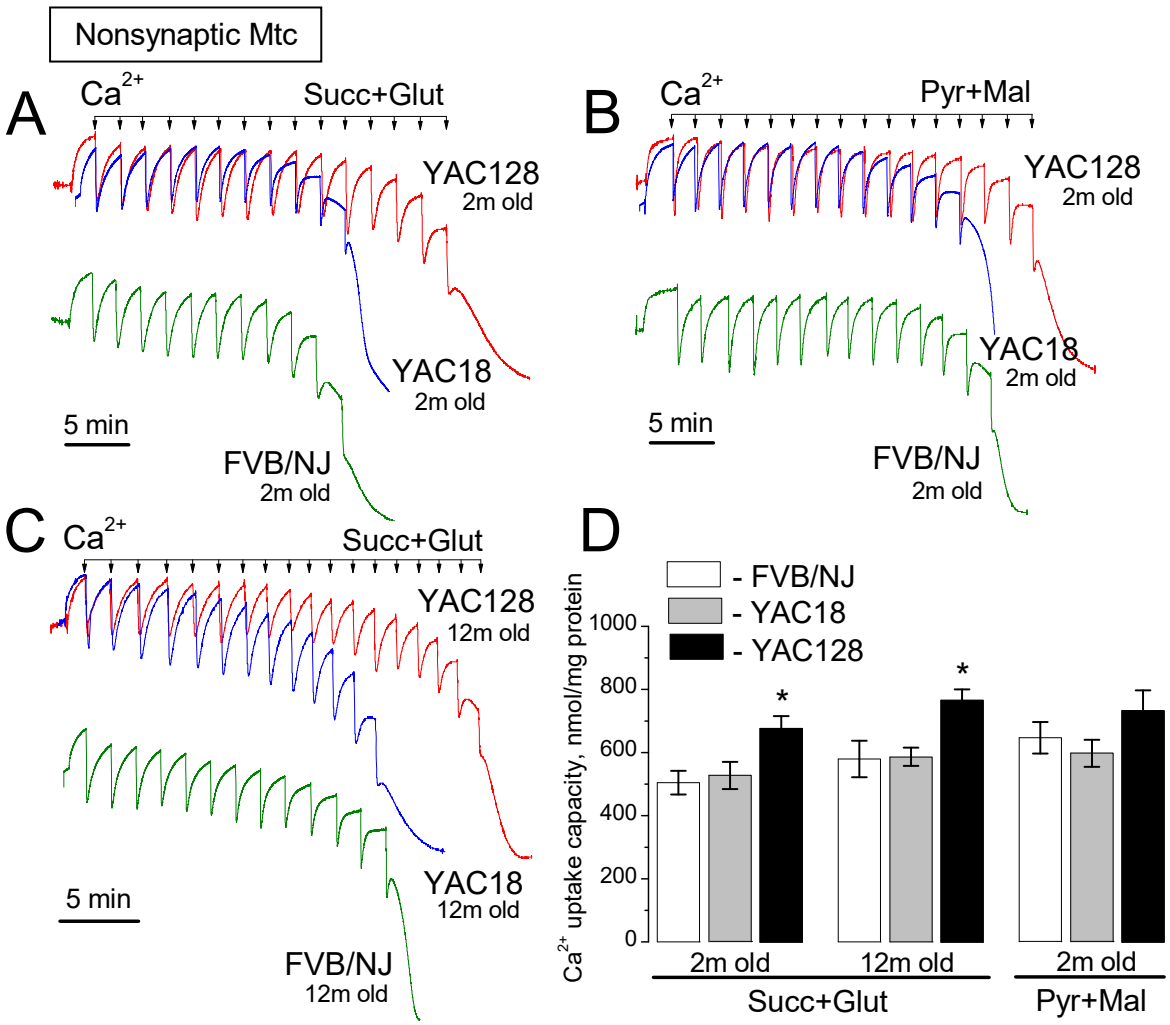

Figure 6. Ca^{2+} uptake capacity of brain nonsynaptic mitochondria isolated from YAC128, YAC18, and WT (FVB/NJ) mice. Mitochondria were incubated at 37ºC in the standard incubation medium supplemented either with 3 mM succinate plus 3 mM glutamate or with 3 mM pyruvate plus 1 mM malate as indicated in the Figure. In all Ca^{2+} uptake experiments, 100μM ADP and 1μM oligomycin were present in the incubation medium. In A and B, mitochondria were isolated from 2-month-old mice. In C, mitochondria were isolated from 12-month-old mice. In A-C, where indicated 10μM Ca^{2+} pulses were applied to mitochondria until mitochondria fail to take Ca^{2+} up. In D, statistical analysis of Ca^{2+} uptake capacity of mitochondria from YAC128, YAC18, and WT (FVB/NJ) mice. Data are mean±SEM, *p<0.05, N=5.

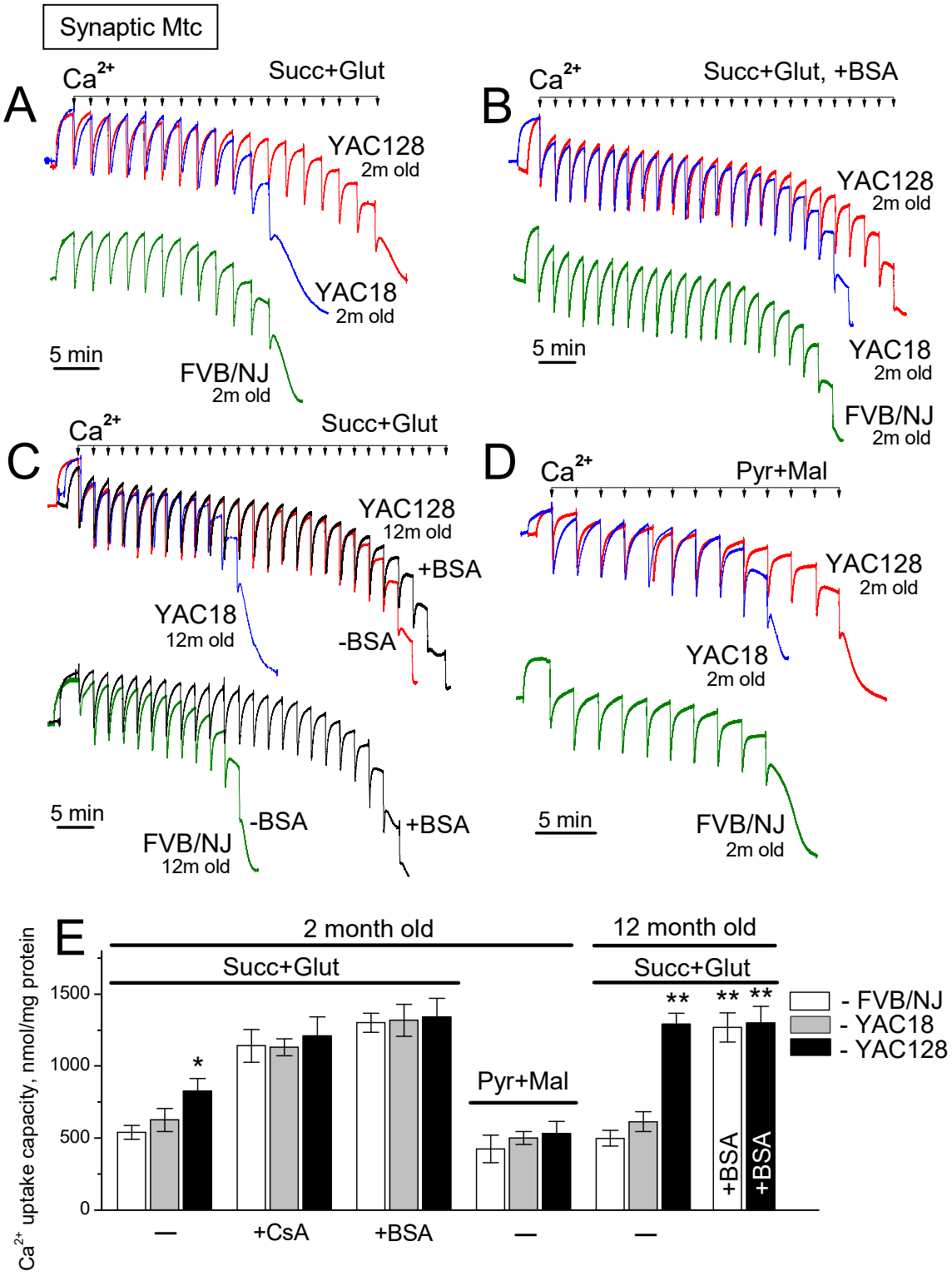
Synaptic Mtc
A
Ca2+
Succ+Glut
YAC128
2m old
YAC18
2m old
5 min
FVB/NJ
2m old
B
Ca2+
Succ+Glut, +BSA
YAC128
2m old
5 min
YAC18
2m old
FVB/NJ
2m old
C
Ca2+
Succ+Glut
YAC128
12m old
+BSA
YAC18
12m old
-BSA
5 min
-BSA
+BSA
FVB/NJ
12m old
D
Ca2+
Pyr+Mal
YAC128
2m old
YAC18
2m old
5 min
FVB/NJ
2m old
E
2 month old
12 month old
Succ+Glut
Succ+Glut
Pyr+Mal
Ca2+ uptake capacity, nmol/mg protein
1500
1000
500
0
*
**
**
**
+BSA
+BSA
—
+CsA
+BSA
—
—
- FVB/NJ
- YAC18
- YAC128

Figure 7.

Figure 7. Ca^{2+} uptake capacity of brain synaptic mitochondria isolated from YAC128, YAC18, and WT (FVB/NJ) mice. Ca^{2+} uptake capacity of brain synaptic mitochondria isolated from YAC128, YAC18, and WT (FVB/NJ) mice. Mitochondria were incubated at 37°C in the standard incubation medium supplemented either with 3 mM succinate plus 3 mM glutamate or with 3 mM pyruvate plus 1 mM malate as indicated in the Figure. In all Ca^{2+} uptake experiments, 100 μM ADP and 1 μM oligomycin were present in the incubation medium. In **B**, incubation medium was additionally supplemented with 0.1% bovine serum albumin (BSA) (free from fatty acids). In (a, b, and d), mitochondria were isolated from 2-month-old mice. In **C**, mitochondria were isolated from 12-month-old mice. In **A-D**, where indicated 10 μM Ca^{2+} pulses were applied to mitochondria until mitochondria fail to uptake additional Ca2+. In **E**, statistical analysis of Ca^{2+} uptake capacity of mitochondria from YAC128, YAC18, and wildtype FVB/NJ mice. Data are mean ±SEM, *$p < 0.05$ comparing with FVB/NJ and YAC18 mitochondria; **$p < 0.01$ compared with mitochondria from 12-month-old FVB/NJ and YAC18 mice, $n = 9$.

These experiments also showed that Ca^{2+} uptake capacity of mitochondria from YAC18 mice was indistinguishable from Ca^{2+} capacity of mitochondria derived from WT mice. Therefore, in the following experiments we used only mitochondria from YAC128 and WT mice.

d. Cyclophilin D expression and ROS levels are not altered by mHtt

Previously, it was reported that the level of cyclophilin D (CyD), a key regulatory component of the PTP that sensitizes it to Ca^{2+} (Baines *et al.*, 2005; Schinzel *et al.*, 2005), was reduced in mitochondria from older animals (Eliseev *et al.*, 2007). Therefore, we asked whether the increased Ca^{2+} uptake capacity in mitochondria from YAC128 mice, particularly, in synaptic mitochondria from 12-month-old transgenic animals, correlates with a decrease in CyD. Our experiments revealed a lack of difference in the amount of CyD in synaptic and nonsynaptic mitochondria from 2- and 12-month-old YAC128 and WT mice (Fig. 8A, B). Consequently, this could not explain increased Ca^{2+} uptake capacity in mitochondria from YAC128 mice compared with mitochondria from WT animals.

ROS are major activators of the PTP (Bernardi, 1999) and PTP induction is the key factor that restricts Ca^{2+} uptake capacity (Chalmers & Nicholls, 2003). It seemed conceivable that altered ROS production could underlie the difference in Ca^{2+} uptake capacity. Therefore, in the following experiments we examined mitochondrial H_2O_2 generation by synaptic mitochondria from YAC128 and WT mice using Amplex Red assay (Brustovetsky *et al.*, 2003).

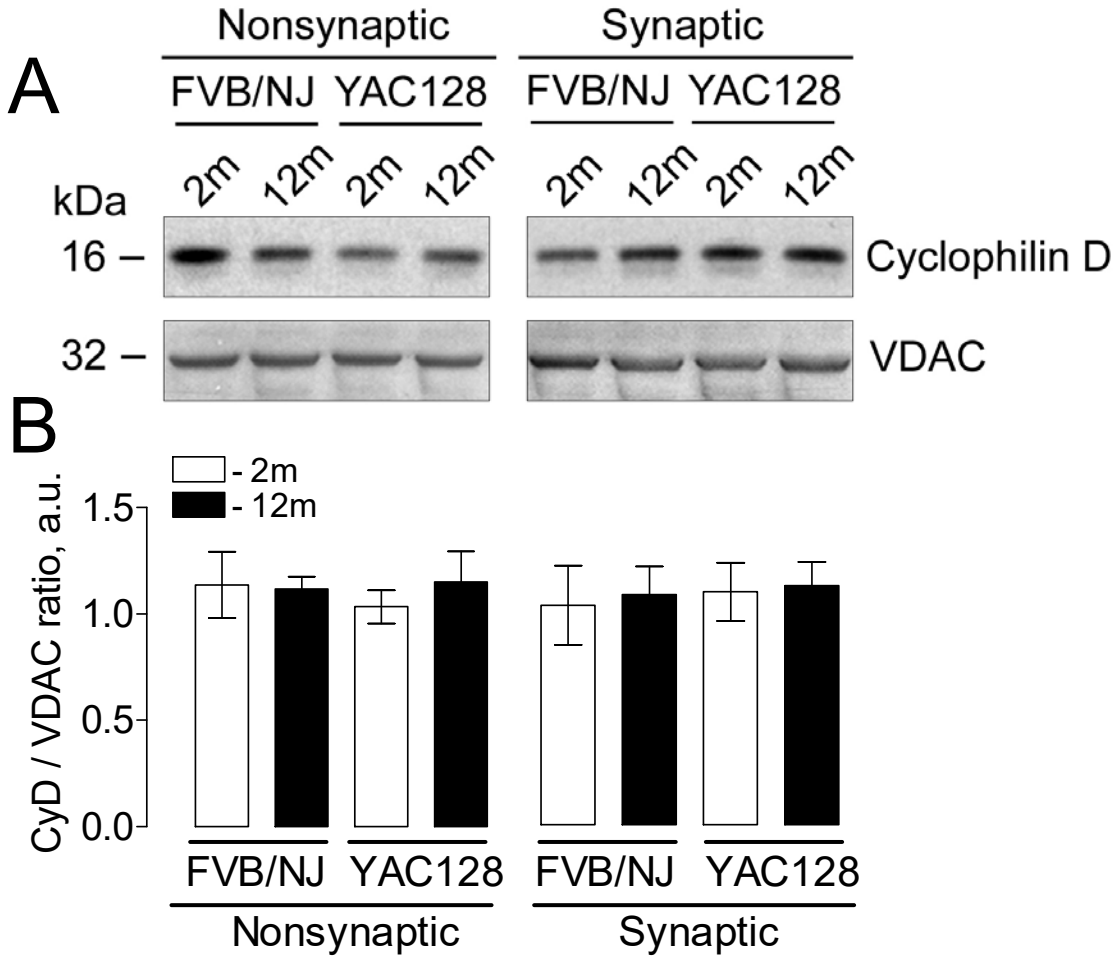

Figure 8. Expression of mitochondrial cyclophilin D in brain mitochondria isolated from 2- and 12-month-old YAC128 and WT (FVB/NJ) mice. In A, representative western blots of brain nonsynaptic and synaptic mitochondria from 2- and 12-month-old FVB/NJ and YAC128 mice with anti-cyclophilin D antibodies. Isolated mitochondria were solubilized and proteins were resolved by SDS-PAGE using 12% Bis-Tris gels. Mitochondrial porin (voltage-dependent anion channel, VDAC) was used as a loading control. In B, statistical analysis of western blot densitometry with data expressed in arbitrary units (a.u.) as a ratio of cyclophilin D band intensity to band intensity of VDAC. Data are mean ± SEM, N=5.

With succinate plus glutamate, ROS generation was much higher than with pyruvate plus malate. BSA further augmented ROS generation (Fig. 9A,B), presumably due to an increase in membrane potential in both YAC128 and WT mitochondria that may lead to an increase in ROS generation (Korshunov *et al.*, 1997). Ca^{2+}, on the other hand, depolarizes mitochondria (Bernardi, 1999) and, consequently, inhibited ROS generation with succinate plus glutamate (Fig. 9C), but did not significantly change ROS generation in the presence of pyruvate plus malate (Fig. 9D). Importantly, there was no difference in ROS generation between mitochondria from YAC128 and WT mice. Thus, ROS production could not account for the difference in Ca^{2+} uptake capacity between mitochondria from transgenic and WT animals.

e. Greater levels of mHtt are associated with synaptic mitochondria from 12- compared with 2-month-old YAC128 mice

To further examine the increase in Ca^{2+} uptake capacity in 12-month compared with 2-month-old YAC128 mice, we asked if the level of mHtt associated with mitochondria changes with age. We found a 2-fold increase in the amount of mHtt bound to synaptic mitochondria from 12-month-old YAC128 mice compared with mitochondria from 2-month-old YAC128 mice (Fig. 10A, B). This increase was not due to an increase in cytosolic mHtt because cytosolic levels remained the same (Fig. 10C, D).

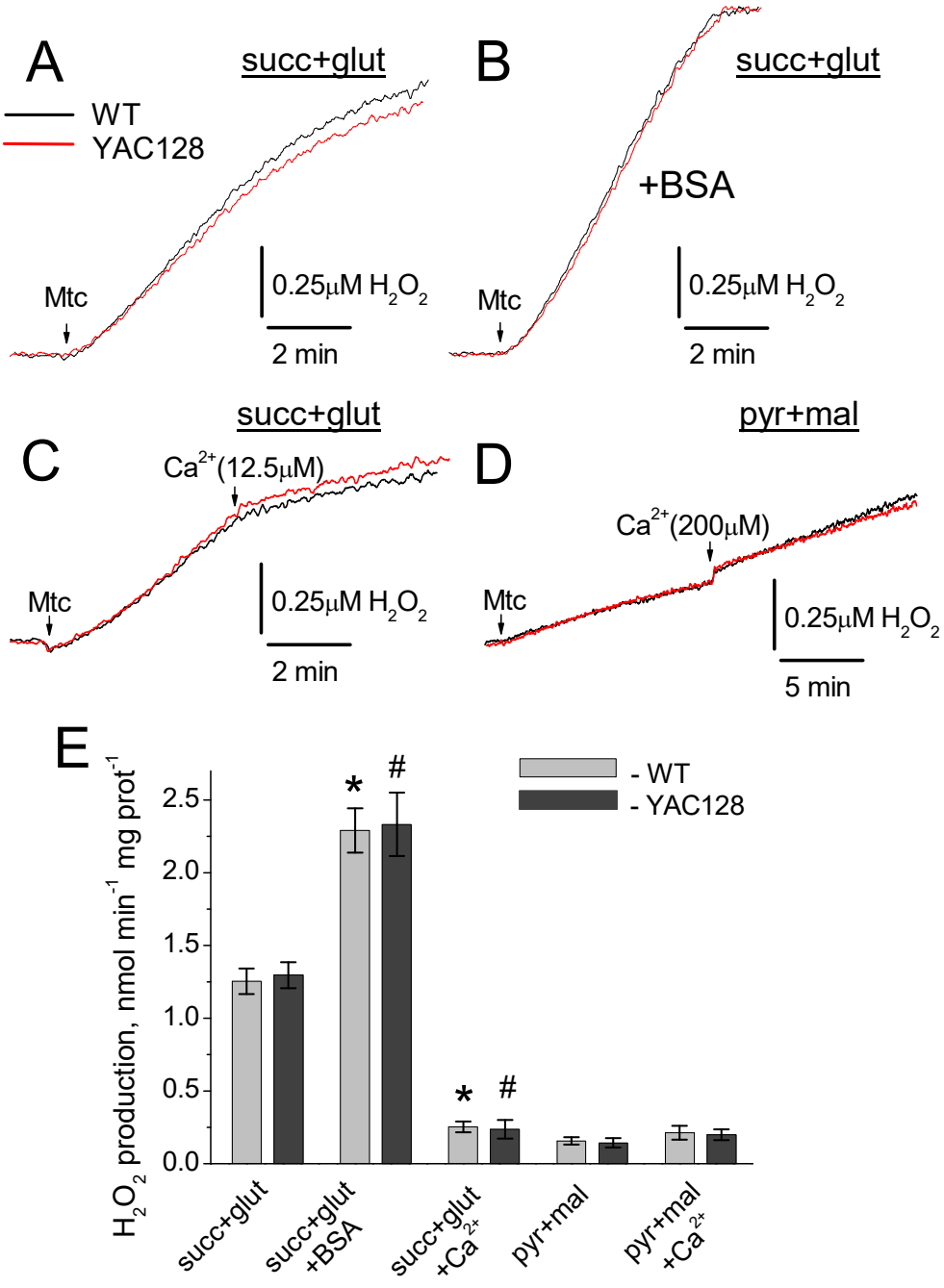
A
succ+glut
WT
YAC128
Mtc
0.25μM H2O2
2 min
B
succ+glut
+BSA
Mtc
0.25μM H2O2
2 min
C
succ+glut
Ca2+(12.5μM)
Mtc
0.25μM H2O2
2 min
D
pyr+mal
Ca2+(200μM)
Mtc
0.25μM H2O2
5 min
E
- WT
- YAC128
H2O2 production, nmol min-1 mg prot-1
0.0
0.5
1.0
1.5
2.0
2.5
*
#
*
#
succ+glut
succ+glut +BSA
succ+glut +Ca2+
pyr+mal
pyr+mal +Ca2+

Figure 9

Figure 9. H_2O_2 production by synaptic mitochondria from 2-month-old YAC128 and WT (FVB/NJ) mice. Mitochondrial H_2O_2 production was measured under continuous stirring in 0.4 ml cuvette at 37ºC in the standard KCl-based incubation medium. In A-C, the standard incubation medium was supplemented with 3 mM succinate plus 3 mM glutamate. In D, the incubation medium was supplemented with 3 mM pyruvate plus 1 mM malate. In B, 0.1% BSA (free from fatty acids) was present in the medium. 12.5 or 200μM Ca^{2+} was applied to mitochondria in C and D, as indicated. In E, a statistical analysis of H_2O_2 production under different experimental conditions. Data are mean±SEM, N=6. *p<0.01 compared to H_2O_2 generation by WT mitochondria oxidizing succinate plus glutamate, but without BSA and Ca^{2+}; #p<0.01 compared to H_2O_2 generation by YAC128 mitochondria oxidizing succinate plus glutamate, but without BSA and Ca^{2+}

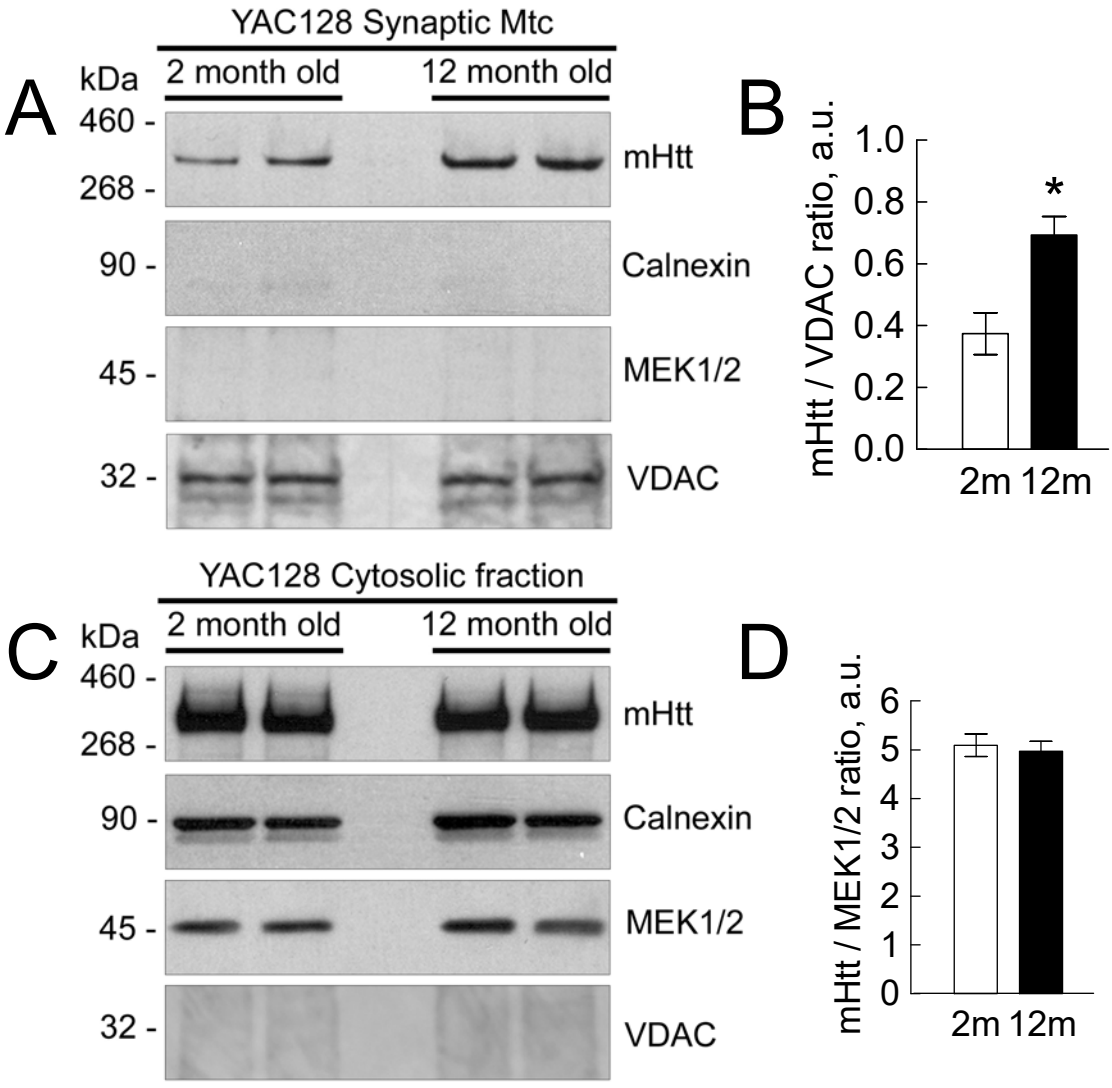
A
YAC128 Synaptic Mtc
kDa
2 month old
12 month old
460 -
268 -
mHtt
90 -
Calnexin
45 -
MEK1/2
32 -
VDAC
B
mHtt / VDAC ratio, a.u.
1.0
0.8
0.6
0.4
0.2
0.0
*
2m 12m
C
YAC128 Cytosolic fraction
kDa
2 month old
12 month old
460 -
268 -
mHtt
90 -
Calnexin
45 -
MEK1/2
32 -
VDAC
D
mHtt / MEK1/2 ratio, a.u.
6
5
4
3
2
1
0
2m 12m

Figure 10.

Figure 10. The level of mutant huntingtin (mHtt) associated with brain mitochondria isolated from 2- and 12-month-old YAC128 mice. The level of mutant huntingtin (mHtt) associated with brain mitochondria isolated from 2- and 12-month-old YAC128 mice. In A, western blots of brain synaptic mitochondria from 2- and 12-month-old YAC128 mice with anti-polyQ 1C2 antibody, specific for mHtt. Isolated mitochondria were solubilized and proteins were resolved by sodium dodecyl sulfate–polyacrylamide gel electrophoresis (SDS–PAGE) using 3–8% Trisacetate gels. Calnexin was used as a marker of endoplasmic reticulum. MEK1/2 was used as a cytosolic marker. Mitochondrial porin (voltage-dependent anion channel, VDAC) was used as a mitochondrial marker and loading control. In B, statistical analysis of western blot densitometry with data expressed as a ratio of mHtt band intensity to band intensity of VDAC. Data are mean ± SEM, *$p < 0.05$ compared with mitochondria from 2-month-old YAC128 mice, n = 8. In C, western blots of brain cytosolic fractions from 2- and 12-month-old YAC128 mice with anti-polyQ 1C2 antibody, specific for mHtt. Cytosolic fractions were resolved by SDS-PAGE using 3–8% Tris-acetate gels. MEK1/2 was used as a cytosolic marker and loading control. In D, statistical analysis of western blot densitometry with data expressed as a ratio of mHtt band intensity to band intensity of MEK1/2. Data are mean ±SEM, n = 8.

Thus, augmented Ca^{2+} uptake capacity of synaptic mitochondria from 12-month-old YAC128 mice correlated with the increased amount of mHtt associated with these mitochondria. These data suggest that mHtt association with mitochondria may augment mitochondrial Ca^{2+} uptake capacity.

B. Ca^{2+}dysregulation in culture neurons from a mouse model of HD

Studies with isolated mitochondria provide important information about the function of the organelles, but under these conditions mitochondria are removed from the complexity of the whole cell. To further examine Ca^{2+} handling in the presence of mHtt, we used primary striatal neurons plated with glia. Ca^{2+} has been shown to be altered in HD contributing to neurodegeneration (Tang *et al.*, 2003; Bezprozvanny & Hayden, 2004). This is likely due to increased activation of NMDAR in striatal neurons expressing mHtt (Zeron *et al.*, 2002).

a. Characterization of striatal neurons in culture

Prior to experiments with primary striatal neurons, characterization was required to confirm that the neurons were medium spiny neuron, the primary neuronal type in the straium. A representative bright-field image of cell culture is shown in Fig. 11A. All pups used for harvesting neurons were genotyped and cultured cells were tested for the presence of mHtt using Western blotting (Fig.11B). Our cell culture contained both neurons and astrocytes stained by neuronal marker, microtubule associated protein (MAP-2, green) and glial marker, glial fibrillary acidic protein (GFAP, red) (Mao & Wang, 2001),

respectively (Fig.11D). To characterize that the striatal neurons were medium spiny neurons, the primary neuronal type in the striatum, we stained with anti-GABA (red) (Ivkovic & Ehrlich, 1999; Mao & Wang, 2001) (Fig.11F) and anti-dopamine and cyclic AMP-regulated phosphoprotein relative molecular mass 32,000 (DARPP-32, red) (Ivkovic & Ehrlich, 1999) (Fig. 11H) antibodies. The majority of neurons (85%) were GABA positive, and 50% of neurons were positive for DARPP-32, typical for striatal neurons (Ivkovic & Ehrlich, 1999). Figures 11C, E, and G show bright-field images for the corresponding immunofluorescence images.

To determine consistency in glia/neuron ratio, we performed western blotting with antibodies against MAP-2 and GFAP. GAPDH was used as a loading control. Then, we performed densitometry and calculated MAP2/GFAP ratio as a characteristic of our cell cultures (Figure 12). These experiments showed very small variability (mean ± SEM: 1.10 ± 0.08 for FVB/NJ mice, n = 6, and 1.12 ± 0.07 for YAC128 mice, n = 6) between different platings as well as the lack of difference between cell cultures prepared from YAC128 and WT littermates.

We next asked if the basal cytosolic Ca^{2+} concentration was altered in striatal neurons from YAC128 mice compared with their WT littermates. Other groups have previously shown no difference in basal cytosolic Ca^{2+} concentration in medium spiny neurons plated from the R6/2 (Cepeda *et al.*, 2001) and YAC128 (Zhang *et al.*, 2008) mouse models of HD.

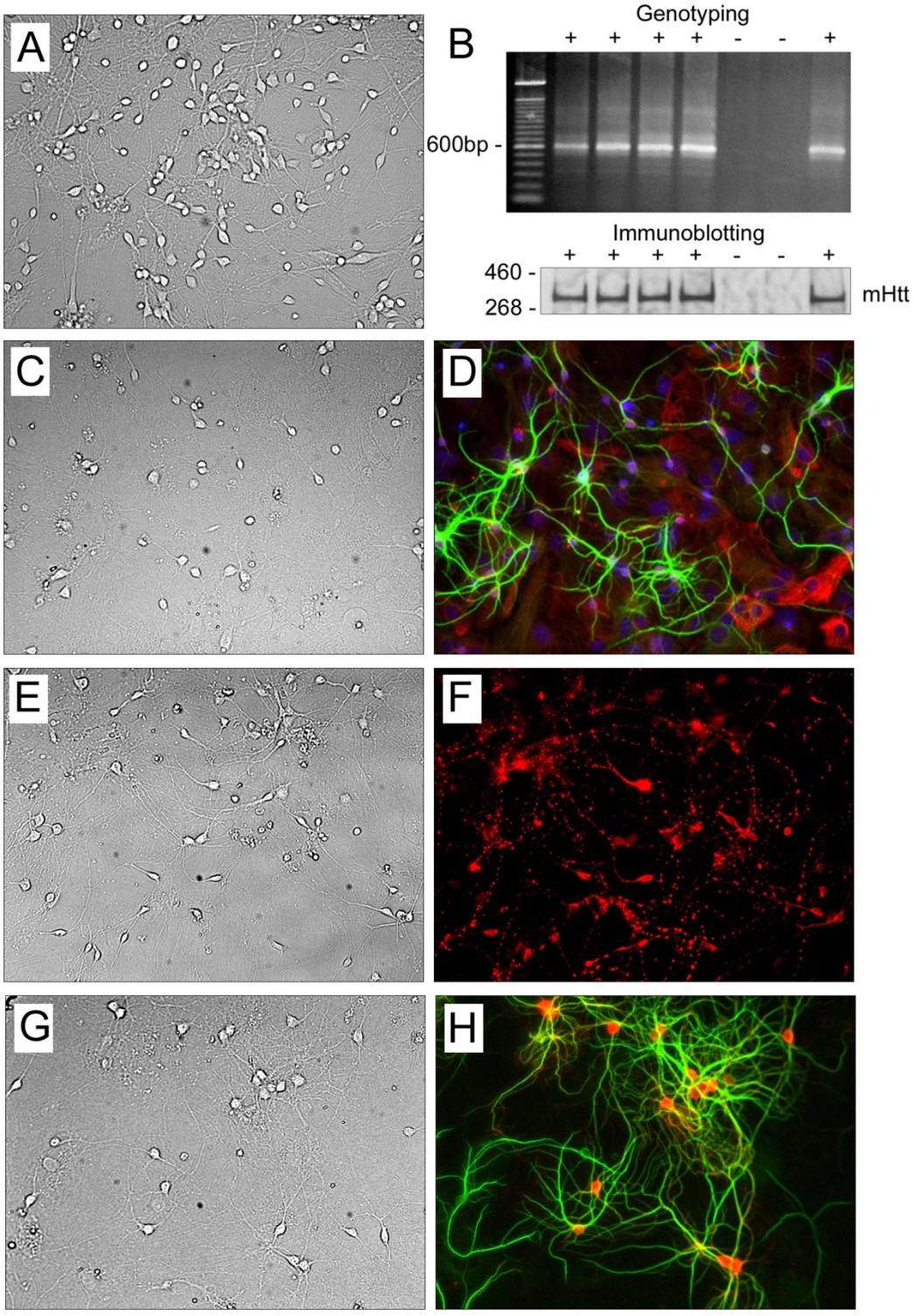

Figure 11.

Figure 11. Characterization of striatal neuronal culture from YAC128 mice. A, a representative live-cell, bright field image of striatal neuronal-glial co-culture used in this study; B, genotyping of mice and western blotting of striatal neuronal cultures from the same animals, “+” – YAC128 mice, “-“ – WT littermates; C and D, bright field image (C) and immunofluorescence image (D) of neuronal culture stained with anti-MAP-2 antibody (neuronal marker), anti-GFAP antibody (astroglial marker), and DAPI (nuclear marker); E and F, bright field image (E) and immunofluorescence image (F) of neuronal culture stained with anti-GABA antibody; G and H, bright field image (G) and immunofluorescence image (H) of neuronal culture stained with anti-DARPP-32 antibody (marker of medium spiny neurons), anti-MAP-2 antibody (general neuronal marker).

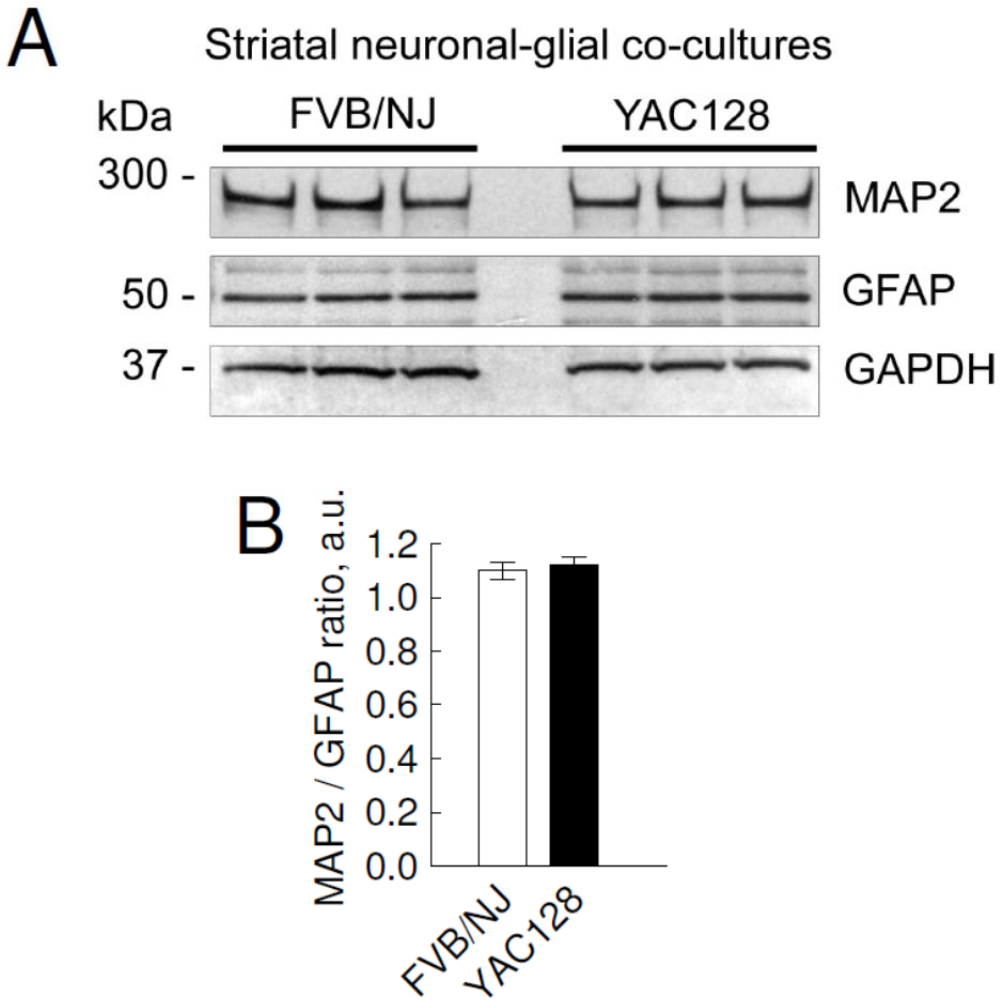

Figure 12. Consistency in neuron to glia ratio in neuronal-glial co-cultures. In **A**, western blotting with three representative neuronalglial co-cultures from three different platings derived from WT (FVB/NJ) and YAC128 mice. MAP2, neuronal marker; GFAP, glial marker; GAPDH, loading control. In **B**, MAP2 to GFAP ratio in arbitrary unites (a.u.) based on densitometry analysis. N=7.

To characterize the cells in our culture system, we evaluated resting (basal) Ca^{2+} concentrations using fluorescent microscopy. Representative traces are shown in Fig. 13A and B. The cytosolic Ca^{2+} concentration was calculated for individual cells and then averaged. There was no significant difference in cytosolic Ca^{2+} concentration between WT (0.087 ± 0.007μM) and YAC128 (0.090 ± 0.004 μM) mice.

To further characterize striatal neurons in culture, we examined resting (basal) cytosolic Na^{+} concentration. This has not previously been investigated in cultured neurons. Representative traces of Na^{+} calibration are shown in Figure 14 A and B. Cytosolic Na^{+} concentration was calculated for each neuron separately and concentrations were averaged. Na^{+} concentrations in striatal neurons derived from YAC128 mice were slightly but statistically significantly elevated ($p<0.05$, N=62-75 individual neurons), although only slightly greater (10.49 ± 0.32 mM) than WT (8.39 ± 0.47 mM) (Fig. 14C). Increased Na^{+} concentration has been reported in the striatum of HD patients *in vivo* in studies using magnetic resonance imaging (MRI) (Reetz *et al.*, 2012; Gramsbergen *et al.*, 1986). These data could suggest increased activity or expression of sodium calcium exchangers to maintain basal cytosolic Ca^{2+} concentration.

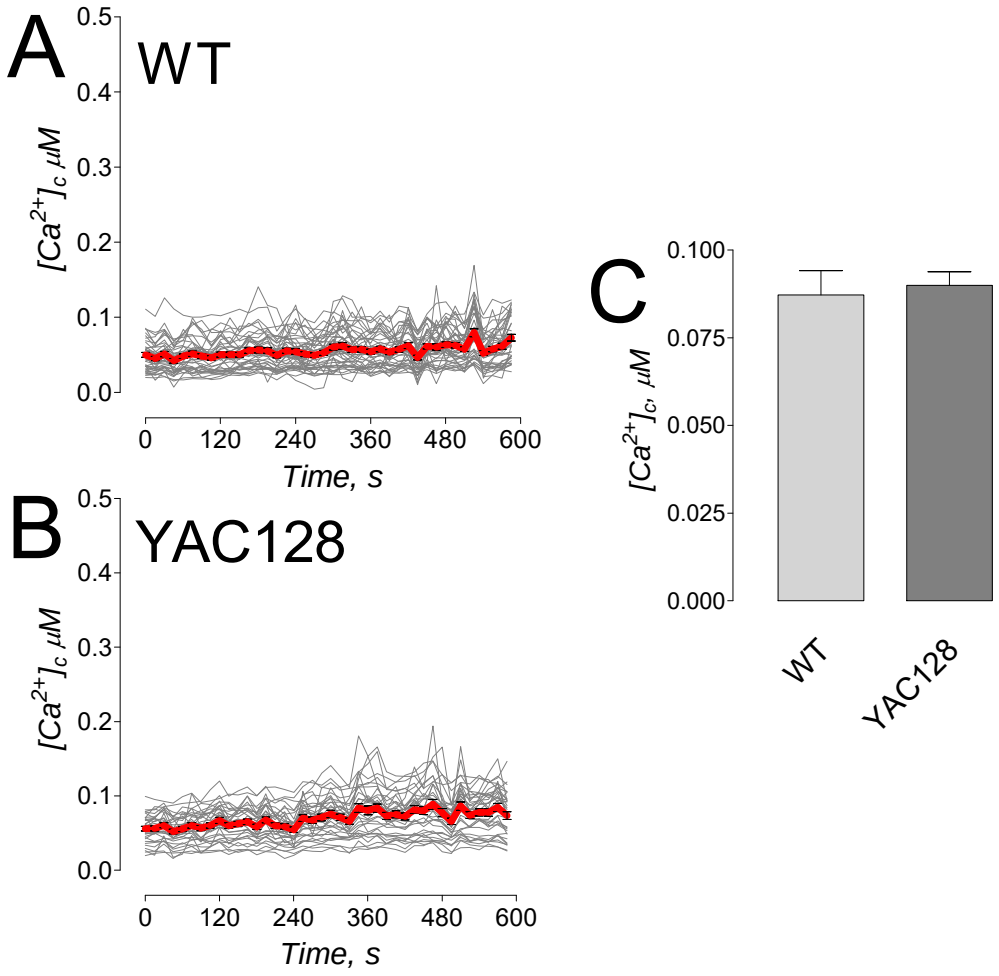

Figure 13. Resting (basal) cytosolic Ca^{2+} concentrations are similar in striatal neurons from YAC128 and WT mice. In A and B, the individual (thin grey traces obtained from individual neurons) and the averaged fluorescence signals (thick red traces, mean±SEM) from the representative experiments are shown. Cytosolic Ca^{2+} was followed by monitoring Fura-2 F_{340}/F_{380} fluorescence ratio at 37ºC. In these experiments, neurons were recorded for ten minutes without any treatment. Data are mean±SEM. In C, averages of individual neurons, n=95-97 individual neurons evaluated for each strain.

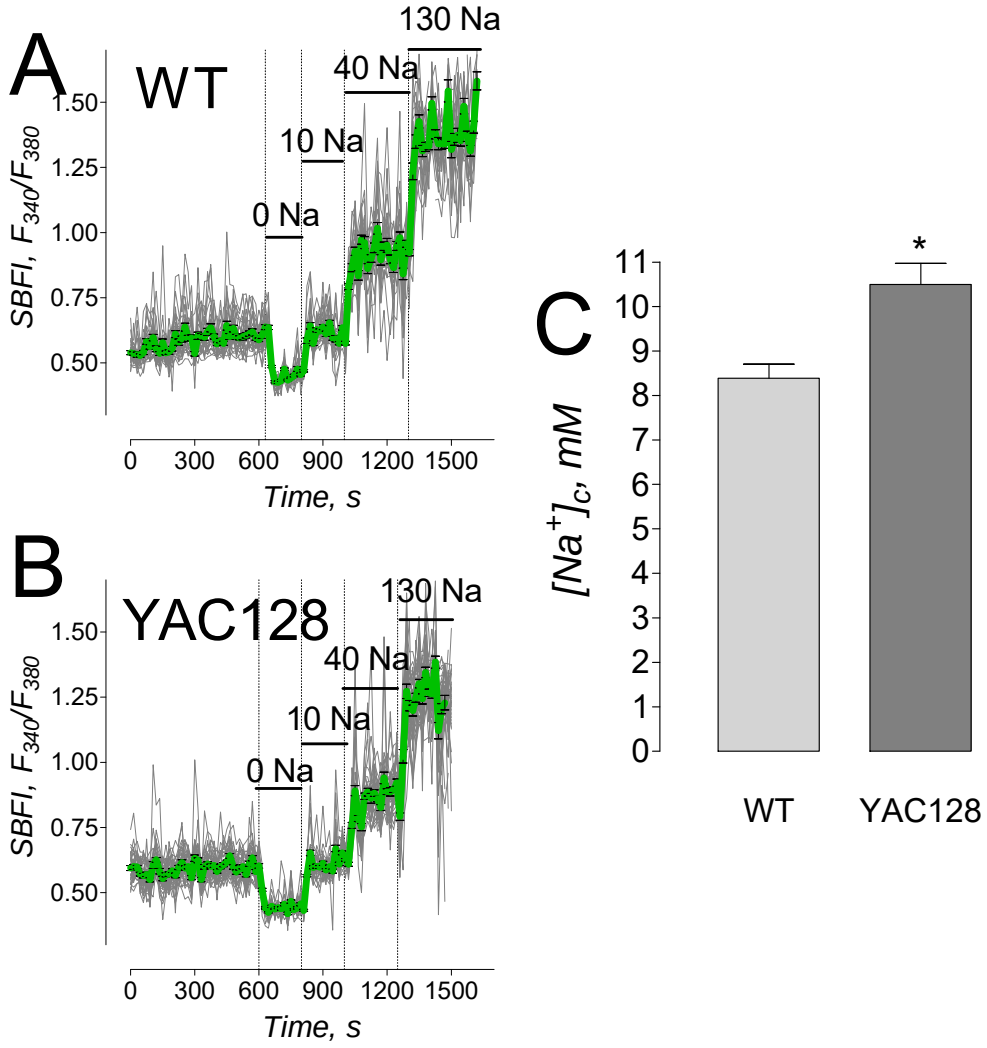

Figure 14. Resting (basal) cytosolic Na^+ concentration is slightly but statistically significantly greater in striatal neurons from YAC128 mice compared with WT mice. In A and B, the individual (thin grey traces obtained from individual neurons) and the averaged fluorescence signals (thick green traces, mean±SEM) from the representative experiments are shown. Cytosolic Na^+ was followed by monitoring SBFI F_{340}/F_{380} fluorescence ratio at 37ºC. In these experiments, neurons were recorded for ten minutes without any treatment then gramicidin was applied along with solutions of known Na^+ concentration for calibration. Data are mean±SEM. In C, averages of individual neurons, n=62-75 individual neurons evaluated for each strain.

b. Striatal neurons undergo DCD more quickly than cortical neurons

Striatal neurons are the most vulnerable neuronal population in HD. We asked if striatal neurons are more vulnerable to excitotoxic insult in WT cultured neurons, without the contribution of mHtt. To evaluate this, we cultured striatal and cortical neurons from WT mice and evaluated glutamate-induced increase in cytosolic Ca^{2+} concentration. The recording was performed at 1 image per 15 seconds acquisition rate for 20 minutes to ensure DCD plateau. Application of 15μM glutamate plus 10μM glycine resulted in DCD within 5 minutes of glutamate application (Fig. 15A). Cortical neurons, on the other hand, recovered to basal levels, eventually undergoing DCD after 20 minutes (Fig.15B). These data were quantified by calculating the area under the curve (AUC). AUC indicates the increase in cytosolic Ca^{2+} over time. AUC for striatal neurons was significantly greater than cortical neurons ($p<0.05$, N=4), 2318 ± 335.8 arbitrary units (a.u.) compared with 594 ± 229.4 a.u. respectively (Fig. 15C). These data suggest that striatal neurons from WT animals are more vulnerable to excitotoxicity than cortical neurons from WT animals.

c. Delayed calcium dysregulation occurs more quickly in striatal neurons from YAC128 mice compared with striatal neurons from WT mice

Next, we asked if mHtt expression further increased the vulnerability of striatal neurons to excitotoxic insult. To evaluate the effect of mHtt, we applied 25μM glutamate plus 10μM glycine to striatal neurons from YAC128 and WT mice.

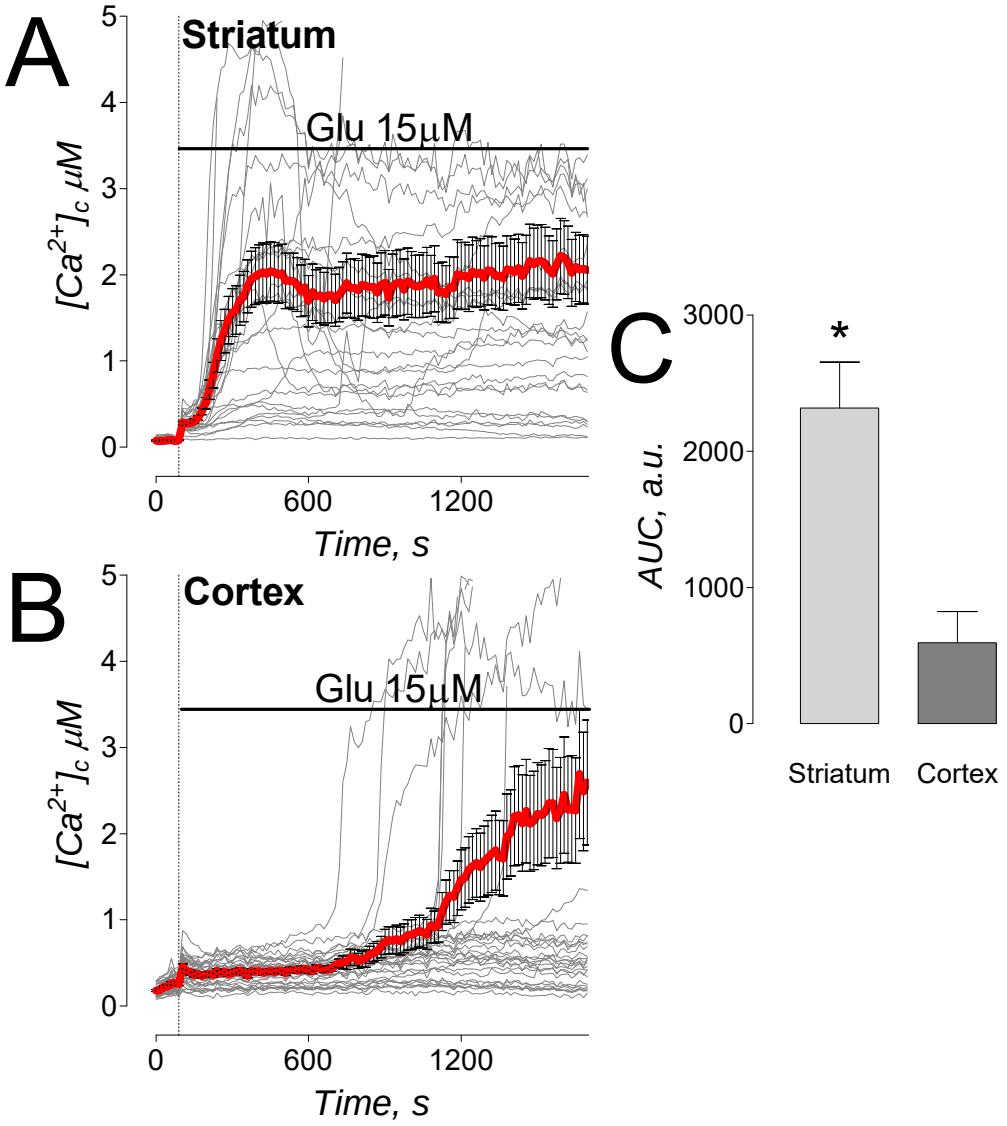

Figure 15. Ca^{2+} dysregulation occurs more quickly in striatal neurons compared with cortical neurons. Striatal and cortical neurons (10-14 days *in vitro*) from WT mice were loaded with Ca^{2+}-sensitive dye Fura-2FF-AM to monitor changes in cytosolic Ca^{2+} concentration ($[Ca^{2+}]_c$). In A and B, thin, grey traces show fluorescent signals from individual neurons whereas thick, red traces represent mean±SEM from individual experiments (n=20-25 neurons per experiment). Where indicated, 15μM glutamate plus 10μM glycine (Glu) were applied to neurons. In C, the summary graph shows average area under the curve (AUC; a.u., arbitrary units), that represents a measure of $[Ca^{2+}]_c$ increase over time. (*p<0.05, N=3-4).

We assessed glutamate-induced increase in cytosolic Ca^{2+} concentration using fluorescent imaging (Figure 16A, B). These data were quantified in two ways. In Figure 16C, the slopes of the average traces are reported. The slope indicates the rate of the response to glutamate. A greater slope correlates with faster onset of DCD. The slope of glutamate-induced increase in cytosolic Ca^{2+} concentration from YAC128 striatal neurons (0.019±0.004) is significantly greater ($p<0.05$, N=4) than the slope observed in WT neurons (0.007±0.002). These data are also represented as AUC in Figure 16D. Evaluation of the AUC also shows statistically significant ($p<0.05$, N=4) increase in neurons from YAC128 striatal neurons (1236±117.3 a.u.) compared with WT neurons (885±87.4 a.u.). These data suggest that the presence of mHtt further increases the vulnerability of striatal neurons to excitotoxic insult.

d. NMDA-induced Ca^{2+} increases are similar in striatal neurons from YAC128 and WT mice

In response to glutamate application, Ca^{2+} predominantly enters the neuron through NMDARs. It has been proposed that NMDAR activity is increased in HD but there are contradictory results in the literature. Fernandes and colleagues (Fernandes *et al.*, 2007) have shown in electrophysiological studies that NMDAR are more active in striatal neurons from YAC72 but not in YAC46 or YAC128 models of HD.

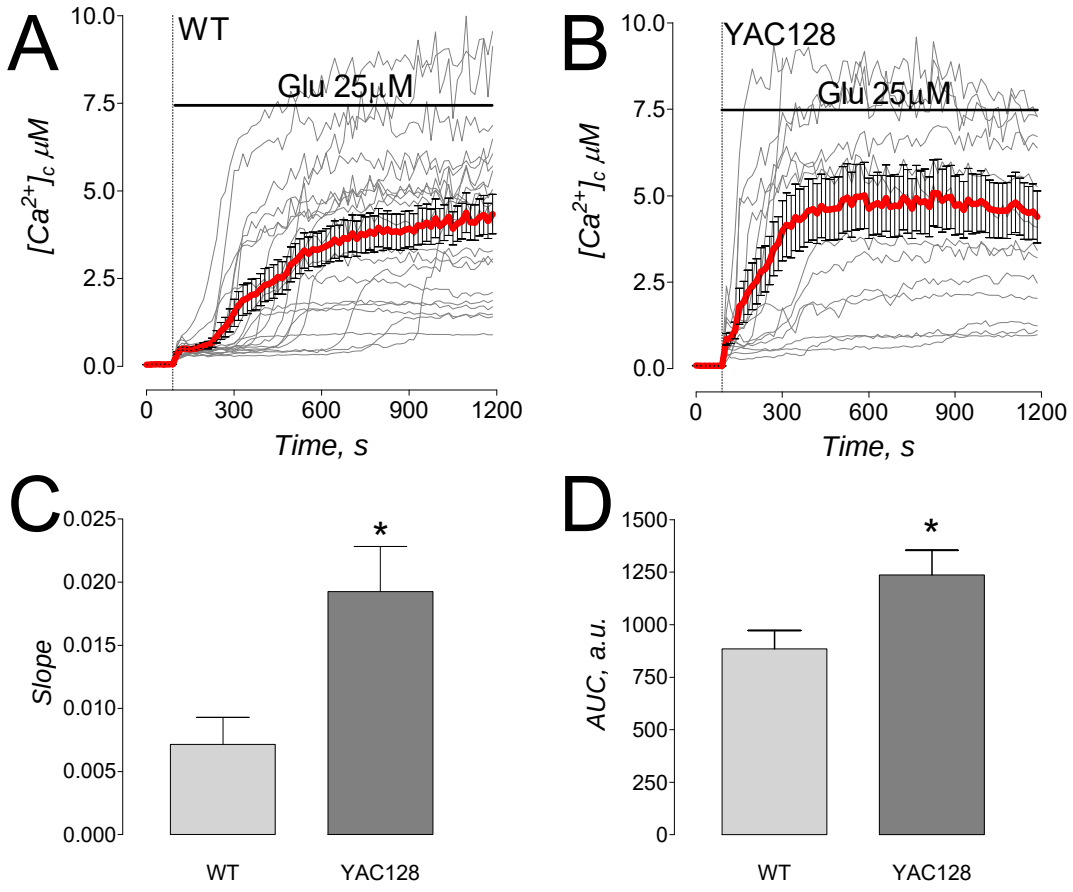

Figure 16. Ca^{2+} dysregulation occurs more quickly in YAC128 striatal neurons compared with WT neurons. Striatal neurons (10-13 days *in vitro*) were loaded with Ca^{2+}-sensitive dye Fura-2FF-AM to monitor changes in cytosolic Ca^{2+} concentration ($[Ca^{2+}]_c$). In A and B, thin, grey traces show fluorescent signals from individual neurons whereas thick, red traces represent mean±SEM from individual experiments (n=20-25 neurons per experiment). Where indicated, 25μM glutamate plus 10μM glycine (Glu) were applied to WT (A) and YAC128 (B) neurons. In C, the summary graph shows the slope, indicating the rate of the response to glutamate. (*p<0.05 N=4). In D, the graph shows average area under the curve (AUC; a.u., arbitrary units), that represents a measure of $[Ca^{2+}]_c$ increase over time. (*p<0.05, N=4)

Other laboratories, however, have shown increased NMDAR currents in striatal neurons derived from YAC128 mice (Zhang *et al.*, 2008), although all conditions are reported as similar to those used by Fernandes et al. This research group also used fluorescent imaging to measure cytosolic Ca^{2+} concentration in response to 100μM or 500μM NMDA for 5 minutes and reported no difference between WT and YAC128 (Fernandes *et al.*, 2007). Many factors contribute to cytosolic Ca^{2+} concentration, not only Ca^{2+} influx, but also mechanisms of Ca^{2+} removal to maintain Ca^{2+} homeostasis and fight excitotoxicity. Furthermore, we have previously used a lower concentration of NMDA (30μM plus 10μM glycine) in a 30 second pulse protocol to evaluate NMDAR activity (Brustovetsky *et al.*, 2011; Brittain *et al.*, 2012a). To decrease the possibility of a ceiling effect, we used lower concentrations of NMDA than the previous study (10μM, 15μM, and 30μM) plus 10μM glycine. Representative traces of cytosolic Ca^{2+} concentration from WT striatal neurons are shown in Figure 17A, B, and C and neurons from YAC128 in Fig. 17D, E, and F. Data are quantified as peak cytosolic Ca^{2+} concentration in Fig. 17G and AUC in Fig. 17H. The peak Ca^{2+} concentration indicates the initial Ca^{2+} increase, whereas AUC indicates the increase in Ca^{2+} over time. Regardless of the quantification, there is no statistically significant difference between NMDA-induced cytosolic Ca^{2+} increases from WT or YAC128 striatal neurons using this protocol. These data could suggest that there is no difference in NMDAR activity in mHtt expressing striatal neurons or that mechanisms of Ca^{2+} removal are compensating for increased Ca^{2+} influx.

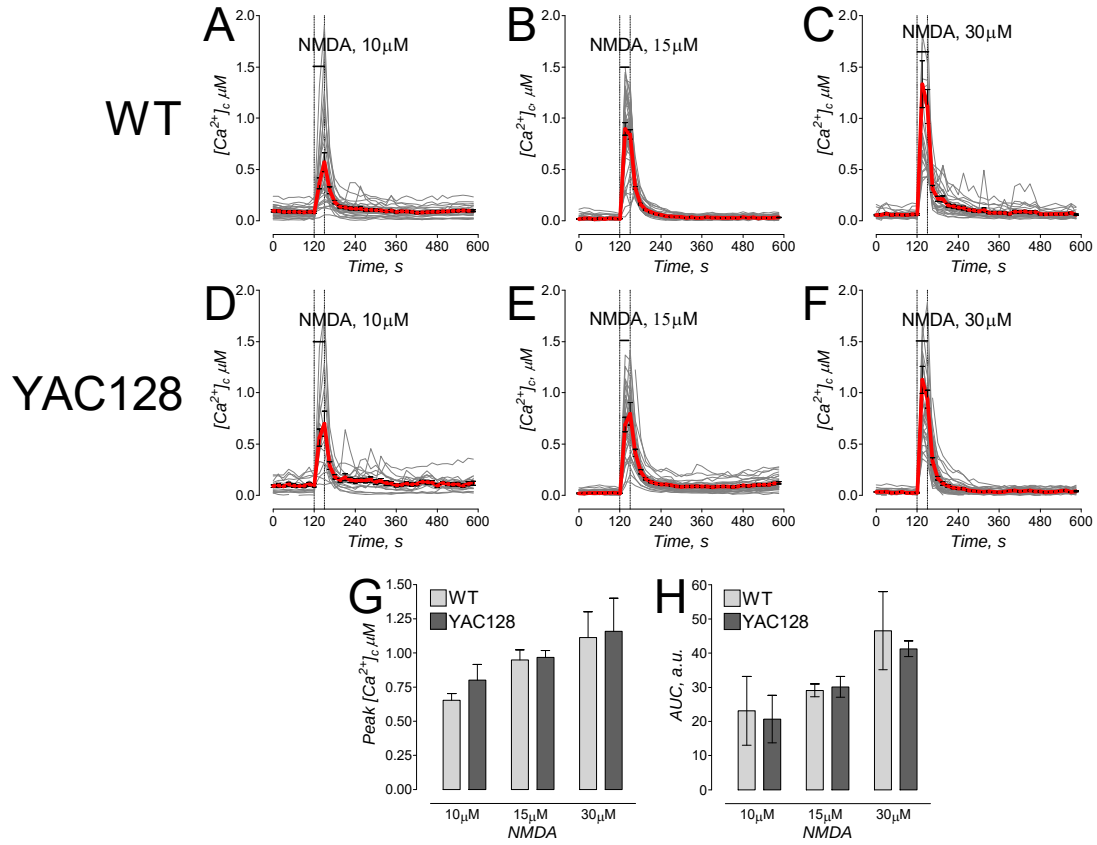

Figure 17. NMDA-induced cytosolic Ca^{2+} increases are similar in striatal neurons from YAC128 and WT mice. Striatal neurons (10-13 days *in vitro*) were loaded with Ca^{2+}-sensitive dye Fura-2AM to monitor changes in $[Ca^{2+}]_c$. In these experiments, where indicated, short pulses of 10μM (A,D), 15μM (B,E) or 30μM (C,F) NMDA (plus 10μM glycine) were applied to WT (A,B,C) or YAC128 (D, E, F) neurons. In G, the summary graph shows changes in average peak cytosolic Ca^{2+} concentration in response to various NMDA concentrations. In H, data is shown as area under the curve. N=3-4 separate, individual experiments.

e. Mitochondrial Ca^{2+} uptake is similar in striatal neurons from YAC128 mice compared with neurons from WT mice

We showed that synaptic and nonsynaptic isolated mitochondria from 2- and 12-month-old YAC128 mice are capable of taking up as much and more Ca^{2+} compared with WT isolated mitochondria. Therefore, we asked if mitochondrial Ca^{2+} uptake is also increased in striatal neurons expressing mHtt. We evaluated the mitochondrial accumulation of Ca^{2+} in striatal neurons exposed to excitotoxic glutamate. Previously, this approach was used in studies with cortical neurons expressing mHtt (Chang & Reynolds, 2006). We used short applications of 25 and 100μM glutamate and after recovery to resting concentration, evaluated subsequent release of mitochondrial Ca^{2+} into the cytosol induced by depolarization of the organelles with 1μM FCCP. The magnitude of elevation in cytosolic Ca^{2+} due to Ca^{2+} release from mitochondria was used to evaluate mitochondrial Ca^{2+} uptake capacity *in situ* (Chang *et al.*, 2006).

Simultaneously with FCCP application, we replaced external Na^{+} for N-methyl-D-glucamine (NMDG), a bulk organic cation that cannot be transported by the Na^{+}/Ca^{2+} exchanger and hence prevents Ca^{2+} extrusion from the cell by this mechanism. In these experiments, glutamate applications produced transient increases in cytosolic Ca^{2+} followed by recovery of cytosolic Ca^{2+} to near resting level after removal of glutamate (Fig. 18). Neurons from YAC128 mice had a more robust response to glutamate consistent with Fig. 16.

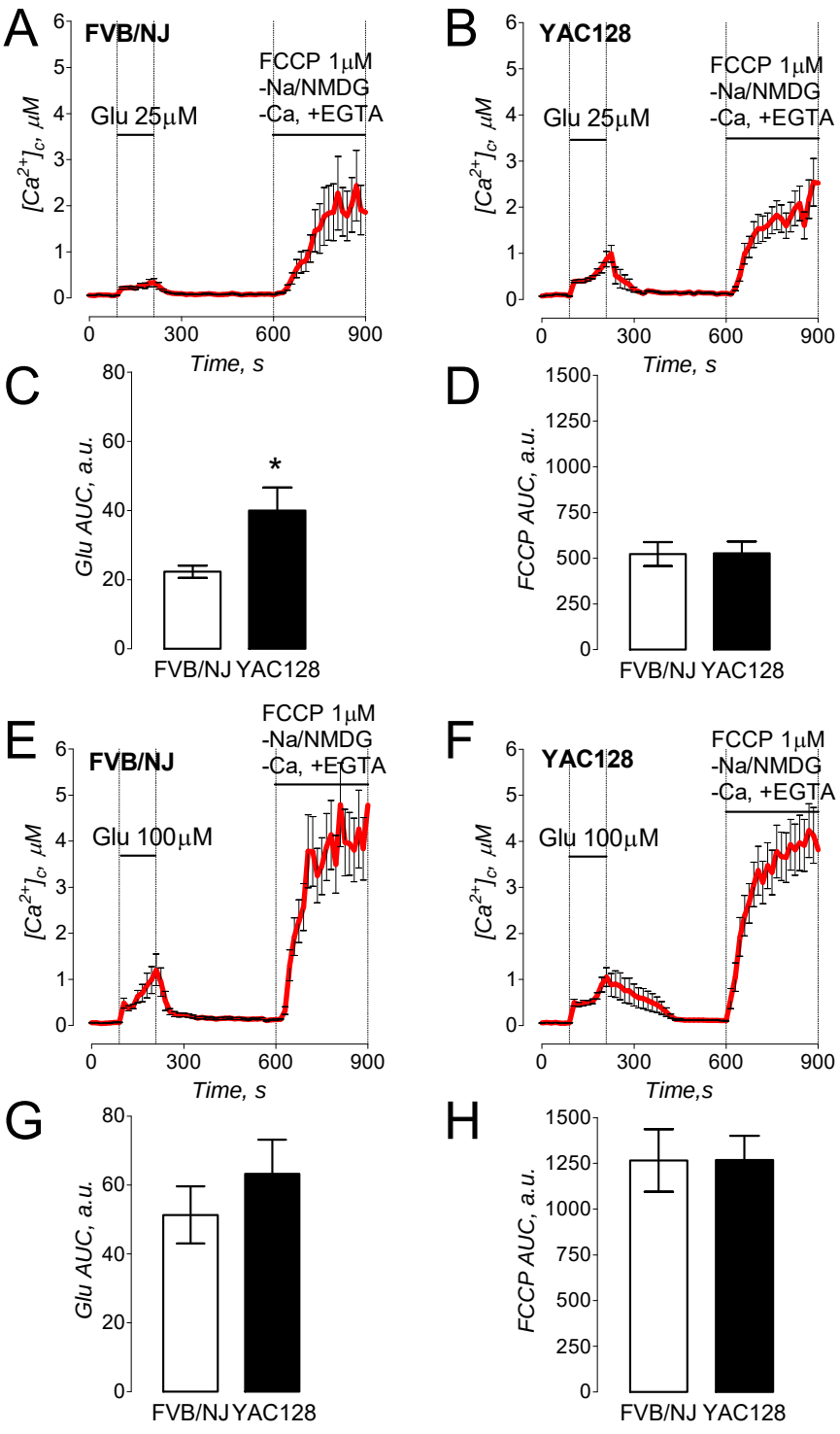
A
FVB/NJ
FCCP 1μM
-Na/NMDG
-Ca, +EGTA
Glu 25μM
[Ca2+]c, μM
Time, s
B
YAC128
FCCP 1μM
-Na/NMDG
-Ca, +EGTA
Glu 25μM
[Ca2+]c, μM
Time, s
C
Glu AUC, a.u.
*
FVB/NJ YAC128
D
FCCP AUC, a.u.
FVB/NJ YAC128
E
FVB/NJ
FCCP 1μM
-Na/NMDG
-Ca, +EGTA
Glu 100μM
[Ca2+]c, μM
Time, s
F
YAC128
FCCP 1μM
-Na/NMDG
-Ca, +EGTA
Glu 100μM
[Ca2+]c, μM
Time,s
G
Glu AUC, a.u.
FVB/NJ YAC128
H
FCCP AUC, a.u.
FVB/NJ YAC128

Figure 18.

Figure 18. Striatal neurons from YAC128 mice have comparable mitochondrial Ca^{2+} accumulation following transient glutamate-induced elevations in cytosolic Ca^{2+}. In A, B, E, and F, the averaged fluorescence signals (mean±SEM) from the representative experiments are shown. Cytosolic Ca^{2+} was followed by monitoring Fura-2FF F_{340}/F_{380} fluorescence ratio at 37ºC. In these experiments, neurons were exposed to 25μM or 100μM glutamate (in both cases, with 10μM glycine) for 2 minutes as indicated. Then, glutamate and glycine were removed to let $[Ca^{2+}]_c$ recover. After $[Ca^{2+}]_c$ reached near resting level (7 minutes after glutamate removal) neurons were treated with 1μM FCCP to depolarize mitochondria and release accumulated Ca^{2+}. To avoid ambiguity concerning possible Ca^{2+} influx from the outside of the cell, external Ca^{2+} was removed simultaneously with glutamate and glycine. In addition, to prevent Ca^{2+} extrusion from the cell by Na^+/Ca^{2+} exchanger, the external Na^+ was replaced by equimolar N-methyl-D-glucamine (NMDG) as indicated. In C, D, G, and H, the areas under the curve (AUC) for the averaged fluorescence signals are shown. The AUC for glutamate-induced increase in $[Ca^{2+}]_c$ (Glu AUC) was calculated for the 120 second period beginning with glutamate application. The AUC for FCCP-induced increase in $[Ca^{2+}]_c$ (FCCP Glu) was calculated for the 300 second period following FCCP application. Data are mean±SEM. In C, *p<0.05 compared to WT cells, n=6-9 separate experiments with 20-25 individual neurons in each experiment.

Depolarization of mitochondria with 1μM FCCP in Ca^{2+}-free bath solution (to prevent influx of external Ca^{2+}) triggered a massive increase in cytosolic Ca^{2+} that was similar in neurons from both YAC128 and WT mice. This result suggests that mHtt does not decrease the ability of neuronal mitochondria to accumulate Ca^{2+} and, therefore, most likely does not affect mitochondrial contribution to maintenance of Ca^{2+} homeostasis in striatal neurons exposed to excitotoxic glutamate.

f. NCX1 expression in striata of YAC128 mice increases with age

NCX is a low affinity, high capacity exchanger and therefore another major mechanism important in the removal of elevated cytosolic Ca^{2+}. We asked if the expression of plasmalemmal NCX isoforms present in lysate from striatum, NCX1 and NCX3, were altered. Our earlier findings of a slight but statistically significant increase in resting sodium concentrations in neurons from YAC128 compared with WT neurons (Fig. 14) suggest increased NCX activity or increased NCX expression. Therefore, we examined the expression of NCX1 and NCX3 in striatal lysate from both 3-week and 3-month-old WT and YAC128 mice. These time points correlate with pre-symptomatic in YAC128 and show no detectable striatal atrophy (Slow *et al.*, 2003). NCX1 expression is statistically significantly increased, by two-fold, at 3 months compared with striata from age matched WT mice ($p<0.05$, N=5) (Fig. 19B, D). At 3-weeks, however, NCX1 expression is not significantly different in striatal lysate from YAC128 mice compared with striatal lysate from WT mice (Fig. 19 A,C).

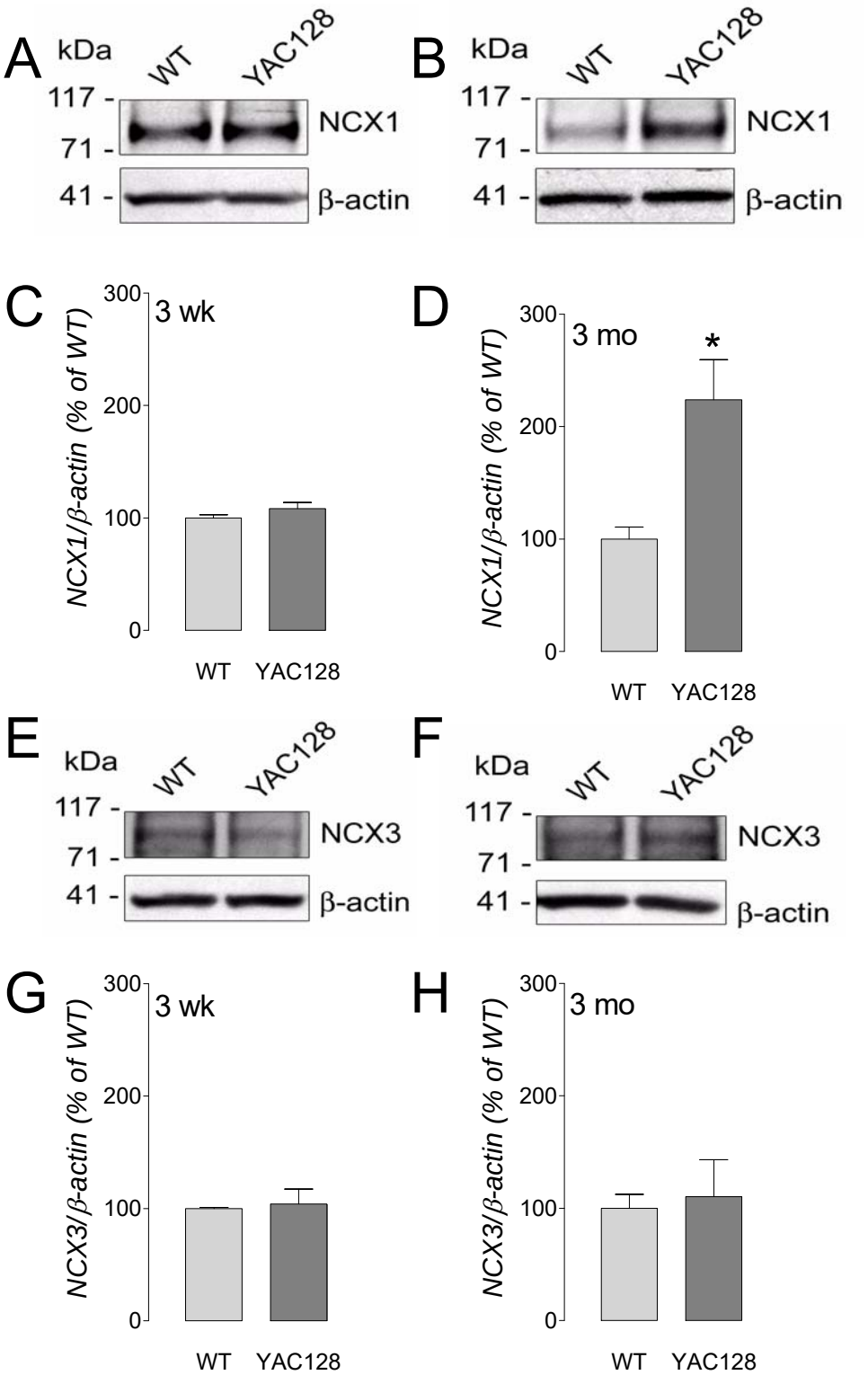
A
kDa
WT
YAC128
117 -
71 -
41 -
NCX1
β-actin
B
kDa
WT
YAC128
117 -
71 -
41 -
NCX1
β-actin
C
3 wk
NCX1/β-actin (% of WT)
300
200
100
0
WT
YAC128
D
3 mo
*
NCX1/β-actin (% of WT)
300
200
100
0
WT
YAC128
E
kDa
WT
YAC128
117 -
71 -
41 -
NCX3
β-actin
F
kDa
WT
YAC128
117 -
71 -
41 -
NCX3
β-actin
G
3 wk
NCX3/β-actin (% of WT)
300
200
100
0
WT
YAC128
H
3 mo
NCX3/β-actin (% of WT)
300
200
100
0
WT
YAC128

Figure 19.

Figure 19. Expression of NCX1 and NCX3 in striata from 3-week and 3-month-old YAC128 and WT mice. In A, Western blots of lysate from striata from 3-week-old YAC128 and WT mice with anti-NCX1 antibody. Lysate from striata from 3-month-old YAC128 and WT mice are show in B. In C and D, statistical analysis of Western blot densitometry with data expressed as percent of WT. In E, Western blots of lysate from striata from 3-week-old YAC128 and WT mice with anti-NCX3 antibody and striata from 3-month-old YAC128 and WT mice are show in F. In C and D, statistical analysis of Western blot densitometry with data expressed as a percentage of WT. β-actin was used as a loading control. Data are mean±SEM, (*$p<0.05$, N=3-4).

There was no change in NCX3 expression at either age (Fig. 19 E-H). These data suggest that the increase in NCX1 expression could be a compensation for increased cytosolic Ca^{2+} concentrations mediated by increased extracellular Ca^{2+} influx or dysfunction of other Ca^{2+} removal mechanisms.

C. Role of CRMP2 in glutamate-induced Ca^{2+} dysregulation

Our laboratory, in collaboration with Dr. Khanna's laboratory, recently found that CRMP2 is involved in regulation of cytosolic Ca^{2+} in neurons exposed to glutamate (Brittain *et al.*, 2011a). The mechanism of CRMP2's involvement in Ca^{2+} regulation is not fully understood. As a first step in our research, we chose to use rat hippocampal neurons in culture to examine the role of CRMP2 without the added variable of mHtt.

a. Glutamate-induced Ca^{2+} dysregulation is reduced after application of tat-CBD3, a small peptide derived from CRMP2

First, we asked if CRMP2 is involved in glutamate-induced Ca^{2+} dysregulation. We used tat-CBD3, a 15-amino acid peptide derived from CRMP2 fused to the cell penetrating motif of HIV-1 (tat), as a tool to disrupt CRMP2 binding. Tat-CBD3 has previously been shown to disrupt interaction between CRMP2 and CaV2.2 (Brittain *et al.*, 2011b). Application of tat-CBD3 significantly decreased glutamate-induced DCD (Fig. 20A) compared with vehicle control (Fig. 20B).

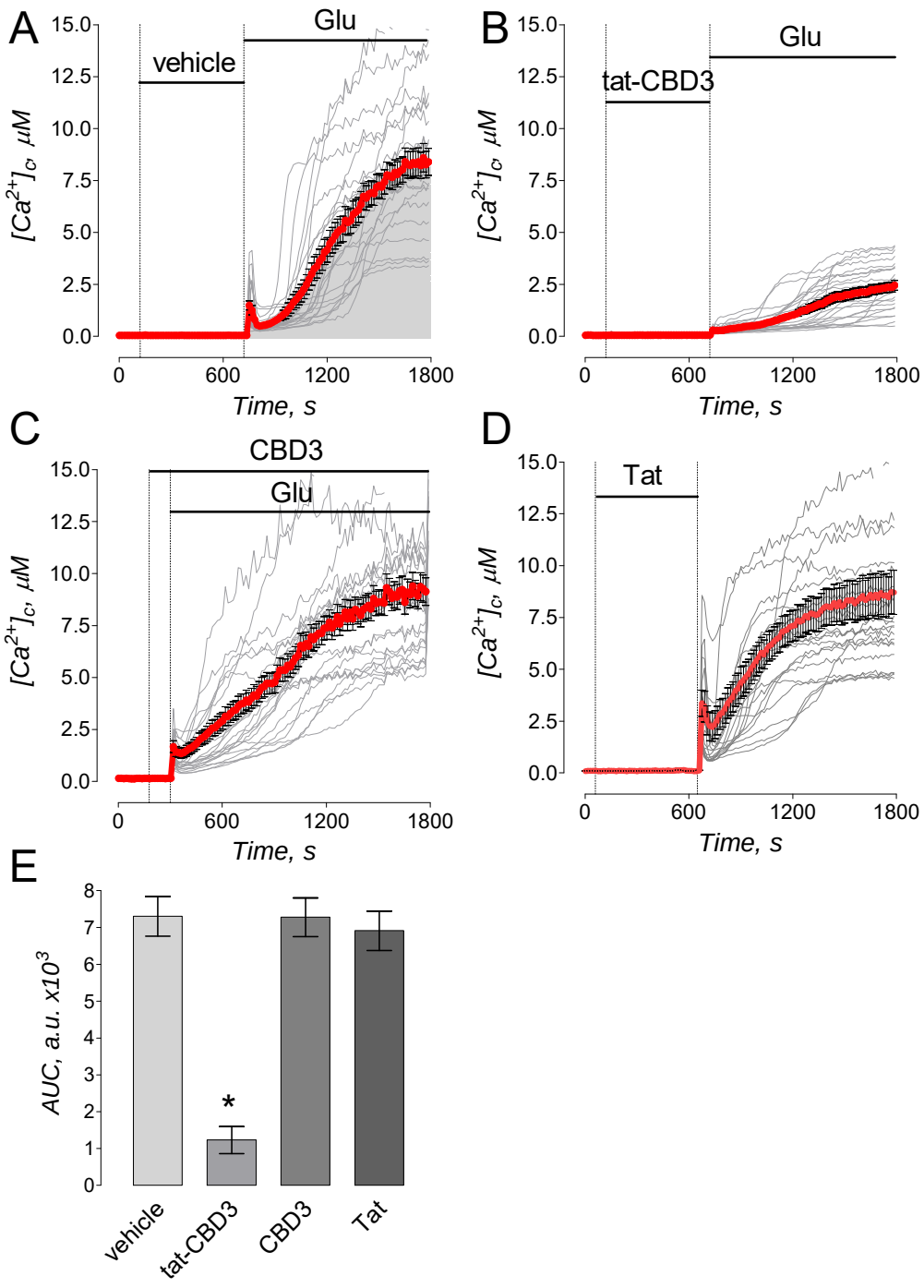
A
vehicle
Glu
B
tat-CBD3
Glu
C
CBD3
Glu
D
Tat
[Ca2+]c, μM
Time, s
E
AUC, a.u. x10^3
*
vehicle
tat-CBD3
CBD3
Tat

Figure 20.

Figure 20. **Tat-CBD3, but not CBD3 sans tat or tat alone, strongly inhibits glutamate-induced Ca^{2+} dysregulation.** Rat hippocampal neurons (12-14 days *in vitro*) were loaded with Ca^{2+}-sensitive dye Fura-2FF-AM to monitor changes in cytosolic Ca^{2+} concentration ($[Ca^{2+}]_c$). Thin, grey traces show fluorescent signals from individual neurons whereas thick, red traces represent mean±SEM from individual experiments (n=20-25 neurons per experiment). Here and in all subsequent Figures, where indicated, neurons were treated either with vehicle (A, DMSO, 0.1%) or 10μM tat-CBD3 (B) for 10 minutes prior to glutamate exposure. In C, neurons were treated with 10μM CBD3 sans tat. The peptide remained in the bath solution throughout the experiment. In D, neurons were treated with 10μM tat for 10 minutes prior to glutamate exposure. Where indicated, 25μM glutamate plus 10μM glycine (Glu) were applied. In E, the summary graph shows the average area under the curve (AUC; a.u., arbitrary units), that represents a measure of $[Ca^{2+}]_c$ increase over time. A representative AUC is shown in panel A as a grey area under the mean±SEM trace. Under each experimental condition, the AUC was calculated for the same time (1080 seconds) following glutamate application. *p<0.01 comparing vehicle- and tat-CBD3-treated neurons. N=5 separate, individual experiments; total number of analyzed neurons is 383.

Furthermore, CBD3 alone (without the tat motif) which cannot cross the membrane, resulted in no change in DCD (Fig. 20B). Treatment with tat alone also had no effect on DCD (Fig. 20D).

The change in cytosolic Ca^{2+} concentration in neurons exposed to tat-CBD3, expressed as AUC, showed a 70% decrease compared with control treatments (Fig. 20E). These data suggest that CRMP2 may be involved in Ca^{2+} handling mechanisms important in DCD.

b. NMDA-induced cytosolic Ca^{2+} concentration increase is reduced after application of tat-CBD3

Since NMDAR is a primary source of Ca^{2+} influx in response to glutamate and CRMP2 has previously been shown to modulate NMDAR (Brittain *et al.*, 2011a), we asked if tat-CBD3 alters cytosolic Ca^{2+} concentration in response to NMDA application. We used an NMDA pulse protocol where NMDA was applied for 30 seconds then cytosolic Ca^{2+} was allowed to return resting. A treatment was applied followed by a second pulse. The treatment was then removed and a final pulse was applied. Similar to glutamate-induced DCD, tat-CBD3 (10μM) statistically significantly reduced NMDA-evoked increases in cytosolic Ca^{2+} concentration (0.17±0.05μM) compared with vehicle treated (1.03±0.05μM) neurons (Fig. 21 A,C). CBD3 without tat was ineffective (1.10±0.07μM) (Fig. 21D). As a positive control, we used AP-5 (20μM), a potent NMDAR antagonist (Morris *et al.*, 1986). AP-5 completely blocked NMDA-induced increase in cytosolic Ca^{2+} (Fig. 21B).

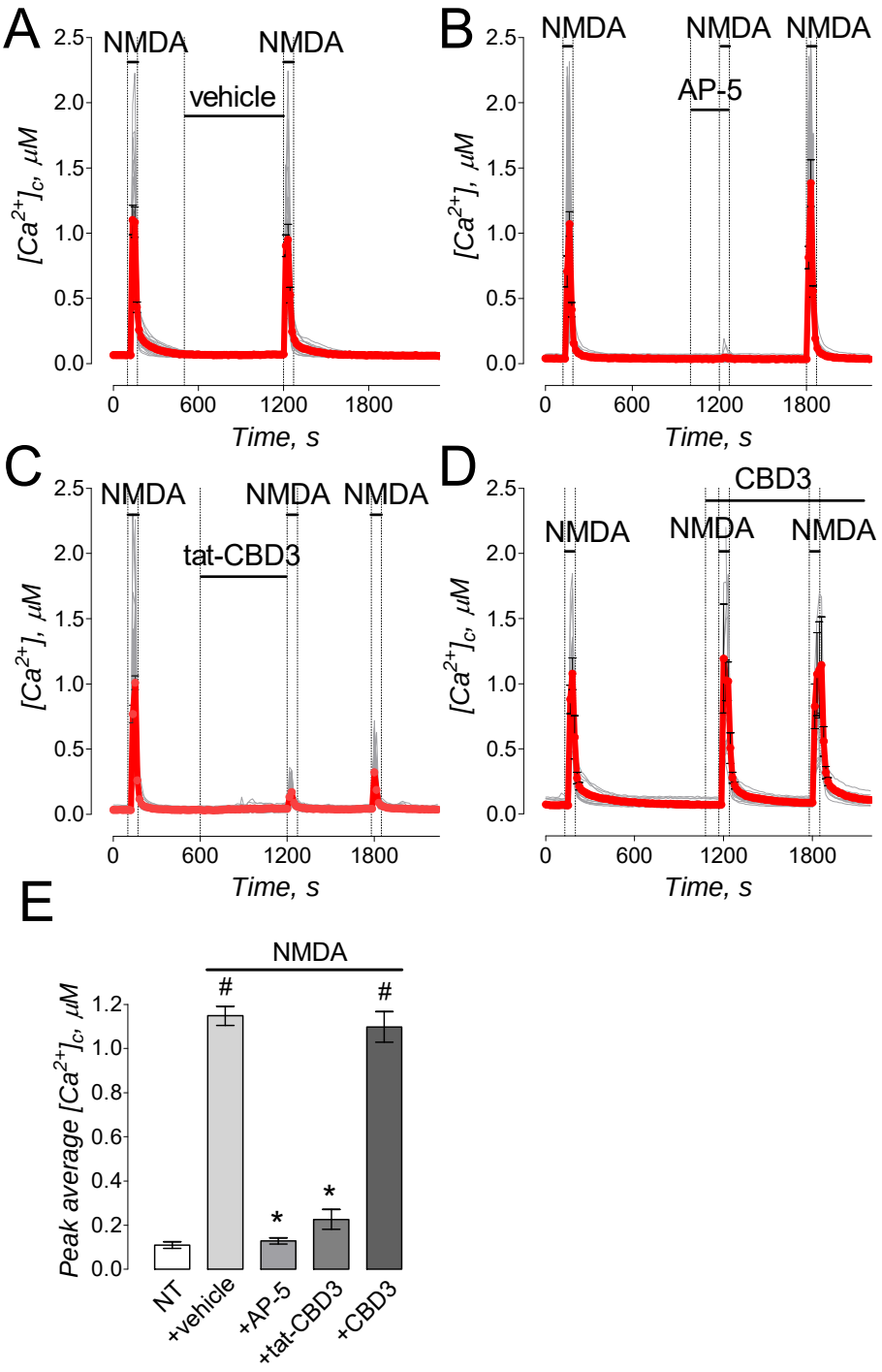
A
NMDA
NMDA
vehicle
[Ca2+]c, μM
Time, s
B
NMDA
NMDA
NMDA
AP-5
[Ca2+], μM
Time, s
C
NMDA
NMDA
NMDA
tat-CBD3
[Ca2+], μM
Time, s
D
CBD3
NMDA
NMDA
NMDA
[Ca2+]c, μM
Time, s
E
NMDA
Peak average [Ca2+]c, μM
NT
+vehicle
+AP-5
+tat-CBD3
+CBD3

Figure 21.

Figure 21. Tat-CBD3, but not CBD3 sans tat, strongly inhibits NMDA-induced increases in cytosolic Ca^{2+}. Rat hippocampal neurons (12-14 days *in vitro*) were loaded with Ca^{2+}-sensitive dye Fura-2AM to monitor changes in $[Ca^{2+}]_c$. In these experiments, where indicated, short pulses of 30μM NMDA (plus 10μM glycine) were applied to neurons. Following recovery of $[Ca^{2+}]_c$ after the first NMDA pulse, neurons were treated with either vehicle (A, DMSO, 0.1%), 10μM tat-CBD3 (C), or 10μM CBD3 (D) as indicated. Then, one or two more NMDA pulses were applied. In B, before the second NMDA pulse, neurons were treated with 20μM AP-5 as a positive control. In E, the summary graph shows changes in average peak cytosolic Ca^{2+} concentration under different conditions. #p<0.01 compared to $[Ca^{2+}]_c$ before treatment (NT, non-treated cells). N=5 separate, individual experiments, total number of analyzed neurons is 217. *p<0.01 compared to changes in average peak $[Ca^{2+}]_c$ in NMDA-treated cells. N=5 separate, individual experiments; total number of analyzed neurons is 205.

These data suggest that tat-CBD3 interacts with an intracellular target to reduce NMDA-induced increases in cytosolic Ca^{2+} concentration.

c. CRMP2 interacts with NR2B-NMDAR and tat-CBD3 disrupts this interaction

Inhibition of NMDAR activity by tat-CBD3 suggested a direct interaction between CRMP2 and NMDAR. Therefore we asked if CRMP2 interacts with NMDAR and if tat-CBD3 disrupts this interaction. We used co-IP experiments to examine an interaction between CRMP2 and NMDAR. Probing for the NR2B subunit of NMDAR, shown previously to be involved in excitotoxicity (Zhou & Baudry, 2006; Liu *et al.*, 2007), we found an interaction between CRMP2 and NR2B-containing NMDARs (Fig. 22A). This is consistent with previous findings (Al-Hallaq *et al.*, 2007). Moreover, tat-CBD3 disrupted the interaction between CRMP2 and NMDAR (Fig. 22A). These data suggest that CRMP2 regulates NMDAR activity via binding to the NR2B subunit and tat-CBD3-mediated dissociation of CRMP2 from NMDAR leads to decreased NMDAR activity.

d. CRMP2 is not required for NMDAR localization to the membrane

Another possibility to explain the impact of CRMP2 on NMDAR activity is that CRMP2 anchors NMDAR to the plasma membrane. If this is how the interaction works, disruption of the interaction between CRMP2 and NMDAR should lead to NMDAR internalization.

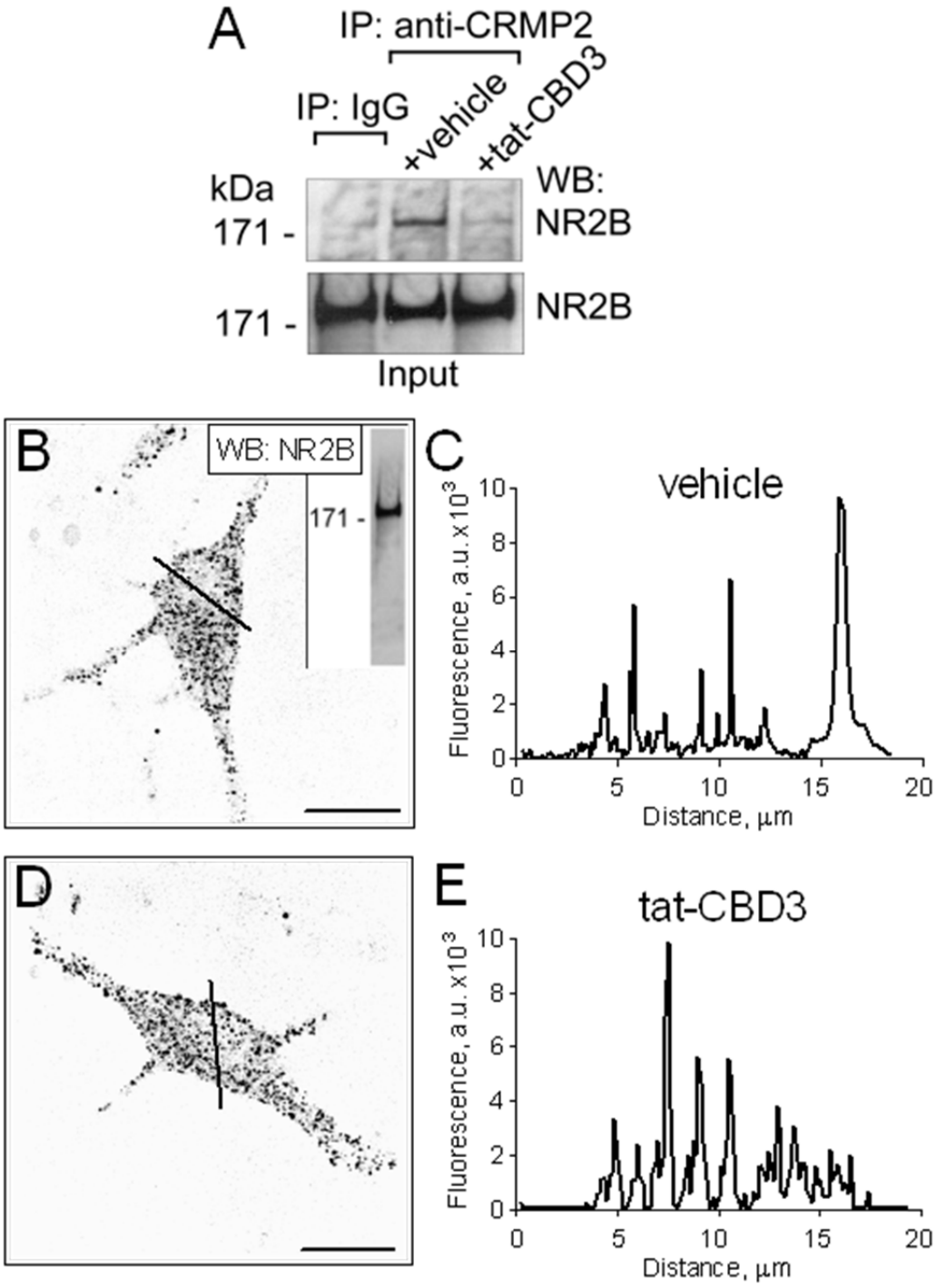
A
IP: anti-CRMP2
IP: IgG
+vehicle
+tat-CBD3
kDa
171 -
WB:
NR2B
171 -
NR2B
Input
B
WB: NR2B
171 -
C
vehicle
Fluorescence, a.u. x10³
Distance, µm
D
E
tat-CBD3
Fluorescence, a.u. x10³
Distance, µm

Figure 22.

Figure 22. Tat-CBD3 disrupts CRMP2 interaction with NR2B-NMDAR, but does not cause NMDAR re-localization. In A, immunoprecipitation was performed with IgG or anti-CRMP2 antibody (Sigma-Aldrich) followed by western blotting with anti-NR2B antibody (BD Biosciences). Where indicated, prior to immunoprecipitation cells were incubated with a vehicle (0.1% DMSO) or 10μM tat-CBD3 for 10 minutes. In B and D, confocal, inverted fluorescence images of representative neurons stained with anti-NR2B antibody (BD Bioscience). In C and E, fluorescence intensity profiles for straight lines in panels B and D, respectively. N=3 separate, individual experiments. The *Inset* in B shows western blot produced with cell lysate and anti-NR2B antibody (BD Bioscience) to illustrate antibody specificity. Scale bars are 15 μm.

Internalization of NMDAR could explain tat-CBD3-evoked suppression of NMDAR activity. We asked if CRMP2 interaction with NMDAR is required for NMDAR membrane localization. To test this possibility, we used immunocytochemistry in conjunction with confocal fluorescent microscopy. Figure 22B-E shows representative inverted fluorescent images and fluorescence intensity profiles for the respective images. All analyzed cells, regardless of treatment, had similar patterns of NR2B distribution (Fig. 22, B, D). NMDARs appear to be localized at the plasma membrane as well as the cytoplasm. The cytoplasmic localization is likely internalized NMDAR (Fig. 22B-E). These patterns of localization are consistent with previous reports of NMDAR distribution (Hallett *et al.*, 2006). The monoclonal anti-NR2B antibody used in these experiments detected only a single band in immunoblotting experiments (Fig. 22B, *Inset*) indicating specificity. This assures that immunostaining shown in Fig. 22B,D is due to NR2B NMDARs. These data suggest that disruption of CRMP2 interaction with NR2B affects NMDAR activity without altering its localization in the plasma membrane.

e. NCX_{rev} is decreased by tat-CBD3

Our laboratory has shown that inhibition of both NMDAR and NCX_{rev} is required for ablation of glutamate-induced Ca^{2+} dysregulation (Brittain *et al.*, 2012b). Based on these findings and the results show in Figure 20, we hypothesized that tat-CBD3, in addition to inhibiting NMDAR, also inhibits NCX_{rev}.

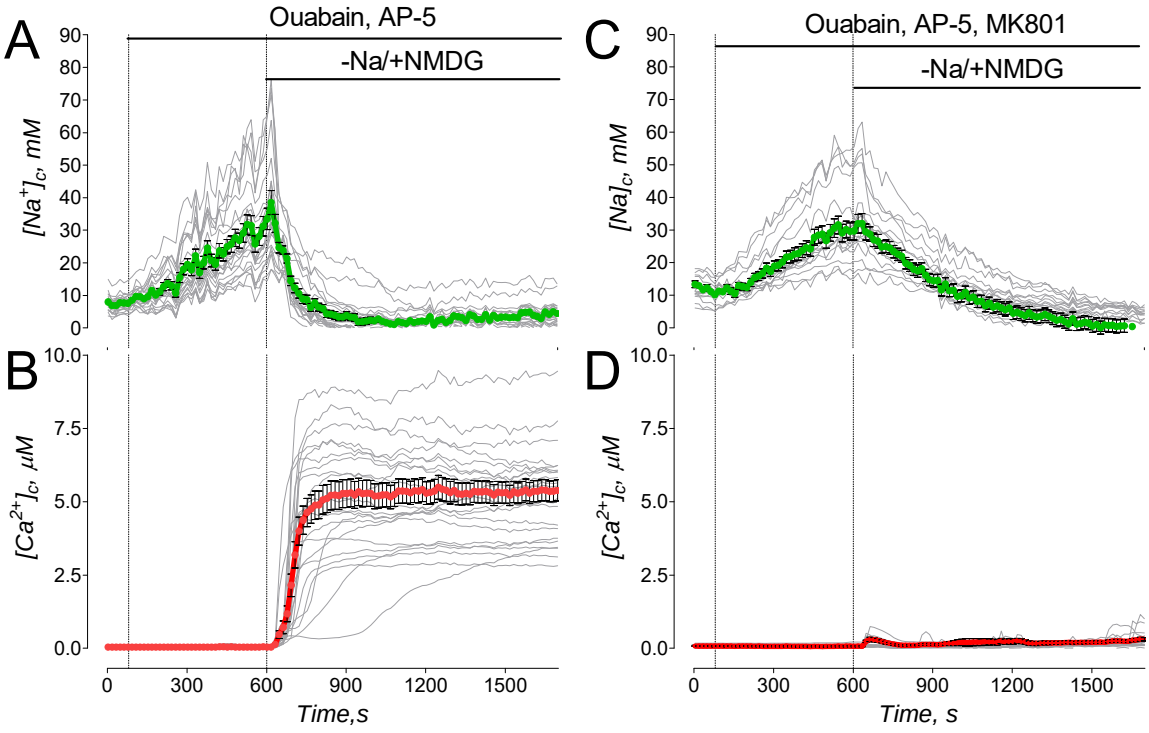

Figure 23. Na^+/NMDG replacement in the bath solution induces reversal of Na^+/Ca^{2+} exchanger. Neurons were co-loaded with a Na^+-sensitive dye SBFI-AM (A and C) and Ca^{2+}-sensitive dye Fluo-4FFAM (B and D). Measurements of cytosolic Ca^{2+} and Na^+ were performed simultaneously. The thin, grey traces show fluorescent signals from individual neurons. The thick, red traces represent cytosolic Ca^{2+} mean±SEM whereas thick, green traces represent cytosolic Na+ mean±SEM from individual experiments (n=20-25 neurons per experiment). The bath solution was supplemented with 5μM nifedipine to block L-type voltage-gated Ca^{2+} channels, 1μM tetrodotoxin (TTX) to block Na^+ channels, and 20μM AP-5, to antagonize NMDA receptor. To elevate cytosolic Na^+, neurons were pre-incubated for 10 minutes with 1 mM ouabain (Ouab). Ouabain remained in the bath solution throughout the experiment. Where indicated, Na+ was replaced by equimolar NMDG to trigger NCX reversal. In C and D, 10μM MK801, an inhibitor of reverse NCX (12), was applied to link Na^+/NMDG-induced increase in cytosolic Ca^{2+} to NCX_{rev} activity. N=5 separate, individual experiments; total number of analyzed neurons is 121.

To examine NCX_{rev} activity, we induced NCX reversal by replacing external Na^+ for equimolar N-methyl-D-glucamine (NMDG). Prior to Na^+/NMDG replacement, neurons were incubated with ouabain (1 mM), an inhibitor of Na^+/K^+-ATPase, for 10 minutes to increase cytosolic Na^+ and thus facilitate NCX reversal.

The Na^+/NMDG replacement produced an increase in cytosolic Ca^{2+} and a decrease in cytosolic Na^+ (Fig. 23A,B). Since Na^+/NMDG replacement could evoke release of endogenous glutamate (Brittain *et al.*, 2012a), these experiments were performed in the presence of AP-5 (20μM) to prevent activation of NMDAR and exclude Ca^{2+} influx via this mechanism. Our laboratory has also previously demonstrated that MK801, an NMDAR antagonist, inhibits NCX_{rev} (Brittain *et al.*, 2012b). In these experiments we used MK801 to demonstrate inhibition of NCX_{rev}. Application of MK801 completely inhibited Na^+/NMDG-induced increase in cytosolic Ca^{2+} concentration and slowed a decrease in cytosolic Na^+ concentration (Fig. 23 C,D), implicating NCX_{rev} in these ion alterations. Thus, in our experiments Na^+/NMDG replacement caused an increase in cytosolic Ca^{2+} due to a reversal of NCX.

Next we use the protocol to induce NCX_{rev} shown in Fig. 23 along with application of various treatments. Tat-CBD3 strongly inhibited the Na^+/NMDG-induced increase in cytosolic Ca^{2+} compared with vehicle treatment (Fig. 24A,B). Tat-CBD3 A6K, a mutated version of CBD3 that demonstrated increased conformational stability (Piekarz *et al.*, 2012), also significantly inhibited Na^+/NMDG-induced increase in cytosolic Ca^{2+} concentrations (Fig. 24C).

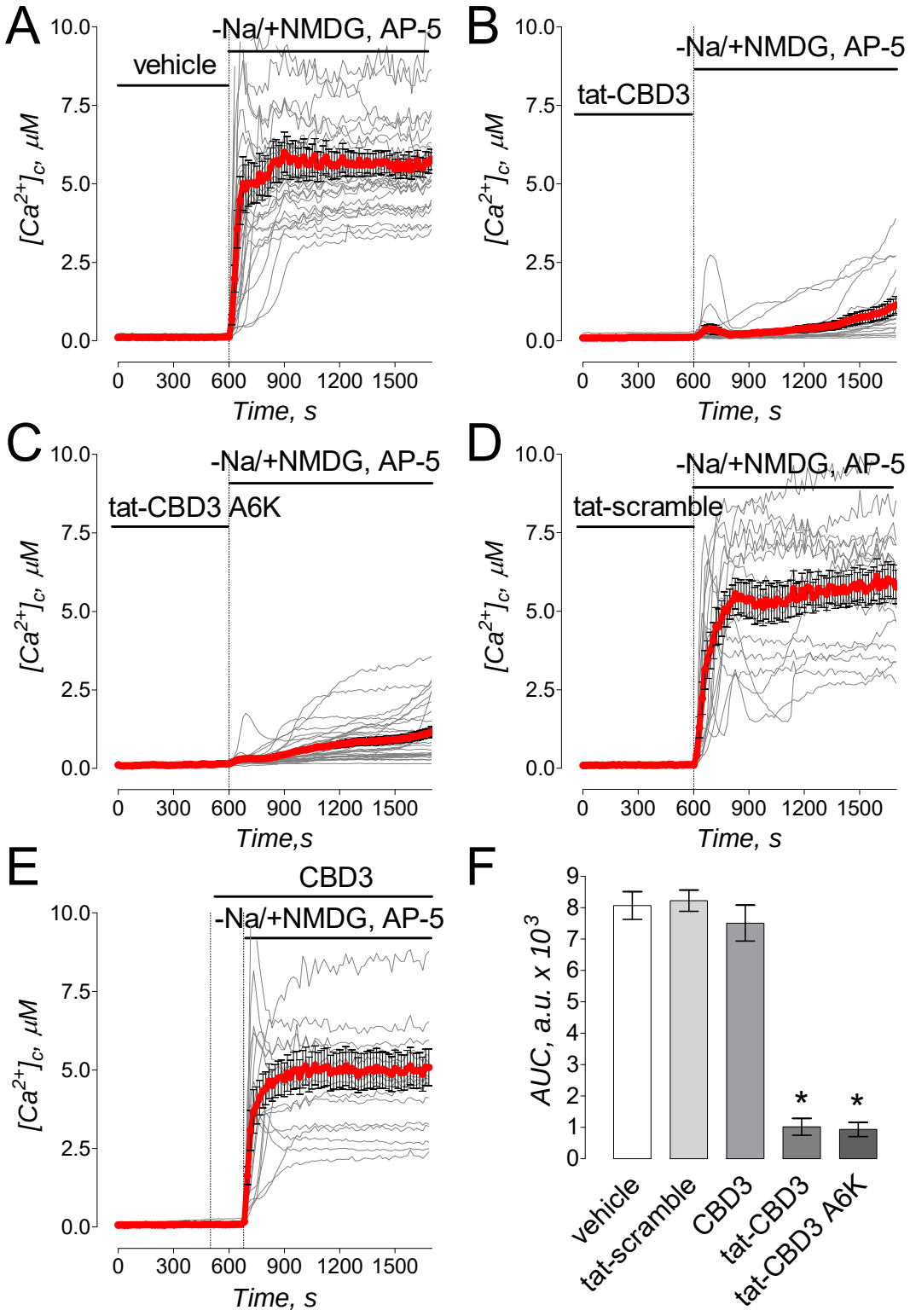
A
vehicle
-Na/+NMDG, AP-5
B
tat-CBD3
-Na/+NMDG, AP-5
C
tat-CBD3 A6K
-Na/+NMDG, AP-5
D
tat-scramble
-Na/+NMDG, AP-5
E
CBD3
-Na/+NMDG, AP-5
F
[Ca2+]c, μM
Time, s
AUC, a.u. x 10^3
vehicle
tat-scramble
CBD3
tat-CBD3
tat-CBD3 A6K

Figure 24.

Figure 24. Na^+/Ca^{2+} exchanger reversal induced by Na^+/NMDG replacement is inhibited by tat-CBD3. Neurons were loaded with Fura-2FF-AM. Where indicated, neurons were treated either with vehicle (A), 10μM tat-CBD3 (B), 10μM tat-CBD3 A6K (C), or 10μM tat-scramble peptide (D) for 10 minutes prior to NCX reversal induced by Na^+/NMDG replacement. In E, neurons were treated with 10μM CBD3 and the peptide remained in the bath solution throughout the experiment. The bath solution was supplemented with 5μM nifedipine, 1μM TTX, and 20μM AP-5. In addition, neurons were preincubated for 10 minutes with 1 mM ouabain (Ouab). Ouabain remained in the bath solution throughout the experiment. In F, the summary graph shows the average area under the curve (AUC; a.u., arbitrary units) that represents a measure of $[Ca^{2+}]_c$ increase over time. Under each experimental condition, the AUC was calculated for the same time (1080 seconds) following Na^+/NMDG replacement. Data are mean±SEM, **p*<0.01 comparing tat-CBD3-, tat-CBD3 A6K- and vehicle-treated neurons. N=4 separate, individual experiments with each condition; total number of analyzed neurons is 404.

Tat-scramble peptide and CBD3 alone were without effect (Fig. 24D,E). Figure 24F shows a summary of the data, expressed as average AUC, obtained with Na^+/NMDG-induced increases in cytosolic Ca^{2+} and the effects of various peptides. These data suggest that tat-CBD3 inhibits NCX_{rev}.

To further investigate NCX_{rev} activity we used electrophysiology. Since Na^+/Ca^{2+} exchange is electrogenic, it is possible to record ion currents mediated by NCX (Kimura *et al.*, 1986; Mechmann & Pott, 1986). This approach was first used in experiments with cardiomyocytes (Convery & Hancox, 1999; Smith *et al.*, 2006) but as also been adapted to neurons in culture (Brustovetsky *et al.*, 2011; Brittain *et al.*, 2012a; Brittain *et al.*, 2012b). The exchange of Na^+ for Ca^{2+} results in a net outward current, which can be used as a measure of NCX_{rev} activity (Brittain *et al.*, 2012b). In Fig. 21A we used Ni^{2+}, an NCX inhibitor (Convery & Hancox, 1999; Smith *et al.*, 2006), as a positive control. Application of 5mM Ni^{2+} significantly decreased (by 62 ± 7%, N=5) the peak ion current generated by the voltage ramp, which indicates that the current is predominantly mediated by NCX_{rev}. Tat-CBD3 (10μM), but not tat-scramble (10μM), applied to neurons for 5 minutes, also significantly attenuated the peak ion current (by 53±6%, N=5), this suggests that CRMP2 regulates NCX_{rev} activity (Fig. 25B,C). Peak currents are summarized in Fig. 25D. These data further suggest that tat-CBD3 decreases NCX_{rev}.

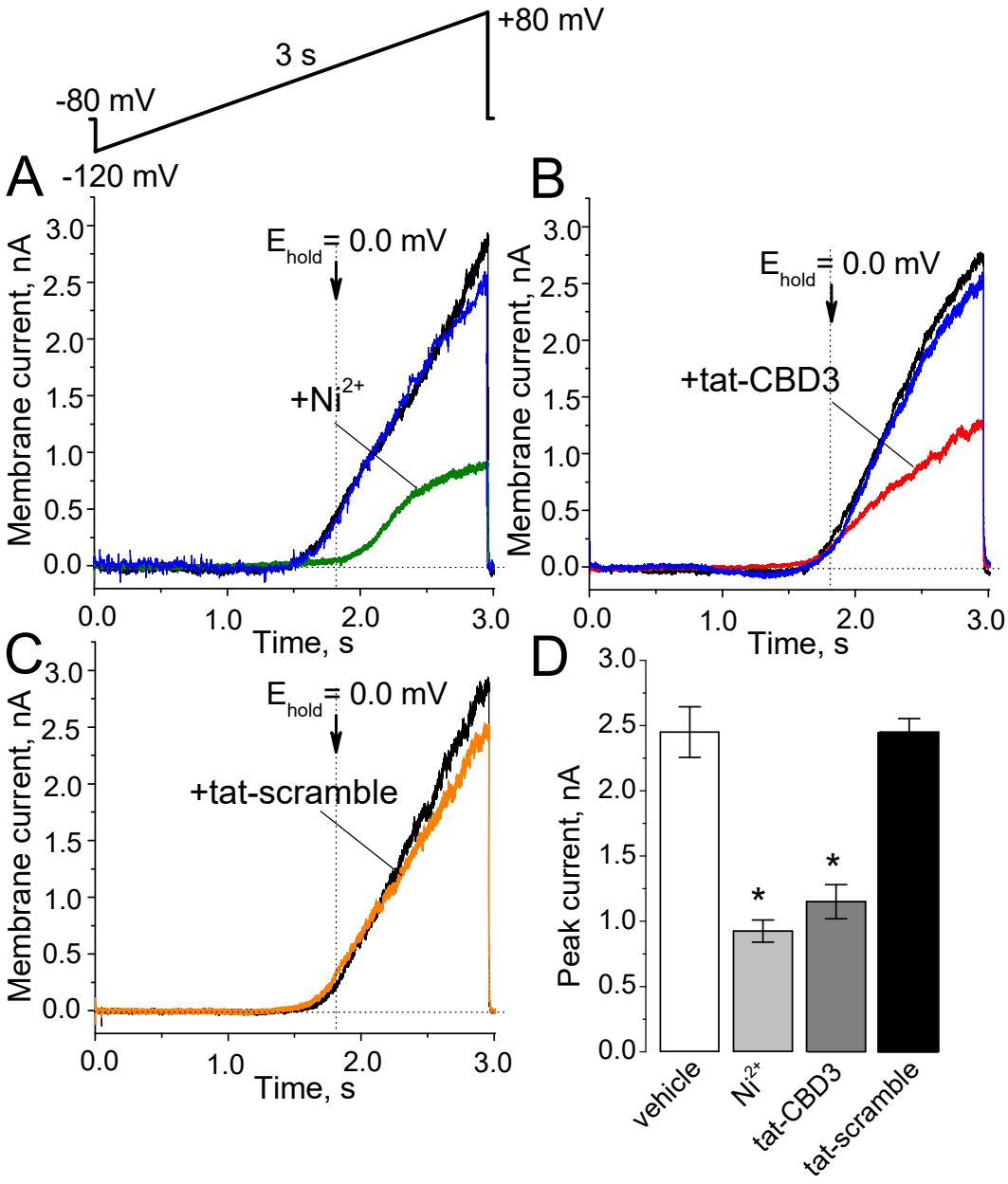

Figure 25. Ni^{2+} and tat-CBD3, but not tat-scramble peptide, suppress ion currents mediated by NCX_{rev}. In A, the ascending voltage ramp protocol employed in these experiments and current traces obtained in the absence (black and blue) and in the presence of 5 mM Ni^{2+} (green) applied to neurons 2 minutes prior to the voltage ramp. In B and C, current traces obtained with untreated neurons (black and blue) and neurons treated with either 10μM tat-CBD3 (B, red trace) or 10μM tat-scramble (C, orange trace) applied 5 minutes prior to the voltage ramp. In D, the summary graph shows changes in the peak ion current under different conditions. *p<0.05 compared to vehicle-treated cells (vehicle). N=5. Kindly provided by Xiao-Fang Yang, Khanna Laboratory.

f. CRMP2 directly interacts with NCX3 and tat-CBD3 strengthens this interaction

To examine how CRMP2 regulates NCX activity and because CRMP2 has been shown to interact with $CaV_{2.2}$ (Brittain *et al.*, 2011b) and NMDAR (Fig. 22) we asked if CRMP2 also interacts with NCX. We used co-IP experiments to investigate an interaction.

We found no evidence for interaction of NCX1 with CRMP2 (Fig. 26A). However, CRMP2 did co-immunoprecipitate with NCX3 (Fig. 26B, C), suggesting a physical interaction between these proteins. Surprisingly, application of tat-CBD3 increased the interaction between CRMP2 and NCX3 interaction instead of disrupting an interaction. Tat-scramble was without effect (Fig. 26C). These data suggest that CRMP2 interacts with NCX3 and could regulate NCX activity.

g. Increased interaction between NCX and CRMP2 leads to NCX3 internalization

In Figure 22, we showed that tat-CBD3 disrupts the interaction between CRMP2 and NMDAR. NMDAR interaction did not alter NMDAR surface expression. Surprisingly, application of tat-CBD3 enhanced the interaction between CRMP2 and NCX3. Therefore, we asked if the increased interaction of CRMP2 and NCX3 caused an increase in NCX3 surface expression. We used immunocytochemistry experiments to examine the expression of NCX3. Neurons were treated and then analyzed using confocal microscopy. Figure 27 shows representative inverted fluorescent images and fluorescence intensity profiles for

the respective images. In vehicle-treated neurons, NCX3 was found to be localized in both plasma membrane and to a lesser extent in the cytoplasm (Fig. 27A,B). The cytoplasmic localization of NCX3 most likely reflects a pool of internalized NCX. The specificity of the anti-NCX3 antibody used in these experiments is demonstrated in the inset of Fig. 27A. This selectivity assures that immunostaining shown in Fig. 27A,C,E is exclusively due to NCX3.

Interestingly, we found that treatment with tat-CBD3 lead to internalization of NCX3, resulting in a decreased expression in the plasma membrane (Fig. 27C,D). Tat scramble did not change NCX3 localization (Fig. 27E,F). These data suggest that increased interaction between CRMP2 and NCX3 leads to internalization.

h. CRMP2 is necessary for tat-CBD3 induced internalization of NCX3 and inhibition of NCX_{rev}

The internalization of NCX3 induced by tat-CBD3 likely explains the decrease in NCX_{rev} activity following pre-incubation with tat-CBD3. Next we asked if CRMP2 was required for NCX3 internalization. To examine the link between CRMP2 and tat-CBD3-triggered NCX3 internalization, we downregulated CRMP2, using siRNA. Neurons were transfected during plating with both a GFP construct and siRNA against CRMP2. Neurons expressing GFP had an almost complete lack of CRMP2 (Fig. 28A-D). In all analyzed neurons (N=21), expression of GFP corresponded with significant CRMP2 downregulation.

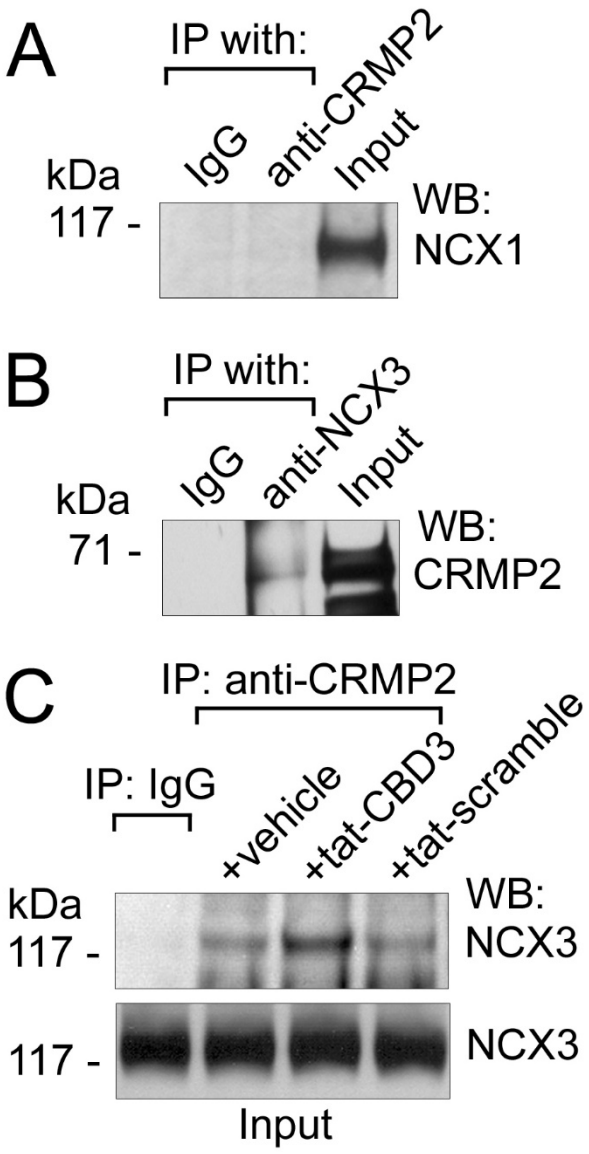

Figure 26. **CRMP2 co-immunoprecipitates with NCX3, but not with NCX1. Tat-CBD3 strengthens CRMP2-NCX3 interaction.** In A, immunoprecipitation was performed with IgG or anti-CRMP2 antibody followed by western blotting with anti-NCX1 antibody. In B, immunoprecipitation was performed with IgG or anti-NCX3 antibody followed by western blotting with anti-CRMP2 antibody. In C, prior to immunoprecipitation, where indicated, neurons were incubated either with 10μM tat-CBD3 or 10μM tat-scramble peptide for 10 minutes. Each experiment was repeated three times.

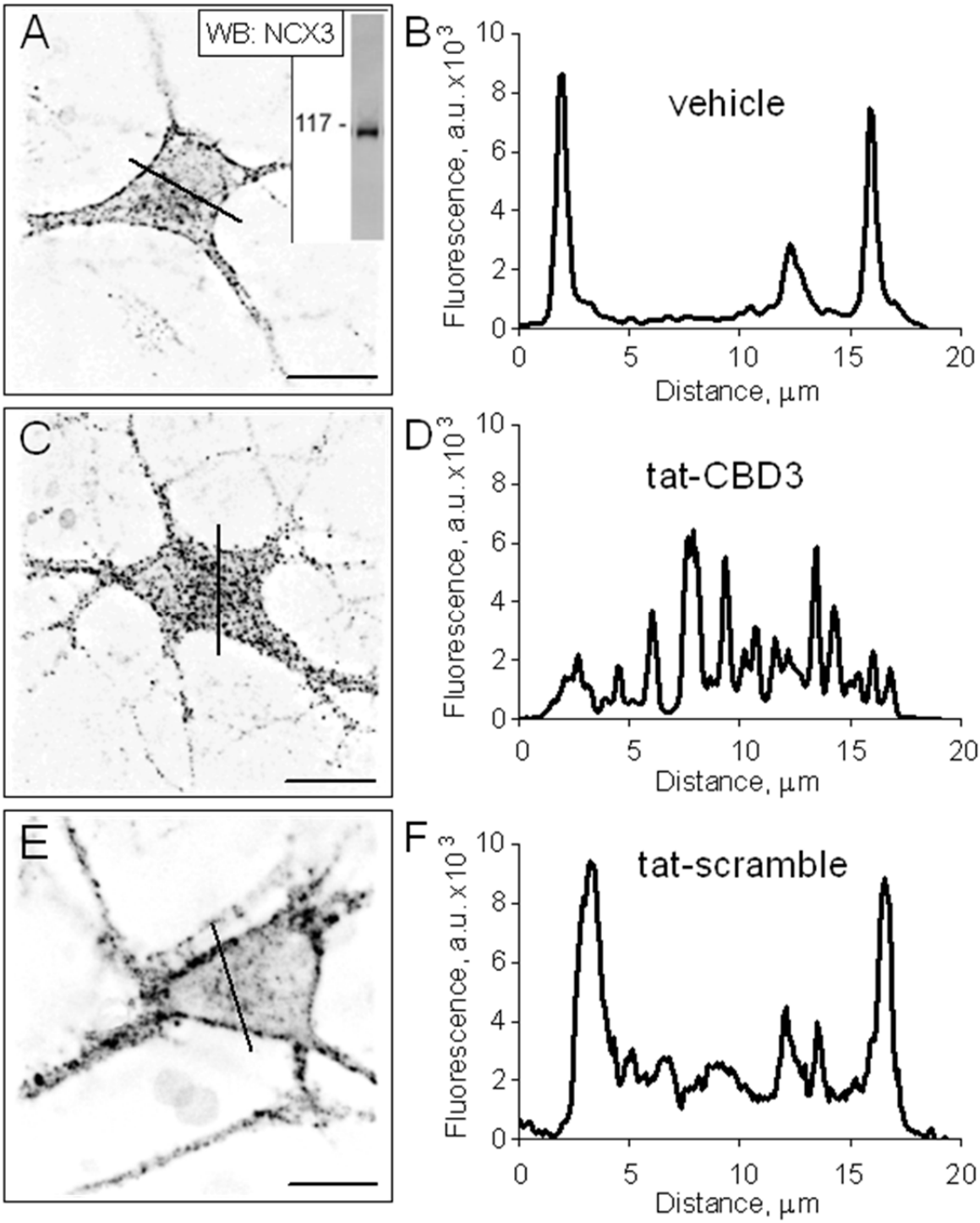
A
WB: NCX3
117 -
B
vehicle
Fluorescence, a.u. x10^3
Distance, µm
C
D
tat-CBD3
Fluorescence, a.u. x10^3
Distance, µm
E
F
tat-scramble
Fluorescence, a.u. x10^3
Distance, µm

Figure 27.

Figure 27. Tat-CBD3 triggers NCX3 internalization. In A, C, and E, confocal, inverted fluorescence images of representative neurons stained with anti-NCX3 antibody. In B, D, and F, fluorescence intensity profiles for straight lines in panels A, C, and E, respectively. N=3 separate, individual experiments. Total number of analyzed neurons is 59 (vehicle-treated), 65 (tat-CBD3-treated) and 51 (tat-scramble-treated). The *Inset* in A shows western blot produced with cell lysate and anti-NCX3 antibody (provided by Drs. Kenneth Philipson and Michela Ottolia, UCLA) to illustrate antibody specificity. Scale bars are 15 μm.

We compared NCX3 expression in non-transfected with transfected cells. NCX3 expression pattern did not differ regardless of transfection (Fig. 28E-H and I,L). Importantly, pre-treatment with tat-CBD3 did not induce internalization of NCX3 in neurons with downregulated CRMP2 (Fig. 28 I-L). Furthermore, GFP transfection alone (Fig. 29) did not alter CRMP2 expression.

Next, we asked if CRMP2 is required tat-CBD3 inhibition of NCX_{rev} activity. We investigated this by downregulating CRMP2 and inducing NCX_{rev}. Application of tat-CBD3 robustly attenuated NCX_{rev} in neurons with CRMP2 (black traces, Fig. 30E) but not in neurons with downregulated CRMP2 (Fig. 30B, green trace, Fig. 30E). The results of these experiments taken together suggest that CRMP2 is necessary for tat-CBD3-induced internalization of NCX3 and subsequent inhibition of NCX_{rev}.

i. NCX_{for} is decreased by tat-CBD3 application

Our data show that the increased CRMP2 association with NCX3 correlates with tat-CBD3-induced NCX3 internalization and subsequent inhibition of NCX_{rev}. Internalization of NCX3 should, in addition to inhibition of NCX_{rev} activity, also decrease NCX_{for}. To test this hypothesis, we treated neurons with ionomycin (5μM), a Ca^{2+} ionophore. Ionomycin caused delayed Ca^{2+} dysregulation in neurons (Fig. 31A), demonstrating that neurons effectively fight against elevations in cytosolic Ca^{2+}. NCX_{for} cannot function in the absence of external Na^{+} (Annunziato *et al.*, 2004).

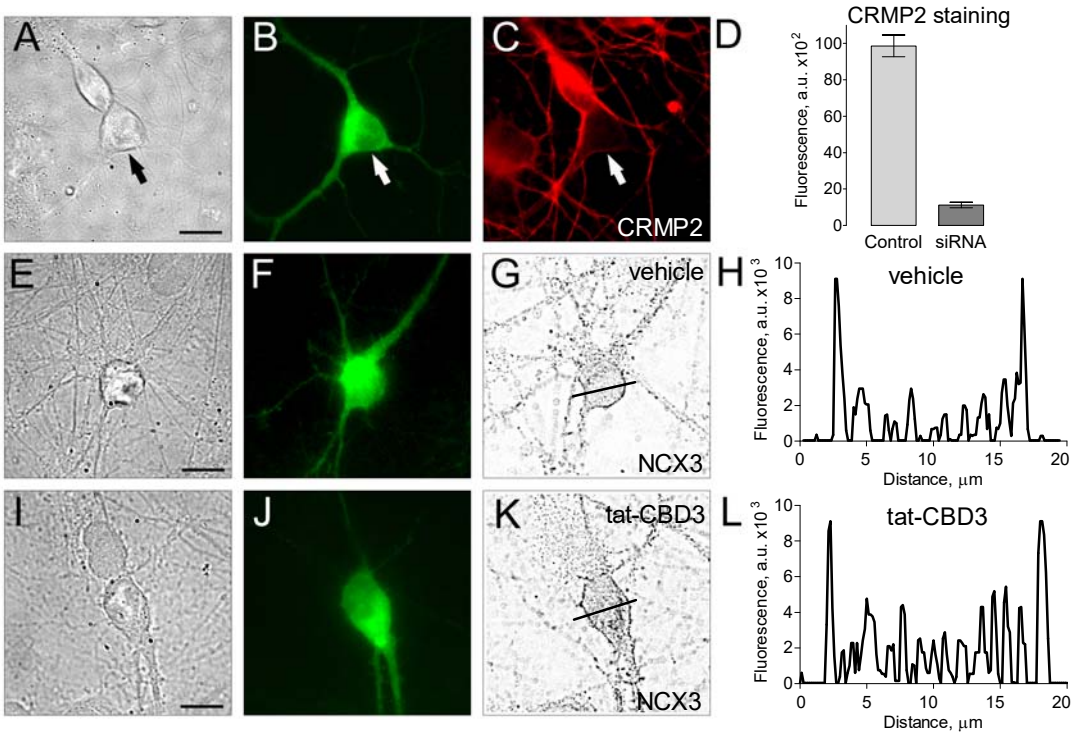

Figure 28. CRMP2 downregulation prevents tat-CBD3-induced NCX3 internalization. Neurons were transfected during plating with a GFP construct and siRNA against CRMP2. In A-C, a representative experiment is shown: A – bright field, B – GFP fluorescence, C – CRMP2 immunostaining. In this experiment, neuron without GFP has robust CRMP2 expression whereas neuron with GFP fluorescence demonstrates significantly decreased CRMP2 expression (marked by arrow). In D, a summary of CRMP2 expression measurements based on fluorescence intensity measurements. The fluorescence measurements were performed in somata of individual neurons, using 3x3μm region of interest. The fluorescence intensity is expressed in arbitrary units (a.u.). The data are mean±SEM, N=21. In E-G, a representative experiment without tat-CBD3 pre-treatment is shown: E – bright field, F – GFP fluorescence, G – NCX3 immunofluorescence (inverted). In H, fluorescence intensity profile for a straight line in panel G. In these experiments, 18 cells were analyzed; each cell had a similar pattern of NCX3 distribution. In I-K, a representative experiment with 10μM tat-CBD3 pre-treatment for 10 minutes: I – bright field, J – GFP fluorescence, K – NCX3 immunofluorescence (inverted). In L, fluorescence intensity profile for a straight line in panel K. In these experiments, 24 cells were analyzed; each cell had a similar pattern of NCX3 distribution. Scale bars are 15 μm.

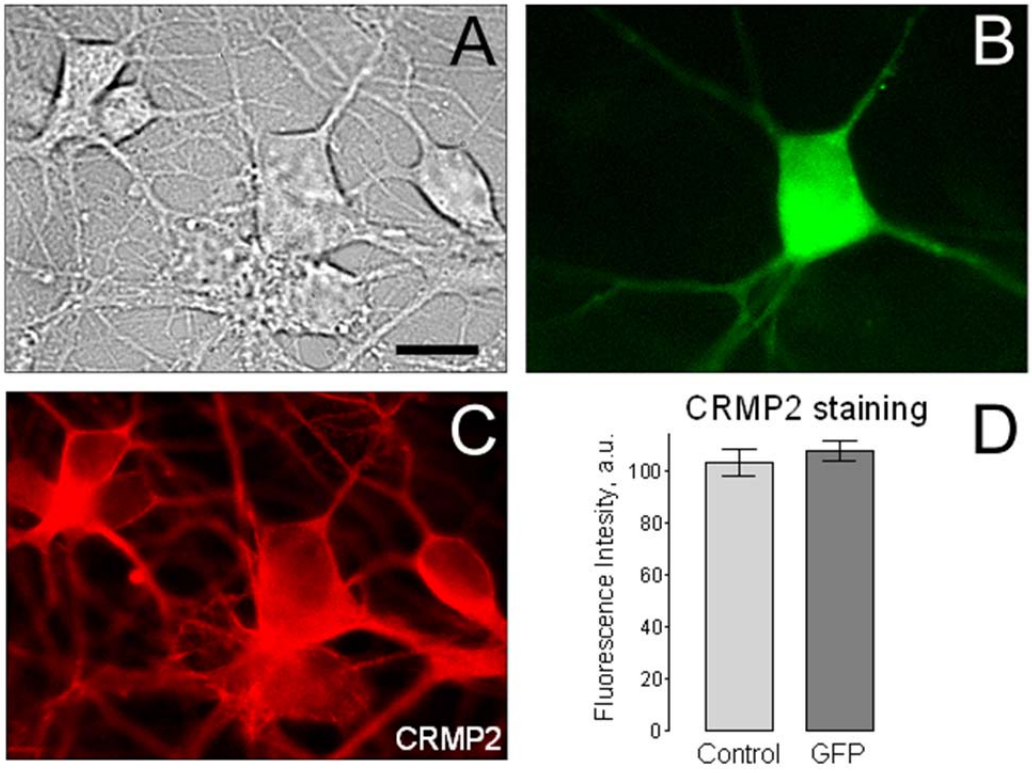

Figure 29. **GFP transfection does not alter CRMP2 expression.** Neurons were transfected during plating with a GFP construct. In A, a representative bright field, B, GFP fluorescence, and C, CRMP2 immunostaining. In this experiment, the neuron expressing GFP has robust CRMP2 expression similar to those without GFP expression. In D, a summary of CRMP2 expression measurements based on fluorescence intensity measurements. The fluorescence measurements were performed in somata of individual neurons, using 3x3μm region of interest. The fluorescence intensity is expressed in arbitrary units (a.u.). The data are mean±SEM, N=3. Scale bars are 15 μm

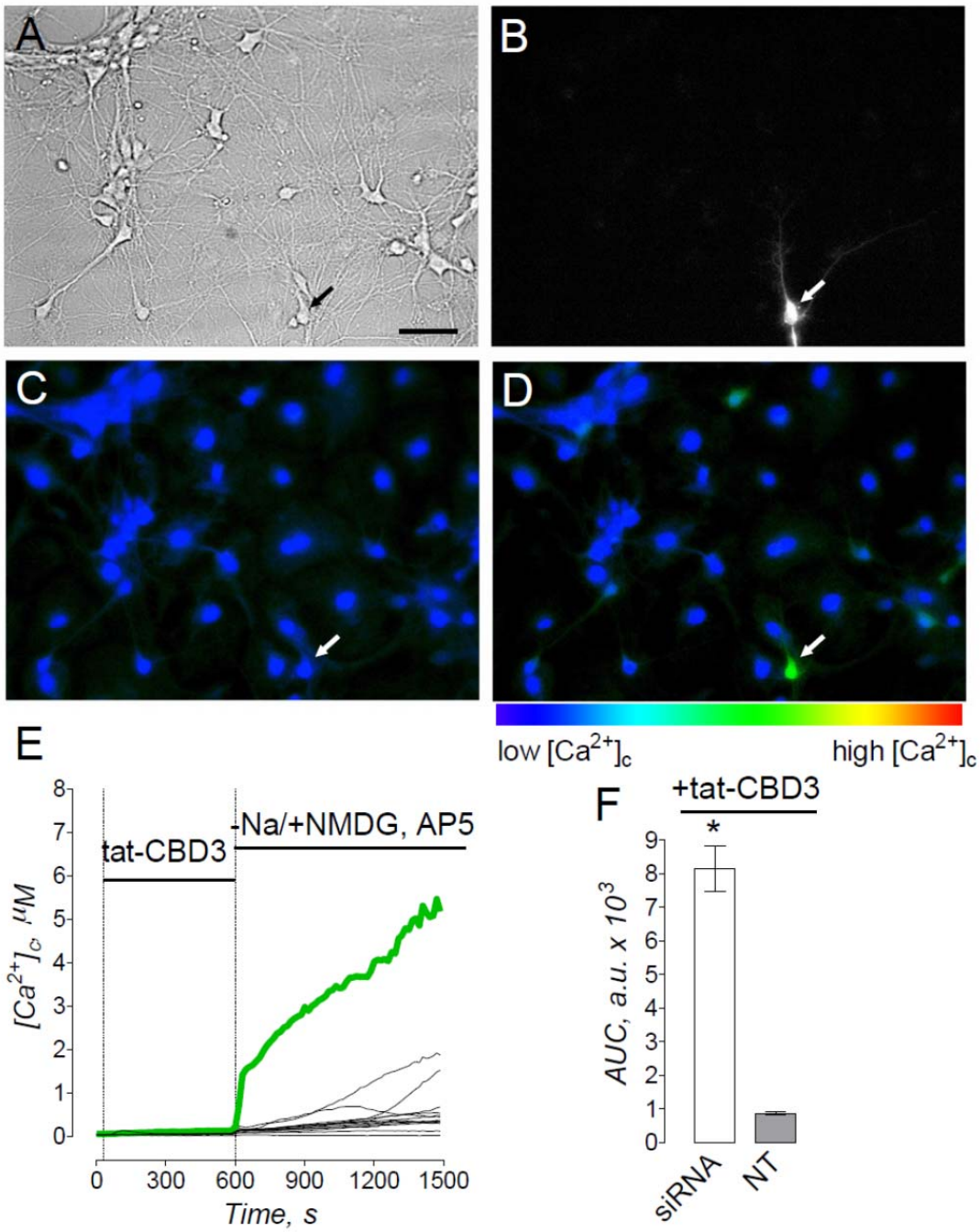
A
B
C
D
low [Ca2+]c
high [Ca2+]c
E
tat-CBD3
-Na/+NMDG, AP5
[Ca2+]c, μM
Time, s
F
+tat-CBD3
AUC, a.u. x 10^3
siRNA
NT

Figure 30.

Figure 30. CRMP2 downregulation strongly attenuates tat-CBD3-induced inhibition of NCX_{rev}. Neurons, transfected during plating with a GFP construct and siRNA against CRMP2, were loaded with Fura-2FF-AM. In **A-E**, a representative experiment is shown: **A** – bright field, **B** – GFP fluorescence, **C** – pseudocolored image of Fura-2FF F340/F380 ratio taken prior to Na+/NMDG replacement at 300 second, **D** – pseudocolored image of Fura-2FF F340/F380 ratio taken after Na+/NMDG replacement at 1500 second, **E** – changes in cytosolic Ca2+ concentration over time in the same experiment. Where indicated, neurons were treated with 10μM tat-CBD3 for 10 minutes. The bath solution was supplemented with 5μM nifedipine, 1μM TTX, and 20μM AP-5. In addition, neurons were pre-incubated for 10 minutes with 1 mM ouabain prior to Na+/NMDG replacement. Ouabain remained in the bath solution throughout the experiment. In **A**-**D**, arrows indicate a neuron that expresses GFP and has downregulated CRMP2. In **E**, green trace shows fluorescent signal from this neuron whereas black traces show fluorescent signals from other neurons in the field. In **F**, the summary graph shows the average area under the curve (AUC; a.u., arbitrary units) that represents a measure of $[Ca^{2+}]_c$ increase over time. Under each experimental condition, the AUC was calculated for the same time (900 seconds) following Na^+/NMDG replacement. Data are mean±SEM, *p<0.01 comparing siRNA-transfected (siRNA) and non-transfected (NT) neurons. N=3 separate, individual experiments; total number of analyzed neurons is 57. Scale bar in panel **A** is 30 μm and is applicable to panels **A**-**D**.

Therefore, to demonstrate the role of NCX_{for} in ionomycin-induced Ca^{2+} increase, we inhibited NCX_{for} activity by removing external Na^+ and replacing it with equimolar NMDG. This protocol differs from that used in Figure 23 by omitting ouabain from the bath solution. Cytosolic Na^+ remained low, so Na^+/NMDG replacement did not cause an increase in cytosolic Ca^{2+}.

These experiments were also performed in the presence of the NMDAR antagonist AP-5 (20μM), to exclude any contribution by NMDARs in ionomycin-induced Ca^{2+} increase. The removal of external Na^+ significantly accelerated the onset of ionomycin-induced Ca^{2+} dysregulation, illustrating a key role for NCX_{for} in maintaining low cytosolic Ca^{2+} (Fig. 31B). Treatment with tat-CBD3 significantly accelerated Ca^{2+} dysregulation in neurons treated with ionomycin (Fig. 31C). These data were quantified by measuring *the time from the beginning of ionomycin application to the onset of* Ca^{2+} *dysregulation* ($\boldsymbol{t}_{dys}$) (Fig. 31D). A similar approach has previously been used to provide analysis of glutamate-induced Ca^{2+} dysregulation (Brustovetsky *et al.*, 2009; Li *et al.*, 2009). These data, summarized in Fig. 27D, show that -Na^+/$NMDG^+$ replacement and tat-CBD3 treatment significantly accelerated the onset of Ca^{2+} dysregulation in neurons. These observations suggest that tat-CBD3 decreases NCX activity, regardless of the mode of operation, likely due to increased interaction between CRMP2 and NCX3 and subsequent NCX3 internalization.

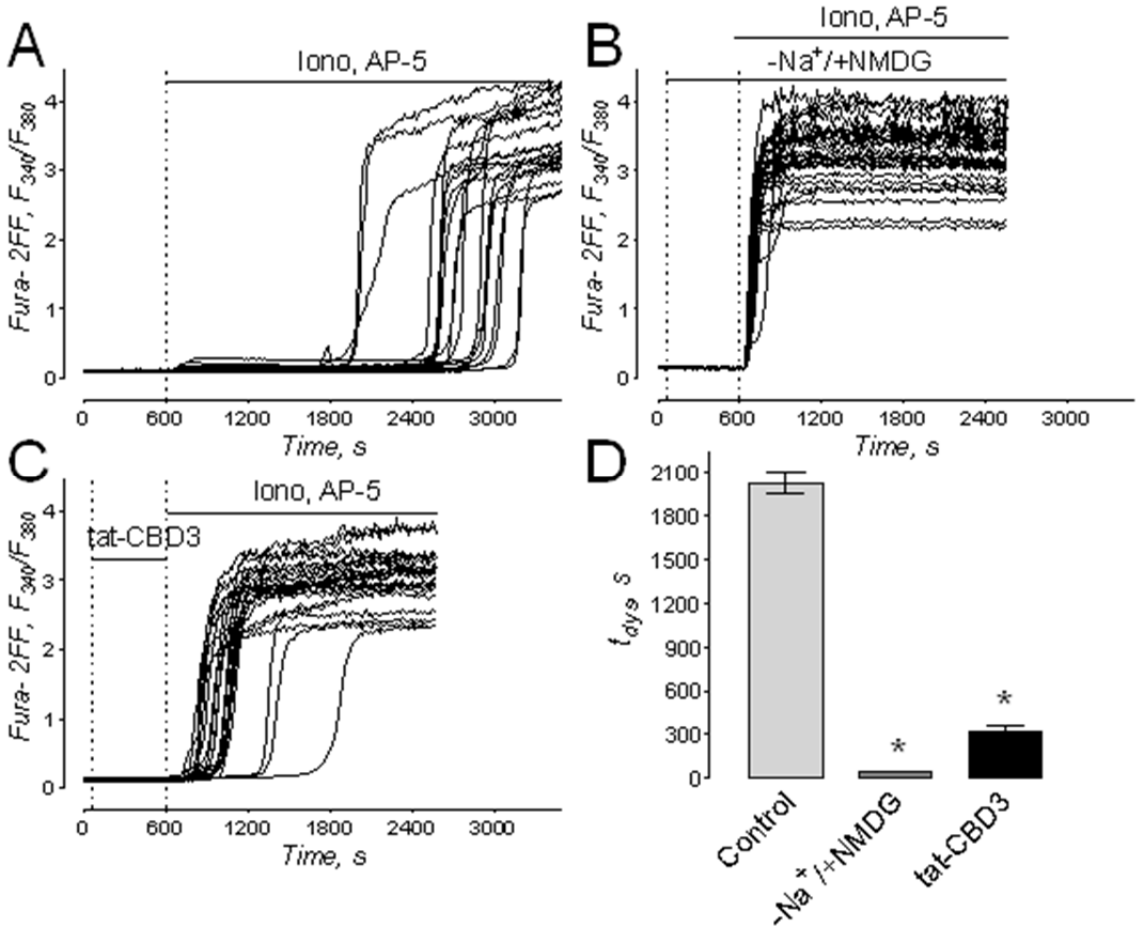

Figure 31. Tat-CBD3 inhibits the forward mode of NCX. Neurons were loaded with Fura-2FF. In A, 5μM ionomycin in combination with 20μM AP-5 was applied to neurons. Where indicated, neurons were subjected to Na^+/NMDG replacement (B) or treated with 10μM tat-CBD3 (C) for 10 minutes prior to addition of ionomycin. In D, the summary graph shows the time from the beginning of ionomycin application to the onset of Ca^{2+} dysregulation (t_{dys}) that reflects NCX_{for} activity. Data are mean±SEM, *p<0.01 comparing the effect of Na^+/NMDG replacement, tat-CBD3- and vehicle-treated neurons; N=5 separate, individual experiments; total number of analyzed neurons is 101.

j. CRMP2 expression is not altered in striata from YAC128 mice and CRMP2 does not interact with Htt or mHtt

Based on our findings that NMDAR and NCX are regulated by CRMP2, we next asked if CRMP2 expression is altered in YAC128 animals. We hypothesized that alteration in CRMP2 expression could alter NCX_{for} activity, leading to faster DCD (as demonstrated in Fig. 15). We used Western blotting to probe for CRMP2. We assessed CRMP2 protein levels in striatal lysate from both 3-week and 3-month-old mice. We found that CRMP2 expression is not altered in striata from either age WT mouse compared with age-matched YAC128 mice (Fig. 32). We showed that alterations in CRMP2 interaction (decreased, Fig. 18 or increased, Fig. 26) with NMDAR and NCX3 could regulate their activity. Therefore, we asked if mHtt interacts with CRMP2. We hypothesized that mHtt could compete with other CRMP2 interacting partners interfering with their interaction with CRMP2. We also investigated the interaction between WT Htt and CRMP2. The interaction between either form of Htt and CRMP2 using co-IP appeared to be below the limit of co-IP resolution (Fig. 32E). These data suggest that CRMP2 expression most likely is not altered by mHtt and that Htt, WT or mutant, may not interact with CRMP2. However, CRMP2 shares many common binding partners with mHtt and Htt. It is possible that CRMP2 does not directly interact with Htt or mHtt, but they interact with the same protein or proteins or as part of a complex. It is also possible that an interaction exists, but it is very weak, and is not captured using this methodology. Given these data, however, CRMP2

may not be involved in the increase in glutamate-induced DCD observed in Figure 15.

k. NCX3 interacts with mHtt and Htt

We showed in Figure 31 that increased CRMP2 interaction with NCX3 correlates with NCX3 internalization and decreased activity in both the reverse and forward modes. Using this model of NCX regulation, we asked if WT Htt or mHtt interacted with NCX1 or NCX3. We found that NCX1 did not interact with either form of Htt (Fig. 33 A). Interestingly, we found that NCX3 interacts with both WT Htt and mHtt (Fig. 33 B, C enlarged). An interaction has not been previously reported between Htt or mHtt and NCX3. These novel interactions could be responsible for additional regulation of NCX, but require further investigation.

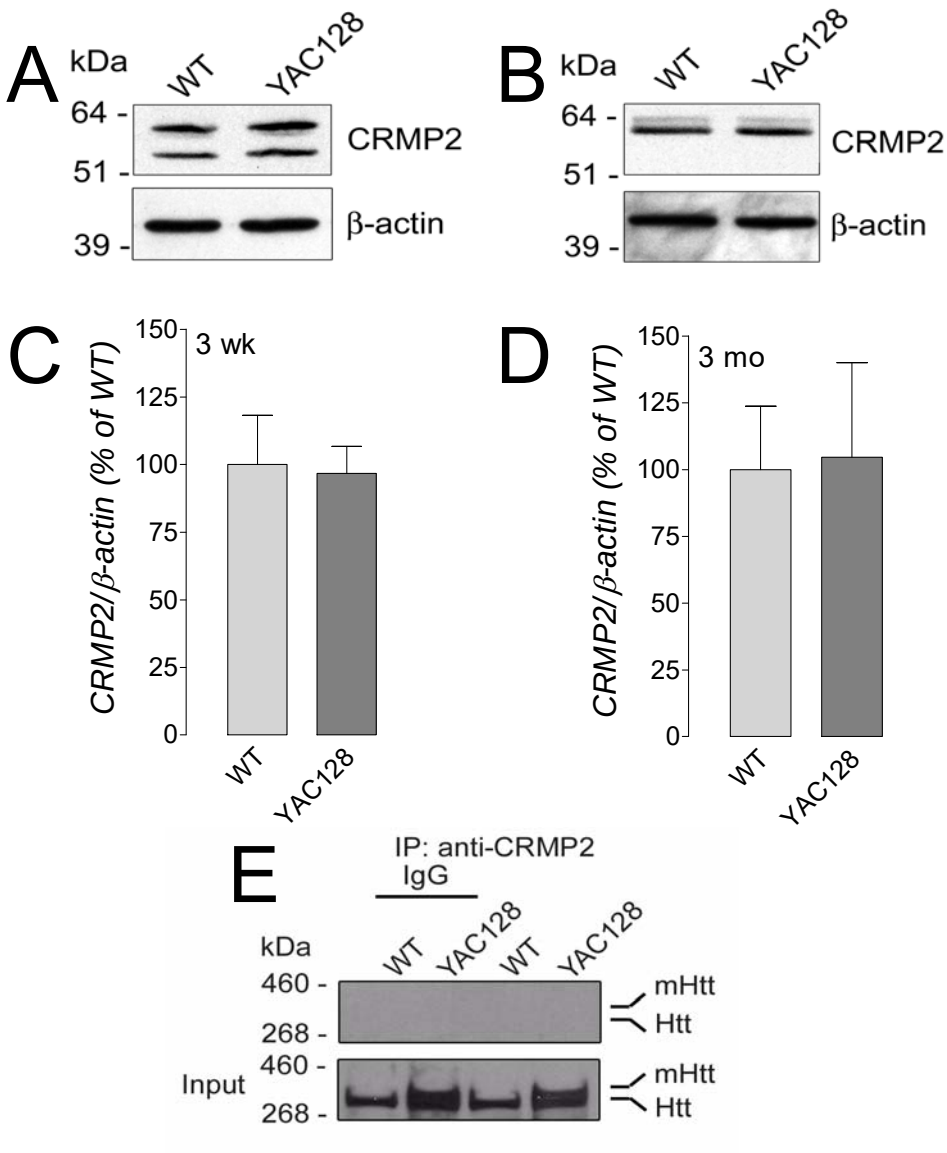

Figure 32. Expression of CRMP2 in striata from 3-week and 3-month-old YAC128 and WT mice. In A, Western blots of lysate from striata from 3-week-old (A,C) YAC128 and WT mice with anti-CRMP2 antibody. Lysate from striata from 3-month-old (B,D) YAC128 and WT mice are show in B. β-actin was used as a loading control. In C and D, statistical analysis of Western blot densitometry with data expressed as a percentage of WT. Data are mean±SEM, N=3. In E, immunoprecipitation was performed with IgG or anti-CRMP antibody followed by Western blotting with 2166 antibody, which recognizes both Htt and mHtt.

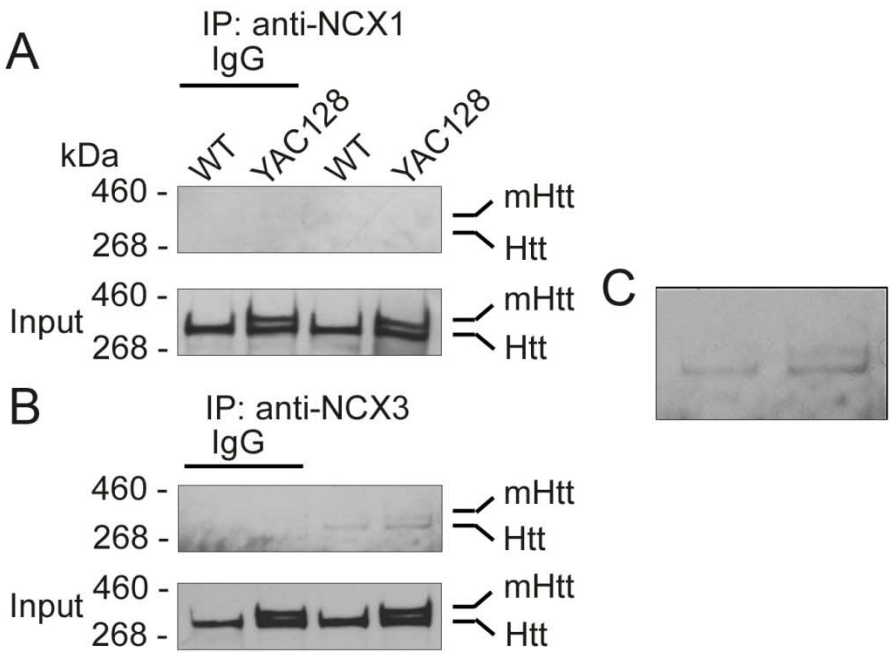

Figure 33. **Htt and mHtt co-immunoprecipitate with NCX3, but not with NCX1.** In A, immunoprecipitation was performed with IgG or anti-NCX1 antibody followed by Western blotting with 2166 antibody, which recognizes both Htt and mHtt. In B, immunoprecipitation was performed with IgG or anti-NCX3 antibody followed by Western blotting with 2166 antibody. In C, a portion of B enlarged for better visualization of the bands corresponding with mHtt and Htt.

IV. DISCUSSION AND CONCLUSIONS

a. Mitochondrial Ca^{2+} uptake capacity is not decreased by mHtt

In earlier studies, mitochondrial dysfunction and a decreased ability of mitochondria to accumulate Ca^{2+} had been proposed to contribute to HD pathogenesis (Panov et al. 2002; Choo et al. 2004). In experiments with non-synaptic mitochondria, we and other investigators failed to find an increase in sensitivity to deleterious Ca^{2+} and instead observed an increase in resistance to Ca^{2+} that was manifested in reduced propensity to PTP induction and augmented Ca^{2+} uptake capacity (Brustovetsky *et al.*, 2005).

In the current work, we demonstrated that both synaptic and non-synaptic mitochondria isolated from YAC128 mice retain their ability to accumulate Ca^{2+} compared with mitochondria from WT animals. Moreover, synaptic mitochondria from 12-month-old YAC128 mice had larger Ca^{2+} uptake capacity compared with mitochondria from WT littermates and this correlated with an increased amount of mHtt associated with these mitochondria.

However, mHtt failed to reduce Ca^{2+} uptake capacity in brain mitochondria from YAC128 mice. On the contrary, the level of mHtt binding to mitochondria positively correlates with mitochondrial resistance to deleterious Ca^{2+}. In our experiments, we found that BSA increased Ca^{2+} uptake capacity of brain mitochondria isolated from both YAC128 mice and their WT littermates.

It is known that ROS production by mitochondria, oxidizing succinate, depends on the reverse electron flow in the mitochondrial electron transport chain that brings electrons back to Complex I. The reverse electron flow, in turn,

depends on mitochondrial membrane potential: hyperpolarization leads to an increase in reverse electron flow and, subsequently, to elevated ROS production (Korshunov *et al.*, 1998; Korshunov *et al.*, 1997). It is established that ROS increase propensity to PTP induction in mitochondria (Zoratti & Szabo, 1995). However, it is also known that free fatty acids (FFA) increase propensity of PTP induction as well (Zoratti & Szabo, 1995). BSA binds FFA (Spector, 1975) and exerts a strong protective effect against PTP (Wieckowski *et al.*, 2000).

Based on these observations, our data concerning BSA effects suggest that the protective action of BSA prevails over deleterious effect of augmented ROS generation. Panov et al. (2003) reported that 'the defect in Ca^{2+} handling in brain mitochondria was consistently observed only if brain mitochondria were isolated without BSA'. The authors presumed that BSA could displace mHtt from its binding sites on mitochondria. Our data do not support this hypothesis. We found that mHtt is associated with mitochondria, consistent with previous reports (Choo et al. 2004), but BSA does not displace mHtt from mitochondria.

In a previous study in our laboratory, we did not observe an increased predisposition to Ca^{2+}-induced PTP induction in striatal and cortical non-synaptic mitochondria from HD mice compared with mitochondria from WT littermates (Brustovetsky *et al.*, 2005). On the contrary, we found increased resistance to Ca^{2+} in striatal mitochondria exposed to mHtt. Other researchers also reported that non-synaptic mitochondria from R6/2 and YAC128 mice had increased Ca^{2+} uptake capacity compared with mitochondria from WT animals. Both our study (Brustovetsky *et al.*, 2005) and a study by Oliveira et al. (2007) suggested the

lack of mHtt-induced impairment of mitochondrial Ca^{2+} handling, argued against facilitation of PTP induction by mHtt, and did not support involvement of PTP in HD pathogenesis.

In our study, we did not find evidence of impaired Ca^{2+} uptake capacity in either synaptic or non-synaptic mitochondria from YAC128 mice. On the contrary, both types of mitochondria had increased Ca^{2+} capacity, especially, synaptic mitochondria from 12-month-old YAC128 mice. The mechanism underlying augmented Ca^{2+} uptake capacity of mitochondria that are associated with increased levels of mHtt remains unknown. At the moment, we can only speculate about a possible scenario. Mitochondrial Ca^{2+} uptake capacity mainly depends on the ability of mitochondria to resist an induction of the PTP (Chalmers and Nicholls 2003). Induction of the PTP causes mitochondrial depolarization that precludes further Ca^{2+} uptake and results in a release of previously accumulated Ca^{2+} (Rasola & Bernardi 2011).

FFA are effective activators of PTP (Zoratti and Szabo 1995) and FFA binding by BSA most likely underlies BSA-mediated protection against PTP induction (Wieckowski et al. 2000). In our experiments, BSA significantly increased Ca^{2+} uptake capacity of synaptic and non-synaptic mitochondria from 2-month-old FVB/NJ, YAC18, and YAC128 mice. Furthermore, in experiments with 12-month-old mice, we found that BSA significantly increased Ca^{2+} uptake capacity of mitochondria from FVB/NJ mice, but was ineffective in mitochondria from YAC128 mice. Keeping in mind the increased amount of mHtt associated with mitochondria from 12-month-old YAC128 mice and elevated Ca^{2+} uptake

capacity in these mitochondria, the lack of further augmentation with BSA suggests that mHtt and BSA effects may have a similar mechanism, for example, binding of FFA. Although additional experiments are necessary to test this hypothesis and untangle the potential mechanism of FFA binding to mHtt, existing literature lends support to this notion.

The increased Ca^{2+} uptake capacity of mitochondria from YAC128 mice may reflect compensatory adaptation to augmented Ca^{2+} influx via over-activated NMDA receptors and/or increased Ca^{2+} release from endoplasmic reticulum via abnormally activated IP_3 receptors (Bezprozvanny and Hayden 2004). Similar to findings by Chang et al. (2006) and Wang et al. (2013), in experiments with cultured striatal neurons from YAC128 mice and WT littermates, we did not find evidence of the decreased ability of neuronal mitochondria to accumulate Ca^{2+}. Consequently, comparable susceptibility to PTP induction and the lack of mHtt-induced deficiency in mitochondrial Ca^{2+} uptake capacity in mitochondria from YAC128 and WT mice argue against possible involvement of these mechanisms in HD pathogenesis.

b. Striatal neurons from YAC128 are more sensitive to glutamate than neurons from WT mice

In HD, the striatum is the most vulnerable brain region (Vonsattel & DiFiglia, 1998; Bates *et al.*, 2002; Walker & Raymond, 2004; Li *et al.*, 2014). Striatal atrophy also occurs in most mouse models of HD ((Bates *et al.*, 2002; Slow *et al.*, 2003; Ramaswamy *et al.*, 2007). In our experiments, we found that

striatal neurons in culture are more sensitive to glutamate than cultured cortical neurons. This is in agreement with the striatal vulnerability seen in HD patients and mouse models. The mechanism responsible for the increased vulnerability in striatum is not known. Other investigators have shown increased NR2B expression in striatum compared with other brain regions (Li *et al.*, 2003). NR2B subunits of NMDAR are linked to cell death compared with NR2A, making increased expression a conceivable reason for increased sensitivity.

Consistent with previous findings, striatal neurons from YAC128 mice underwent DCD more quickly (reaching phase 3) than neurons from WT animals. Interestingly, no difference was seen in NMDA-induced Ca^{2+} influx. This is likely because the Ca^{2+} influx from a 30 second application of NMDA can be removed from the cytosol by Ca^{2+} removal mechanisms. Increased Ca^{2+} influx may occur, but there is no additional increase in the total cytosolic Ca^{2+} concentration due to the efficacy of the removal mechanisms. This may suggest some compensation by these mechanisms to maintain tight control on cytosolic Ca^{2+} concentration

Application of glutamate to cultured striatal neurons from YAC128 mice to 'load' neuronal mitochondria, showed that mitochondria accumulated similar amounts of Ca^{2+} compared with mitochondria in striatal neurons from WT animals. This data supports but does not match the isolated mitochondria data. There could be multiple reasons for this. Most likely, in isolated mitochondria experiments no other Ca^{2+} removal mechanisms present therefore only mitochondrial Ca^{2+} is observed. However, in the presence of high and low capacity mechanisms for Ca^{2+} regulation, the mitochondria have assistance in

Ca^{2+} removal and control. Furthermore, we found that mHtt association with isolated mitochondria increased with age. Primary neurons in culture are DIV 10-13 from PN1 mice, therefore they do not likely have the increased levels of mHtt seen associated with mitochondria from older animals.

c. NCX1 expression is increased in striatal lysate from older YAC128 mice

The contribution of NCX to Ca^{2+} homeostasis in HD deserves additional investigation. We found augmented basal cytosolic Na^{+} concentrations in striatal neurons from YAC128 mice compared with WT. This was a slight but statistically significant increase which could suggest a few different scenarios. One possibility is that the increased striatal sensitivity to glutamate requires frequent action of NCX_{for} resulting in increased intracellular Na^{+} concentrations. Another possibility is that another mechanism, an ion channel or exchanger, is not operating properly and is allowing influx of Na^{+}. This could result in an increased propensity for NCX reversal. Since NCX_{rev} is a major contributor to DCD, high Na^{+} levels could lead to aberrant NCX_{rev} and Ca^{2+} dysregulation. It is also possible that the increased Na^{+} concentration is not great enough to have a physiological consequence. Further investigation of NCX actvity in both the forward and reverse modes in neurons expressing mHtt should be done to better understand the possible effect of mHtt on NCX activity.

We found increased NCX1 expression in striatal lysate from 3-month-old YAC128 mice compared with WT. This could suggest upregulation due to compensation for increased Ca^{2+} influx. Transcriptional regulation has been

shown to be altered by mHtt which could potentially explain the upregulation (Hogel *et al.*, 2012). Another possiblity is that NCX1 upregulation is compensatory for aberrant Ca^{2+} signalling. In ischemic preconditioning studies, upregulation of both NCX1 and NCX3 bas been observed, and the upregulation correlated with neuroprotection (Pignataro *et al.*, 2013). Interestingly, NCX3 expression is unchanged. Further experiments are required to understand the increased expression of NCX1 with age in striata expressing mHtt, as well as the differential expression between the subtypes in a mouse model of HD.

NCX3 and CRMP2 interaction may also contribute to NCX1 upregulation. CRMP2, mHtt, and Htt interact with NCX3 but not NCX1. These interacting proteins (or others) may regulate NCX3 localization and expression. It is conceivable that mHtt leads to increased CRMP2 binding to NCX3, leading to internalization. Furthermore, the localization of NCX1 should be investigated. If NCX1 in HD is intrenalized instead of localized to the plasma membrane, this could suggest that the increased expression is not altering function. Electrophysiology should be done to study the activity of NCX in striatal neurons from HD mouse models. These experiments were attempted with Ca^{2+} imaging but the number of manipulations required made the data difficult to interpret.

d. CRMP2 regulates NMDAR and NCX

Sustained elevations in cytosolic Ca^{2+} play a causative role in glutamate-induced neuronal death. Elevated cytosolic Ca^{2+} activates Ca^{2+}-dependent degradation enzymes, such as proteases and phospholipases, and thus hastens

cell death (Bano *et al.*, 2005; Farooqui *et al.*, 2006; Brustovetsky *et al.*, 2010). Therefore, it is vitally important for neurons to remove excessive Ca^{2+} elevations and maintain low cytosolic Ca^{2+}. In neurons, Ca^{2+} extrusion by NCX_{for} and Ca^{2+} uptake by mitochondria are major mechanisms that antagonize Ca^{2+} increases in the cytosol. Mitochondria may accumulate substantial amounts of Ca^{2+} before they undergo permeability transition and become damaged (Chalmers & Nicholls, 2003). Following Ca^{2+}-dependent activation of the permeability transition pore, mitochondria lose the ability to accumulate Ca^{2+} and, subsequently, release previously accumulated Ca^{2+} (Bernardi, 1999). Thus, although mitochondria can accumulate large amounts of Ca^{2+}, their Ca^{2+} uptake capacity is finite. On the other hand, the amount of Ca^{2+} in the extracellular milieu is practically infinite, and consequently, attenuation of Ca^{2+} influx into neurons could be a much more effective strategy in neuronal defense against glutamate-induced Ca^{2+} dysregulation.

Ca^{2+} influx via NMDAR and NCX_{rev} are two major mechanisms of Ca^{2+} entry into neurons exposed to glutamate (Tymianski *et al.*, 1993b; Czyz & Kiedrowski, 2002). Recently, we demonstrated that both mechanisms have to be suppressed to prevent glutamate-induced Ca^{2+} dysregulation (Brittain *et al.*, 2012b). Tat-CBD3 strongly attenuates glutamate-induced Ca^{2+} dysregulation. Based on these observations, we hypothesized that tat-CBD3 should inhibit both NMDAR and NCX_{rev}. The results presented in this study strongly support this hypothesis and link NMDAR and NCX activity to CRMP2 signaling.

CRMP2 is a member of the CRMP protein family originally known as an axon guidance and outgrowth regulator (Schmidt & Strittmatter, 2007; Hensley *et al.*, 2011; Khanna *et al.*, 2012). CRMP2 is cleaved by calpain following focal ischemia, thereby implicating it in neurotoxicity associated with ischemia (Bretin *et al.*, 2006). It appears that cleaved CRMP2 is neuroprotective, whereas cleavage of CRMP3 and CRMP4 is detrimental for neurons (Kowara *et al.*, 2005; Bretin *et al.*, 2006; Liu *et al.*, 2009) . CRMP2 physically interacts with numerous proteins in the cell, including NMDAR and CaV2.2. It has been shown that tat-CBD3 disrupts interaction of CRMP2 with CaV2.2, leading to its internalization and a decrease in ion currents mediated by this channel (Brittain *et al.*, 2011b). In a previous paper from our laboratory, using a pH-sensitive fluorescent NR2B sensor, we showed that tat-CBD3 decreases surface expression of NMDAR in dendritic spines (Brittain *et al.*, 2011a), but it remained unclear whether tat-CBD3 disrupts a CRMP2-NMDAR interaction. It was also unknown whether CRMP2 interacts with NCX and whether tat-CBD3 affects NCX_{rev} activity. In these studies, we demonstrate for the first time that CRMP2 physically interacts with NCX3 and that tat-CBD3 strengthens this interaction, triggers NCX3 internalization, and consequently suppresses NCX activity in both forward and reverse modes. In contrast to strengthening the CRMP2-NCX3 complex, tat-CBD3 disrupted CRMP2-NMDAR interaction, suggesting different mechanisms by which CRMP2 interacts with NMDAR and NCX3.

Although NCX3 internalization may account for the suppression of NCX activity, the mechanism of NCX3 internalization and the role of tat-CBD3-

augmented CRMP2-NCX3 interaction in this process are not clear. It is conceivable that tat-CBD3 competes with CRMP2 for binding with other proteins (e.g. CaV2.2 (and NMDAR)) and releases CRMP2 from complexes with these proteins. If so, then the liberated CRMP2 may bind to other proteins (e.g. NCX3) possibly via a different binding site, with which tat-CBD3 does not interfere. Overall, this may lead to CRMP2 redistribution and increased binding to NCX3. That NCX3 internalization is no longer induced by tat-CBD3 in CRMP2- ablated neurons suggests a causative link between increased CRMP2 association with NCX3 and NCX3 internalization. However, additional experiments are necessary to completely prove this hypothesis.

One of the goals of our study was to test the hypothesis that tat-CBD3 inhibits deleterious NCX_{rev}, which, instead of extruding Ca^{2+} from the cell, causes Ca^{2+} influx (Kiedrowski *et al.*, 1994). Our results strongly support this hypothesis. However, our study also revealed an unexpected consequence of tat-CBD3 treatment. Because tat-CBD3 triggers NCX internalization, it suppresses both forward and reverse modes of NCX. However, NCX_{for} is critical for mitigating increases in cytosolic Ca^{2+} and, thus, maintaining cytosolic Ca^{2+} at the low, physiological level. Consequently, suppression of NCX_{for} should be detrimental for the cell. The question remains, how then can one reconcile this, given tat-CBD3-mediated protection against glutamate-induced Ca^{2+} dysregulation? A likely explanation is that tat-CBD3-induced inhibition of NMDAR plays the dominant role in this protection. The significantly lower Ca^{2+} influx via NMDAR creates conditions in which, despite suppression of NCX_{for}, cytosolic Ca^{2+}

remains at a low level. Mitochondrial Ca^{2+} uptake and Ca^{2+} extrusion by plasma membrane Ca^{2+}-ATPase might also contribute to keeping cytosolic Ca^{2+} low under these conditions. However, as we reported earlier, inhibition of NMDAR alone is not sufficient to prevent glutamate-induced Ca^{2+} dysregulation. Suppression of NCX_{rev}, in addition to NMDAR, is critical for maintaining low cytosolic Ca^{2+} following exposure to glutamate (Brittain *et al.*, 2012b). Our present study unequivocally demonstrates that tat-CBD3 inhibits both NMDAR and NCX_{rev}, hence filling a significant gap in our understanding of the mechanism of TAT-CBD3-mediated neuroprotection. Thus, a sum of the tat-CBD3 inhibitory effects on NMDAR and NCX_{rev} collectively results in a net protection against glutamate-induced Ca^{2+} dysregulation.

For the first time we demonstrated a link between CRMP2 signaling, NMDAR and NCX3 activities, and maintenance of Ca^{2+} homeostasis in neurons exposed to excitotoxic levels of glutamate. Our experiments revealed that CRMP2 physically interacts with both NMDAR and NCX3. Moreover, we showed that TAT-CBD3 strengthens CRMP2-NCX3 interaction and induces NCX3 internalization, leading to suppression of NCX activity. Concomitantly, tat-CBD3 disrupts the CRMP2-NMDAR interaction without detectable relocalization of NMDAR. Nevertheless, this also leads to suppression of NMDAR activity. Thus, our study implicates CRMP2 signaling in regulation of cytosolic Ca^{2+} in neurons exposed to glutamate, suggests different mechanisms of CRMP2 interaction with NMDAR and NCX, and further clarifies the mechanism of tat-CBD3-mediated defense against glutamate-induced Ca^{2+} dysregulation. Our experiments with tat-

CBD3 provide further support to our hypothesis that inhibition of both NMDAR and NCX_{rev} is essential for robust attenuation of glutamate-induced Ca^{2+} dysregulation. Overall, the new knowledge obtained in our study could be instrumental in designing new neuroprotective agents and in a better understanding of the mechanisms of their action.

e. Possiblity for CRMP2 modulation in HD

CRMP2 expression was not found to change in HD models. We were unable to show an interaction between CRMP2 and Htt or mHtt but this does not mean that no interaction exists. Perhaps the interaction is weak or transient and is unable to be detected in co-IP experiments. It is also possible that CRMP2 and mHtt or Htt may both interact with another protein. For example, both CRMP2 and mHtt interact with tubulin. PSD-95 or another scaffold protein may participate in a complex. CRMP2 and PSD-95 both interact with NMDAR and mHtt has been shown to modulate NMDAR via PSD-95 (Sun *et al.*, 2001; Harjes & Wanker, 2003; Fan *et al.*, 2009). Further investigation should be done to further understand the implications of CRMP2 modulation of NMDAR in the presence of mHtt. CRMP2 is a phosphoprotein and phosphorylation of CRMP2 modulates its activity. It is conceivable that the phosphorylation state of CRMP2 may be altered in neurons expressing mHtt. There are many avenues to further explore CRMP2 in HD mouse models beyond expression levels and association with mHtt. CRMP2's modulation of NMDAR makes it an attractive target in further understanding the mechanism of Ca^{2+} dysregulation in neurons expressing mHtt.

f. Conclusion

Taken together, the increased Ca^{2+} uptake capacity of mitochondria from the YAC128 mouse model and the increased NCX1 expression correlated with increased age, suggest a compensation for increased Ca^{2+} influx or perhaps Ca^{2+} removal failure. This may explain the late onset of HD, neurons may compensate for sensitivity to glutamate and subsequent increased cytosolic Ca^{2+} concentrations until the insult overcomes the compensation. The role of Ca^{2+} removal mechanisms and regulation should be investigated further in HD.

Furthermore, CRMP2 modulation of NMDAR and NCX3 may be important in HD as well. Our experiments revealed that CRMP2 physically interacts with both NMDAR and NCX3, important in Ca^{2+} dysregulation. Disrupting the interaction between NMDAR and CRMP leads to decreased activity, whereas increased NCX3-CRMP2 interaction leads to internalization and decreased activity. A model of these interactions is shown in Figure 34. The novel regulation of Ca^{2+} homeostasis in neurons expressing mHtt could help better understand HD and lead to improved therapeutics.

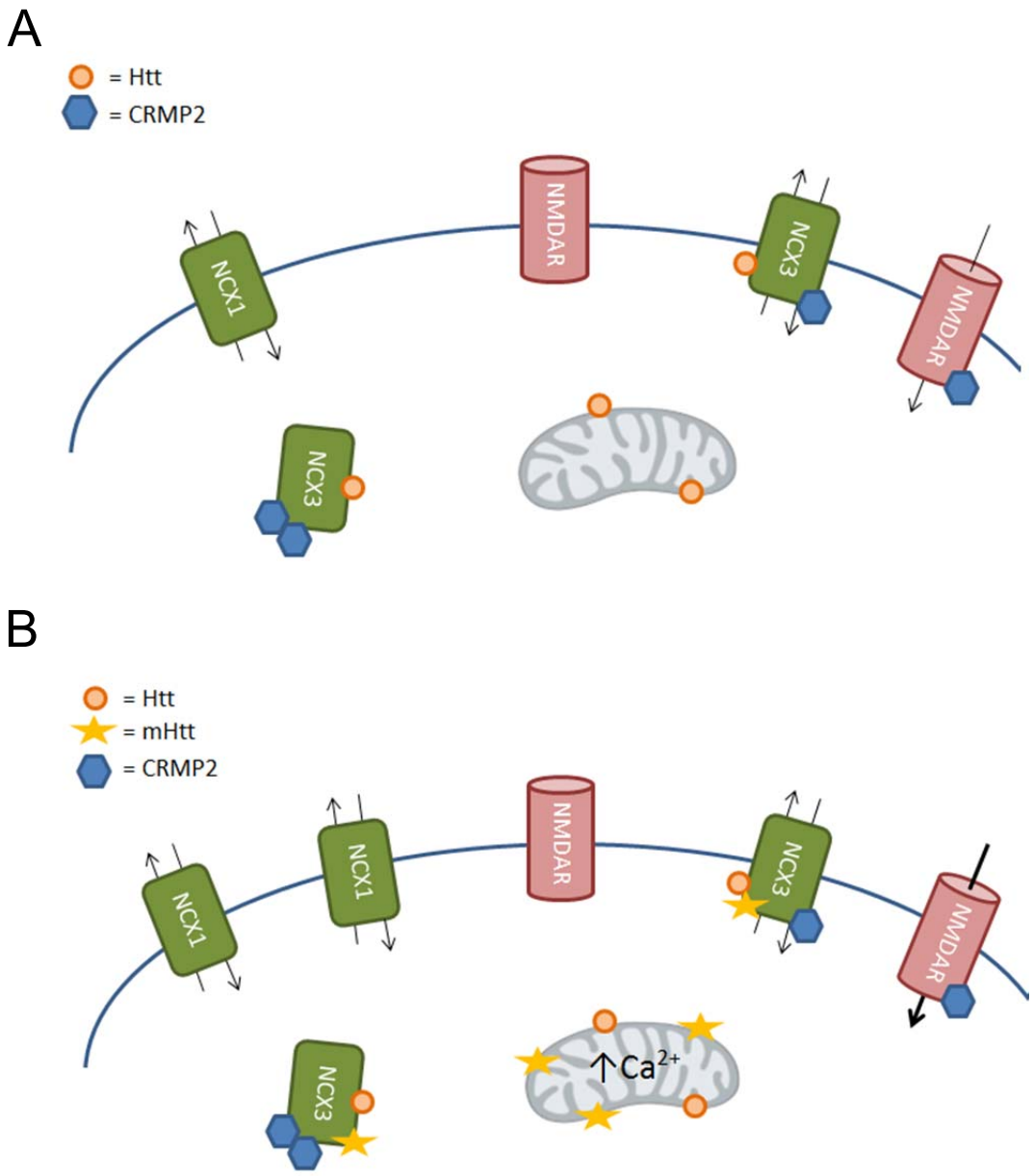

Figure 34. Model of Ca^{2+} regulation in striatal neurons with and without the presence of mHtt. In WT neurons (A), in response to NMDAR activation results in Ca^{2+} influx through NMDAR associated with CRMP2. Mtc and NCX work to maintain Ca^{2+} homeostasis. Increased binding of CRMP2 to NCX3 causes internalization and inactivation. In the presence of mHtt (B), increased NMDAR activity results in greater increase in Ca^{2+} concentrations. To maintain Ca^{2+} homeostasis, Mtc Ca^{2+} uptake is increased and NCX1 expression is upregulated.

Reference List

Al-Hallaq RA, Conrads TP, Veenstra TD, & Wenthold RJ (2007). NMDA di-heteromeric receptor populations and associated proteins in rat hippocampus. *J Neurosci* **27**, 8334-8343.

Ali NJ & Levine MS (2006). Changes in expression of N-methyl-D-aspartate receptor subunits occur early in the R6/2 mouse model of Huntington's disease. *Dev Neurosci* **28**, 230-238.

Anderson KE (2011). Huntington's disease. *Handb Clin Neurol* **100**, 15-24.

Andre VM, Cepeda C, Venegas A, Gomez Y, & Levine MS (2006). Altered cortical glutamate receptor function in the R6/2 model of Huntington's disease. *J Neurophysiol* **95**, 2108-2119.

Annunziato L, Pignataro G, & Di Renzo GF (2004). Pharmacology of brain Na+/Ca2+ exchanger: from molecular biology to therapeutic perspectives. *Pharmacol Rev* **56**, 633-654.

Arimura N, Menager C, Kawano Y, Yoshimura T, Kawabata S, Hattori A, Fukata Y, Amano M, Goshima Y, Inagaki M, Morone N, Usukura J, & Kaibuchi K (2005). Phosphorylation by Rho kinase regulates CRMP-2 activity in growth cones. *Mol Cell Biol* **25**, 9973-9984.

Arzberger T, Krampfl K, Leimgruber S, & Weindl A (1997). Changes of NMDA receptor subunit (NR1, NR2B) and glutamate transporter (GLT1) mRNA expression in Huntington's disease--an in situ hybridization study. *J Neuropathol Exp Neurol* **56**, 440-454.

Ashizawa T, Wong LJ, Richards CS, Caskey CT, & Jankovic J (1994). CAG repeat size and clinical presentation in Huntington's disease. *Neurology* **44**, 1137-1143.

Aylward EH, Sparks BF, Field KM, Yallapragada V, Shpritz BD, Rosenblatt A, Brandt J, Gourley LM, Liang K, Zhou H, Margolis RL, & Ross CA (2004). Onset and rate of striatal atrophy in preclinical Huntington disease. *Neurology* **63**, 66-72.

Baines CP, Kaiser RA, Purcell NH, Blair NS, Osinska H, Hambleton MA, Brunskill EW, Sayen MR, Gottlieb RA, Dorn GW, Robbins J, & Molkentin JD (2005). Loss of cyclophilin D reveals a critical role for mitochondrial permeability transition in cell death. *Nature* **434**, 658-662.

Balasuriya D, Takahashi H, Srivats S, & Edwardson JM (2014). Activation-induced structural change in the GluN1/GluN3A excitatory glycine receptor. *Biochem Biophys Res Commun* **450**, 1452-1457.

Bano D, Young KW, Guerin CJ, Lefeuvre R, Rothwell NJ, Naldini L, Rizzuto R, Carafoli E, & Nicotera P (2005). Cleavage of the plasma membrane Na+/Ca2+ exchanger in excitotoxicity. *Cell* **120**, 275-285.

Basso E, Fante L, Fowlkes J, Petronilli V, Forte MA, & Bernardi P (2005). Properties of the permeability transition pore in mitochondria devoid of Cyclophilin D. *J Biol Chem* **280**, 18558-18561.

Bates GP, Harper PS, & Jones L. Huntington's Disease. 2002. Oxford University Press.
Ref Type: Edited Book

Baughman JM, Perocchi F, Girgis HS, Plovanich M, Belcher-Timme CA, Sancak Y, Bao XR, Strittmatter L, Goldberger O, Bogorad RL, Koteliansky V, & Mootha VK (2011). Integrative genomics identifies MCU as an essential component of the mitochondrial calcium uniporter. *Nature* **476**, 341-345.

Beal MF, Hyman BT, & Koroshetz W (1993). Do defects in mitochondrial energy metabolism underlie the pathology of neurodegenerative diseases? *Trends Neurosci* **16**, 125-131.

Beal MF, Kowall NW, Ellison DW, Mazurek MF, Swartz KJ, & Martin JB (1986). Replication of the neurochemical characteristics of Huntington's disease by quinolinic acid. *Nature* **321**, 168-171.

Bernardi P (1999). Mitochondrial transport of cations: channels, exchangers, and permeability transition. *Physiol Rev* **79**, 1127-1155.

Bernardi P & Petronilli V (1996). The permeability transition pore as a mitochondrial calcium release channel: a critical appraisal. *J Bioenerg Biomembr* **28**, 131-138.

Bezprozvanny I (2011). Role of inositol 1,4,5-trisphosphate receptors in pathogenesis of Huntington's disease and spinocerebellar ataxias. *Neurochem Res* **36**, 1186-1197.

Bezprozvanny I & Hayden MR (2004). Deranged neuronal calcium signaling and Huntington disease. *Biochem Biophys Res Commun* **322**, 1310-1317.

Bizat N, Hermel JM, Boyer F, Jacquard C, Creminon C, Ouary S, Escartin C, Hantraye P, Kajewski S, & Brouillet E (2003). Calpain is a major cell death effector in selective striatal degeneration induced in vivo by 3-nitropropionate: implications for Huntington's disease. *J Neurosci* **23**, 5020-5030.

Bjorkqvist M, Fex M, Renstrom E, Wierup N, Petersen A, Gil J, Bacos K, Popovic N, Li JY, Sundler F, Brundin P, & Mulder H (2005). The R6/2 transgenic mouse model of Huntington's disease develops diabetes due to deficient beta-cell mass and exocytosis. *Hum Mol Genet* **14**, 565-574.

Blaustein MP, Juhaszova M, Golovina VA, Church PJ, & Stanley EF (2002). Na/Ca exchanger and PMCA localization in neurons and astrocytes: functional implications. *Ann N Y Acad Sci* **976**, 356-366.

Blaustein MP & Lederer WJ (1999). Sodium/calcium exchange: its physiological implications. *Physiol Rev* **79**, 763-854.

Bonventre JV (1997). Roles of phospholipases A2 in brain cell and tissue injury associated with ischemia and excitotoxicity. *J Lipid Mediat Cell Signal* **17**, 71-79.

Borlongan CV, Koutouzis TK, Freeman TB, Cahill DW, & Sanberg PR (1995). Behavioral pathology induced by repeated systemic injections of 3-nitropropionic acid mimics the motoric symptoms of Huntington's disease. *Brain Res* **697**, 254-257.

Brandstaetter H, Kruppa AJ, & Buss F (2014). Huntingtin is required for ER-to-Golgi transport and for secretory vesicle fusion at the plasma membrane. *Dis Model Mech* **7**, 1335-1340.

Bretin S, Rogemond V, Marin P, Maus M, Torrens Y, Honnorat J, Glowinski J, Premont J, & Gauchy C (2006). Calpain product of WT-CRMP2 reduces the amount of surface NR2B NMDA receptor subunit. *J Neurochem* **98**, 1252-1265.

Brewer LD, Thibault O, Staton J, Thibault V, Rogers JT, Garcia-Ramos G, Kraner S, Landfield PW, & Porter NM (2007). Increased vulnerability of hippocampal neurons with age in culture: temporal association with increases in NMDA receptor current, NR2A subunit expression and recruitment of L-type calcium channels. *Brain Res* **1151**, 20-31.

Brini M, Manni S, & Carafoli E (2002). A study of the activity of the plasma membrane Na/Ca exchanger in the cellular environment. *Ann N Y Acad Sci* **976**, 376-381.

Brittain JM, Chen L, Wilson SM, Brustovetsky T, Gao X, Ashpole NM, Molosh AI, You H, Hudmon A, Shekhar A, White FA, Zamponi GW, Brustovetsky N, Chen J, & Khanna R (2011a). Neuroprotection against traumatic brain injury by a peptide derived from the collapsin response mediator protein 2 (CRMP2). *J Biol Chem* **286**, 37778-37792.

Brittain JM, Duarte DB, Wilson SM, Zhu W, Ballard C, Johnson PL, Liu N, Xiong W, Ripsch MS, Wang Y, Fehrenbacher JC, Fitz SD, Khanna M, Park CK, Schmutzler BS, Cheon BM, Due MR, Brustovetsky T, Ashpole NM, Hudmon A, Meroueh SO, Hingtgen CM, Brustovetsky N, Ji RR, Hurley JH, Jin X, Shekhar A, Xu XM, Oxford GS, Vasko MR, White FA, & Khanna R (2011b). Suppression of inflammatory and neuropathic pain by uncoupling CRMP-2 from the presynaptic Ca(2) channel complex. *Nat Med* **17**, 822-829.

Brittain JM, Piekarz AD, Wang Y, Kondo T, Cummins TR, & Khanna R (2009). An atypical role for collapsin response mediator protein 2 (CRMP-2) in neurotransmitter release via interaction with presynaptic voltage-gated calcium channels. *J Biol Chem* **284**, 31375-31390.

Brittain MK, Brustovetsky T, Brittain JM, Khanna R, Cummins TR, & Brustovetsky N (2012a). Ifenprodil, a NR2B-selective antagonist of NMDA receptor, inhibits reverse Na+/Ca2+ exchanger in neurons. *Neuropharmacology* **63**, 974-982.

Brittain MK, Brustovetsky T, Sheets PL, Brittain JM, Khanna R, Cummins TR, & Brustovetsky N (2012b). Delayed calcium dysregulation in neurons requires both the NMDA receptor and the reverse Na+/Ca2+ exchanger. *Neurobiol Dis* **46**, 109-117.

Broekemeier KM, Dempsey ME, & Pfeiffer DR (1989). Cyclosporin A is a potent inhibitor of the inner membrane permeability transition in liver mitochondria. *J Biol Chem* **264**, 7826-7830.

Brouillet E, Conde F, Beal MF, & Hantraye P (1999). Replicating Huntington's disease phenotype in experimental animals. *Prog Neurobiol* **59**, 427-468.

Brown MR, Sullivan PG, Dorenbos KA, Modafferi EA, Geddes JW, & Steward O (2004). Nitrogen disruption of synaptoneurosomes: an alternative method to isolate brain mitochondria. *J Neurosci Methods* **137**, 299-303.

Brown TB, Bogush AI, & Ehrlich ME (2008). Neocortical expression of mutant huntingtin is not required for alterations in striatal gene expression or motor dysfunction in a transgenic mouse. *Hum Mol Genet* **17**, 3095-3104.

Brustovetsky N, Brustovetsky T, Jemmerson R, & Dubinsky JM (2002). Calcium-induced cytochrome c release from CNS mitochondria is associated with the permeability transition and rupture of the outer membrane. *J Neurochem* **80**, 207-218.

Brustovetsky N, Brustovetsky T, Purl KJ, Capano M, Crompton M, & Dubinsky JM (2003). Increased susceptibility of striatal mitochondria to calcium-induced permeability transition. *J Neurosci* **23**, 4858-4867.

Brustovetsky N & Dubinsky JM (2000). Dual responses of CNS mitochondria to elevated calcium. *J Neurosci* **20**, 103-113.

Brustovetsky N, LaFrance R, Purl KJ, Brustovetsky T, Keene CD, Low WC, & Dubinsky JM (2005). Age-dependent changes in the calcium sensitivity of striatal mitochondria in mouse models of Huntington's Disease. *J Neurochem* **93**, 1361-1370.

Brustovetsky T, Bolshakov A, & Brustovetsky N (2010). Calpain activation and Na(+)/Ca(2+) exchanger degradation occur downstream of calcium deregulation in hippocampal neurons exposed to excitotoxic glutamate. *J Neurosci Res* **88**, 1317-1328.

Brustovetsky T, Brittain MK, Sheets PL, Cummins TR, Pinelis V, & Brustovetsky N (2011). KB-R7943, an inhibitor of the reverse Na+ /Ca2+ exchanger, blocks N-methyl-D-aspartate receptor and inhibits mitochondrial complex I. *Br J Pharmacol* **162**, 255-270.

Brustovetsky T, Li V, & Brustovetsky N (2009). Stimulation of glutamate receptors in cultured hippocampal neurons causes Ca2+-dependent mitochondrial contraction. *Cell Calcium* **46**, 18-29.

Budd SL & Nicholls DG (1996). A reevaluation of the role of mitochondria in neuronal Ca2+ homeostasis. *J Neurochem* **66**, 403-411.

Byk T, Ozon S, & Sobel A (1998). The Ulip family phosphoproteins--common and specific properties. *Eur J Biochem* **254**, 14-24.

Canitano A, Papa M, Boscia F, Castaldo P, Sellitti S, Taglialatela M, & Annunziato L (2002). Brain distribution of the Na+/Ca2+ exchanger-encoding genes NCX1, NCX2, and NCX3 and their related proteins in the central nervous system. *Ann N Y Acad Sci* **976**, 394-404.

Carafoli E (1988). The intracellular homeostasis of calcium: an overview. *Ann N Y Acad Sci* **551**, 147-157.

Carafoli E & Lehninger AL (1971). A survey of the interaction of calcium ions with mitochondria from different tissues and species. *Biochem J* **122**, 681-690.

Carafoli E, Santella L, Branca D, & Brini M (2001). Generation, control, and processing of cellular calcium signals. *Crit Rev Biochem Mol Biol* **36**, 107-260.

Cepeda C, Ariano MA, Calvert CR, Flores-Hernandez J, Chandler SH, Leavitt BR, Hayden MR, & Levine MS (2001). NMDA receptor function in mouse models of Huntington disease. *J Neurosci Res* **66**, 525-539.

Cha JH (2007). Transcriptional signatures in Huntington's disease. *Prog Neurobiol* **83**, 228-248.

Chalmers S & Nicholls DG (2003). The relationship between free and total calcium concentrations in the matrix of liver and brain mitochondria. *J Biol Chem* **278**, 19062-19070.

Chan SL & Mattson MP (1999). Caspase and calpain substrates: roles in synaptic plasticity and cell death. *J Neurosci Res* **58**, 167-190.

Chang DT & Reynolds IJ (2006). Differences in mitochondrial movement and morphology in young and mature primary cortical neurons in culture. *Neuroscience* **141**, 727-736.

Chang DT, Rintoul GL, Pandipati S, & Reynolds IJ (2006). Mutant huntingtin aggregates impair mitochondrial movement and trafficking in cortical neurons. *Neurobiol Dis* **22**, 388-400.

Charrier E, Reibel S, Rogemond V, Aguera M, Thomasset N, & Honnorat J (2003). Collapsin response mediator proteins (CRMPs): involvement in nervous system development and adult neurodegenerative disorders. *Mol Neurobiol* **28**, 51-64.

Chen N, Luo T, & Raymond LA (1999a). Subtype-dependence of NMDA receptor channel open probability. *J Neurosci* **19**, 6844-6854.

Chen N, Luo T, Wellington C, Metzler M, McCutcheon K, Hayden MR, & Raymond LA (1999b). Subtype-specific enhancement of NMDA receptor currents by mutant huntingtin. *J Neurochem* **72**, 1890-1898.

Chen S, Berthelier V, Hamilton JB, O'Nuallain B, & Wetzel R (2002). Amyloid-like features of polyglutamine aggregates and their assembly kinetics. *Biochemistry* **41**, 7391-7399.

Choi DW & Hartley DM (1993). Calcium and glutamate-induced cortical neuronal death. *Res Publ Assoc Res Nerv Ment Dis* **71**, 23-34.

Choo YS, Johnson GV, MacDonald M, Detloff PJ, & Lesort M (2004). Mutant huntingtin directly increases susceptibility of mitochondria to the calcium-induced permeability transition and cytochrome c release. *Hum Mol Genet* **13**, 1407-1420.

Clements JD & Westbrook GL (1994). Kinetics of AP5 dissociation from NMDA receptors: evidence for two identical cooperative binding sites. *J Neurophysiol* **71**, 2566-2569.

Convery MK & Hancox JC (1999). Comparison of Na+-Ca2+ exchange current elicited from isolated rabbit ventricular myocytes by voltage ramp and step protocols. *Pflugers Arch* **437**, 944-954.

Costa V, Giacomello M, Hudec R, Lopreiato R, Ermak G, Lim D, Malorni W, Davies KJ, Carafoli E, & Scorrano L (2010). Mitochondrial fission and cristae disruption increase the response of cell models of Huntington's disease to apoptotic stimuli. *EMBO Mol Med* **2**, 490-503.

Coyle JT & Schwarcz R (1976). Lesion of striatal neurones with kainic acid provides a model for Huntington's chorea. *Nature* **263**, 244-246.

Crompton M (1999). The mitochondrial permeability transition pore and its role in cell death. *Biochem J* **341 (Pt 2)**, 233-249.

Czyz A & Kiedrowski L (2002). In depolarized and glucose-deprived neurons, Na+ influx reverses plasmalemmal K+-dependent and K+-independent Na+/Ca2+ exchangers and contributes to NMDA excitotoxicity. *J Neurochem* **83**, 1321-1328.

De SD, Raffaello A, Teardo E, Szabo I, & Rizzuto R (2011). A forty-kilodalton protein of the inner membrane is the mitochondrial calcium uniporter. *Nature* **476**, 336-340.

Dehorter N, Vinay L, Hammond C, & Ben-Ari Y (2012). Timing of developmental sequences in different brain structures: physiological and pathological implications. *Eur J Neurosci* **35**, 1846-1856.

Diarra A, Sheldon C, & Church J (2001). In situ calibration and [H+] sensitivity of the fluorescent Na+ indicator SBFI. *Am J Physiol Cell Physiol* **280**, C1623-C1633.

DiFiglia M, Sapp E, Chase K, Schwarz C, Meloni A, Young C, Martin E, Vonsattel JP, Carraway R, Reeves SA, & . (1995). Huntingtin is a cytoplasmic protein associated with vesicles in human and rat brain neurons. *Neuron* **14**, 1075-1081.

Dingledine R, Borges K, Bowie D, & Traynelis SF (1999). The glutamate receptor ion channels. *Pharmacol Rev* **51**, 7-61.

DiPolo R & Beauge L (2006). Sodium/calcium exchanger: influence of metabolic regulation on ion carrier interactions. *Physiol Rev* **86**, 155-203.

Douaud G, Gaura V, Ribeiro MJ, Lethimonnier F, Maroy R, Verny C, Krystkowiak P, Damier P, Bachoud-Levi AC, Hantraye P, & Remy P (2006). Distribution of grey matter atrophy in Huntington's disease patients: a combined ROI-based and voxel-based morphometric study. *Neuroimage* **32**, 1562-1575.

Dragatsis I, Levine MS, & Zeitlin S (2000). Inactivation of Hdh in the brain and testis results in progressive neurodegeneration and sterility in mice. *Nat Genet* **26**, 300-306.

Dubinsky JM (1993). Intracellular calcium levels during the period of delayed excitotoxicity. *Journal of Neuroscience* **13**, 623-631.

Dubinsky JM, Kristal BS, & Elizondo-Fournier M (1995). On the probabilistic nature of excitotoxic neuronal death in hippocampal neurons. *Neuropharmacology* **34**, 701-711.

Ehrlich ME (2012). Huntington's disease and the striatal medium spiny neuron: cell-autonomous and non-cell-autonomous mechanisms of disease. *Neurotherapeutics* **9**, 270-284.

Eliseev RA, Filippov G, Velos J, VanWinkle B, Goldman A, Rosier RN, & Gunter TE (2007). Role of cyclophilin D in the resistance of brain mitochondria to the permeability transition. *Neurobiol Aging* **28**, 1532-1542.

Erecinska M & Silver IA (1996). Calcium handling by hippocampal neurons under physiologic and pathologic conditions. *Adv Neurol* **71**, 119-136.

Faden AI, Demediuk P, Panter SS, & Vink R (1989). The role of excitatory amino acids and NMDA receptors in traumatic brain injury. *Science* **244**, 798-800.

Fan J, Cowan CM, Zhang LY, Hayden MR, & Raymond LA (2009). Interaction of postsynaptic density protein-95 with NMDA receptors influences excitotoxicity in the yeast artificial chromosome mouse model of Huntington's disease. *J Neurosci* **29**, 10928-10938.

Fan MM & Raymond LA (2007). N-methyl-D-aspartate (NMDA) receptor function and excitotoxicity in Huntington's disease. *Prog Neurobiol* **81**, 272-293.

Fan TJ, Xia L, & Han YR (2001). Mitochondrion and Apoptosis. *Sheng Wu Hua Xue Yu Sheng Wu Wu Li Xue Bao (Shanghai)* **33**, 7-12.

Farooqui AA, Ong WY, & Horrocks LA (2006). Inhibitors of brain phospholipase A2 activity: their neuropharmacological effects and therapeutic importance for the treatment of neurologic disorders. *Pharmacol Rev* **58**, 591-620.

Fernandes HB, Baimbridge KG, Church J, Hayden MR, & Raymond LA (2007). Mitochondrial sensitivity and altered calcium handling underlie enhanced NMDA-induced apoptosis in YAC128 model of Huntington's disease. *J Neurosci* **27**, 13614-13623.

Foster AC & Wong EH (1987). The novel anticonvulsant MK-801 binds to the activated state of the N-methyl-D-aspartate receptor in rat brain. *Br J Pharmacol* **91**, 403-409.

Fukata Y, Itoh TJ, Kimura T, Menager C, Nishimura T, Shiromizu T, Watanabe H, Inagaki N, Iwamatsu A, Hotani H, & Kaibuchi K (2002). CRMP-2 binds to tubulin heterodimers to promote microtubule assembly. *Nat Cell Biol* **4**, 583-591.

Fusco FR, Chen Q, Lamoreaux WJ, Figueredo-Cardenas G, Jiao Y, Coffman JA, Surmeier DJ, Honig MG, Carlock LR, & Reiner A (1999). Cellular localization of huntingtin in striatal and cortical neurons in rats: lack of correlation with neuronal vulnerability in Huntington's disease. *J Neurosci* **19**, 1189-1202.

Gafni J, Hermel E, Young JE, Wellington CL, Hayden MR, & Ellerby LM (2004). Inhibition of calpain cleavage of huntingtin reduces toxicity: accumulation of calpain/caspase fragments in the nucleus. *J Biol Chem* **279**, 20211-20220.

Gauthier LR, Charrin BC, Borrell-Pages M, Dompierre JP, Rangone H, Cordelieres FP, De MJ, MacDonald ME, Lessmann V, Humbert S, & Saudou F (2004). Huntingtin controls neurotrophic support and survival of neurons by enhancing BDNF vesicular transport along microtubules. *Cell* **118**, 127-138.

Gellerich FN, Gizatullina ZZ, Nguyen HP, Trumbeckaite S, Vielhaber S, Seppet E, Zierz S, Landwehrmeyer B, Ries O, von HS, & Striggow F (2008). Impaired regulation of brain mitochondria by extramitochondrial Ca2+ in transgenic Huntington disease rats. *J Biol Chem* **283**, 30715-30724.

Glasgow NG, Siegler RB, & Johnson JW (2015). Molecular bases of NMDA receptor subtype-dependent properties. *J Physiol* **593**, 83-95.

Gleichmann M & Mattson MP (2010). Neuronal Calcium Homeostasis and Dysregulation. *Antioxid Redox Signal*.

Goldberg YP, Nicholson DW, Rasper DM, Kalchman MA, Koide HB, Graham RK, Bromm M, Kazemi-Esfarjani P, Thornberry NA, Vaillancourt JP, & Hayden MR (1996). Cleavage of huntingtin by apopain, a proapoptotic cysteine protease, is modulated by the polyglutamine tract. *Nat Genet* **13**, 442-449.

Goldstein JC, Munoz-Pinedo C, Ricci JE, Adams SR, Kelekar A, Schuler M, Tsien RY, & Green DR (2005). Cytochrome c is released in a single step during apoptosis. *Cell Death Differ* **12**, 453-462.

Goll DE, Thompson VF, Li H, Wei W, & Cong J (2003). The calpain system. *Physiol Rev* **83**, 731-801.

Govert F & Schneider SA (2013). Huntington's disease and Huntington's disease-like syndromes: an overview. *Curr Opin Neurol* **26**, 420-427.

Graham RK, Deng Y, Slow EJ, Haigh B, Bissada N, Lu G, Pearson J, Shehadeh J, Bertram L, Murphy Z, Warby SC, Doty CN, Roy S, Wellington CL, Leavitt BR, Raymond LA, Nicholson DW, & Hayden MR (2006). Cleavage at the caspase-6 site is required for neuronal dysfunction and degeneration due to mutant huntingtin. *Cell* **125**, 1179-1191.

Gramsbergen JB, Veenma-Van der Duin L, Venema K, & Korf J (1986). Cerebral cation shifts and amino acids in Huntington's disease. *Arch Neurol* **43**, 1276-1281.

Gray M, Shirasaki DI, Cepeda C, Andre VM, Wilburn B, Lu XH, Tao J, Yamazaki I, Li SH, Sun YE, Li XJ, Levine MS, & Yang XW (2008). Full-length human mutant huntingtin with a stable polyglutamine repeat can elicit progressive and selective neuropathogenesis in BACHD mice. *J Neurosci* **28**, 6182-6195.

Green DR & Kroemer G (2004). The pathophysiology of mitochondrial cell death. *Science* **305**, 626-629.

Gregory KJ, Noetzel MJ, & Niswender CM (2013). Pharmacology of metabotropic glutamate receptor allosteric modulators: structural basis and therapeutic potential for CNS disorders. *Prog Mol Biol Transl Sci* **115**, 61-121.

Griparic L & van der Bliek AM (2005). Assay and properties of the mitochondrial dynamin related protein Opa1. *Methods Enzymol* **404**, 620-631.

Groc L, Heine M, Cousins SL, Stephenson FA, Lounis B, Cognet L, & Choquet D (2006). NMDA receptor surface mobility depends on NR2A-2B subunits. *Proc Natl Acad Sci U S A* **103**, 18769-18774.

Grynkiewicz G, Poenie M, & Tsien RY (1985). A new generation of Ca2+ indicators with greatly improved fluorescence properties. *J Biol Chem* **260**, 3440-3450.

Guerini D, Coletto L, & Carafoli E (2005). Exporting calcium from cells. *Cell Calcium* **38**, 281-289.

Hagberg H (2004). Mitochondrial impairment in the developing brain after hypoxia-ischemia. *J Bioenerg Biomembr* **36**, 369-373.

Haines JL & Conneally PM (1986). Causes of death in Huntington disease as reported on death certificates. *Genet Epidemiol* **3**, 417-423.

Halestrap AP & Davidson AM (1990). Inhibition of Ca2(+)-induced large-amplitude swelling of liver and heart mitochondria by cyclosporin is probably caused by the inhibitor binding to mitochondrial-matrix peptidyl-prolyl cis-trans isomerase and preventing it interacting with the adenine nucleotide translocase. *Biochem J* **268**, 153-160.

Hallett PJ, Spoelgen R, Hyman BT, Standaert DG, & Dunah AW (2006). Dopamine D1 activation potentiates striatal NMDA receptors by tyrosine phosphorylation-dependent subunit trafficking. *J Neurosci* **26**, 4690-4700.

Han I, You Y, Kordower JH, Brady ST, & Morfini GA (2010). Differential vulnerability of neurons in Huntington's disease: The role of cell type-specific features. *J Neurochem*.

Harjes P & Wanker EE (2003). The hunt for huntingtin function: interaction partners tell many different stories. *Trends Biochem Sci* **28**, 425-433.

Harper PS & Jones L (2002). Huntington's disease: genetic and molecular studies. In *Huntington's Disease*, eds. Bates GP, Harper PS, & Jones L, pp. 113-158. Oxford University Press, New York.

Harper PS (2002). Huntgington's Disease: a historical background. In *Huntington's Disease*, eds. Bates GP, Harper PS, & Jones L, pp. 3-27. Oxford University Press, New York.

Heemskerk AW & Roos RA (2012). Aspiration pneumonia and death in Huntington's disease. *PLoS Curr* **4**, RRN1293.

Hensley K, Venkova K, Christov A, Gunning W, & Park J (2011). Collapsin response mediator protein-2: an emerging pathologic feature and therapeutic target for neurodisease indications. *Mol Neurobiol* **43**, 180-191.

Hodgson JG, Agopyan N, Gutekunst CA, Leavitt BR, LePiane F, Singaraja R, Smith DJ, Bissada N, McCutcheon K, Nasir J, Jamot L, Li XJ, Stevens ME, Rosemond E, Roder JC, Phillips AG, Rubin EM, Hersch SM, & Hayden MR (1999). A YAC mouse model for Huntington's disease with full-length mutant huntingtin, cytoplasmic toxicity, and selective striatal neurodegeneration. *Neuron* **23**, 181-192.

Hodgson JG, Smith DJ, McCutcheon K, Koide HB, Nishiyama K, Dinulos MB, Stevens ME, Bissada N, Nasir J, Kanazawa I, Disteche CM, Rubin EM, & Hayden MR (1996). Human huntingtin derived from YAC transgenes compensates for loss of murine huntingtin by rescue of the embryonic lethal phenotype. *Hum Mol Genet* **5**, 1875-1885.

Hogel M, Laprairie RB, & Denovan-Wright EM (2012). Promoters are differentially sensitive to N-terminal mutant huntingtin-mediated transcriptional repression. *PLoS ONE* **7**, e41152.

Hoyt KR, Arden SR, Aizenman E, & Reynolds IJ (1998). Reverse Na+/Ca2+ exchange contributes to glutamate-induced intracellular Ca2+ concentration increases in cultured rat forebrain neurons. *Mol Pharmacol* **53**, 742-749.

Huettner JE & Bean BP (1988). Block of N-methyl-D-aspartate-activated current by the anticonvulsant MK-801: selective binding to open channels. *Proc Natl Acad Sci U S A* **85**, 1307-1311.

Huntington G (1872). On Chorea. *Medical and Surgical Reporter* **26**, 320-321.

Ivkovic S & Ehrlich ME (1999). Expression of the striatal DARPP-32/ARPP-21 phenotype in GABAergic neurons requires neurotrophins in vivo and in vitro. *J Neurosci* **19**, 5409-5419.

Janssens N & Lesage AS (2001). Glutamate receptor subunit expression in primary neuronal and secondary glial cultures. *J Neurochem* **77**, 1457-1474.

Javadov S & Kuznetsov A (2013). Mitochondrial permeability transition and cell death: the role of cyclophilin d. *Front Physiol* **4**, 76.

Jeffs GJ, Meloni BP, Bakker AJ, & Knuckey NW (2007). The role of the Na(+)/Ca(2+) exchanger (NCX) in neurons following ischaemia. *J Clin Neurosci* **14**, 507-514.

Kamo N, Muratsugu M, Hongoh R, & Kobatake Y (1979). Membrane potential of mitochondria measured with an electrode sensitive to tetraphenyl phosphonium and relationship between proton electrochemical potential and phosphorylation potential in steady state. *J Membr Biol* **49**, 105-121.

Kegel KB, Meloni AR, Yi Y, Kim YJ, Doyle E, Cuiffo BG, Sapp E, Wang Y, Qin ZH, Chen JD, Nevins JR, Aronin N, & DiFiglia M (2002). Huntingtin is present in the nucleus, interacts with the transcriptional corepressor C-terminal binding protein, and represses transcription. *J Biol Chem* **277**, 7466-7476.

Kehoe LA, Bernardinelli Y, & Muller D (2013). GluN3A: an NMDA receptor subunit with exquisite properties and functions. *Neural Plast* **2013**, 145387.

Kells AP, Fong DM, Dragunow M, During MJ, Young D, & Connor B (2004). AAV-mediated gene delivery of BDNF or GDNF is neuroprotective in a model of Huntington disease. *Mol Ther* **9**, 682-688.

Khanna R, Wilson SM, Brittain JM, Weimer J, Sultana R, Butterfield A, & Hensley K (2012). Opening Pandora's jar: a primer on the putative roles of CRMP2 in a

panoply of neurodegenerative, sensory and motor neuron, and central disorders. *Future Neurol* **7**, 749-771.

Kiedrowski L (1999). N-methyl-D-aspartate excitotoxicity: relationships among plasma membrane potential, Na(+)/Ca(2+) exchange, mitochondrial Ca(2+) overload, and cytoplasmic concentrations of Ca(2+), H(+), and K(+). *Mol Pharmacol* **56**, 619-632.

Kiedrowski L, Brooker G, Costa E, & Wroblewski JT (1994). Glutamate impairs neuronal calcium extrusion while reducing sodium gradient. *Neuron* **12**, 295-300.

Kiedrowski L & Costa E (1995). Glutamate-induced destabilization of intracellular calcium concentration homeostasis in cultured cerebellar granule cells: role of mitochondria in calcium buffering. *Mol Pharmacol* **47**, 140-147.

Kiedrowski L, Czyz A, Baranauskas G, Li XF, & Lytton J (2004). Differential contribution of plasmalemmal Na/Ca exchange isoforms to sodium-dependent calcium influx and NMDA excitotoxicity in depolarized neurons. *J Neurochem* **90**, 117-128.

Kim SH, Thomas CA, Andre VM, Cummings DM, Cepeda C, Levine MS, & Ehrlich ME (2011). Forebrain striatal-specific expression of mutant huntingtin protein in vivo induces cell-autonomous age-dependent alterations in sensitivity to excitotoxicity and mitochondrial function. *ASN Neuro* **3**, e00060.

Kimura J, Noma A, & Irisawa H (1986). Na-Ca exchange current in mammalian heart cells. *Nature* **319**, 596-597.

Kohr G (2006). NMDA receptor function: subunit composition versus spatial distribution. *Cell Tissue Res* **326**, 439-446.

Korshunov SS, Korkina OV, Ruuge EK, Skulachev VP, & Starkov AA (1998). Fatty acids as natural uncouplers preventing generation of O2.- and H2O2 by mitochondria in the resting state. *FEBS Lett* **435**, 215-218.

Korshunov SS, Skulachev VP, & Starkov AA (1997). High protonic potential actuates a mechanism of production of reactive oxygen species in mitochondria. *FEBS Lett* **416**, 15-18.

Kowara R, Chen Q, Milliken M, & Chakravarthy B (2005). Calpain-mediated truncation of dihydropyrimidinase-like 3 protein (DPYSL3) in response to NMDA and H2O2 toxicity. *J Neurochem* **95**, 466-474.

Kritis AA, Stamoula EG, Paniskaki KA, & Vavilis TD (2015). Researching glutamate-induced cytotoxicity in different cell lines: a comparative/collective analysis/study. *Front Cell Neurosci* **9**.

Kumar A, Kumar SS, Kumar V, Kumar D, Agarwal S, & Rana MK (2015). Huntington's disease: An update of therapeutic strategies. *Gene* **556**, 91-97.

Kushnareva YE, Wiley SE, Ward MW, Andreyev AY, & Murphy AN (2005). Excitotoxic injury to mitochondria isolated from cultured neurons. *J Biol Chem* **280**, 28894-28902.

La Spada AR, Weydt P, & Pineda VV (2011). Huntington's Disease Pathogenesis. In *Neurobiology of Huntington's Disease: Applications to Drug Discovery*, eds. Lo DC & Hughes RE, CRC Press, Boca Raton, FL.

Landwehrmeyer GB, Standaert DG, Testa CM, Penney JB, Jr., & Young AB (1995). NMDA receptor subunit mRNA expression by projection neurons and interneurons in rat striatum. *J Neurosci* **15**, 5297-5307.

Lankiewicz S, Marc LC, Truc BN, Krohn AJ, Poppe M, Cole GM, Saido TC, & Prehn JH (2000). Activation of calpain I converts excitotoxic neuron death into a caspase-independent cell death. *J Biol Chem* **275**, 17064-17071.

Leavitt BR, Guttman JA, Hodgson JG, Kimel GH, Singaraja R, Vogl AW, & Hayden MR (2001). Wild-type huntingtin reduces the cellular toxicity of mutant huntingtin in vivo. *Am J Hum Genet* **68**, 313-324.

Lester RA, Clements JD, Westbrook GL, & Jahr CE (1990). Channel kinetics determine the time course of NMDA receptor-mediated synaptic currents. *Nature* **346**, 565-567.

Li B, Otsu Y, Murphy TH, & Raymond LA (2014). Developmental decrease in NMDA receptor desensitization associated with shift to synapse and interaction with postsynaptic density-95. *Journal of Neuroscience* **23**, 11244-11254.

Li L, Fan M, Icton CD, Chen N, Leavitt BR, Hayden MR, Murphy TH, & Raymond LA (2003). Role of NR2B-type NMDA receptors in selective neurodegeneration in Huntington disease. *Neurobiol Aging* **24**, 1113-1121.

Li SH & Li XJ (2004). Huntingtin-protein interactions and the pathogenesis of Huntington's disease. *Trends Genet* **20**, 146-154.

Li Y, Bondada V, Joshi A, & Geddes JW (2009). Calpain 1 and Calpastatin expression is developmentally regulated in rat brain. *Exp Neurol* **220**, 316-319.

Lim D, Fedrizzi L, Tartari M, Zuccato C, Cattaneo E, Brini M, & Carafoli E (2008). Calcium homeostasis and mitochondrial dysfunction in striatal neurons of Huntington disease. *J Biol Chem* **283**, 5780-5789.

Lim NK, Hung LW, Pang TY, Mclean CA, Liddell JR, Hilton JB, Li QX, White AR, Hannan AJ, & Crouch PJ (2014). Localized changes to glycogen synthase kinase-3 and collapsin response mediator protein-2 in the Huntington's disease affected brain. *Hum Mol Genet* **23**, 4051-4063.

Lin CH, Tallaksen-Greene S, Chien WM, Cearley JA, Jackson WS, Crouse AB, Ren S, Li XJ, Albin RL, & Detloff PJ (2001). Neurological abnormalities in a knock-in mouse model of Huntington's disease. *Hum Mol Genet* **10**, 137-144.

Lin Y, Jover-Mengual T, Wong J, Bennett MV, & Zukin RS (2006). PSD-95 and PKC converge in regulating NMDA receptor trafficking and gating. *Proc Natl Acad Sci U S A* **103**, 19902-19907.

Liu JC, DeFazio RA, Espinosa-Jeffrey A, Cepeda C, de VJ, & Levine MS (2004). Calcium modulates dopamine potentiation of N-methyl-D-aspartate responses: electrophysiological and imaging evidence. *J Neurosci Res* **76**, 315-322.

Liu W, Zhou XW, Liu S, Hu K, Wang C, He Q, & Li M (2009). Calpain-truncated CRMP-3 and -4 contribute to potassium deprivation-induced apoptosis of cerebellar granule neurons. *Proteomics* **9**, 3712-3728.

Liu Y, Wong TP, Aarts M, Rooyakkers A, Liu L, Lai TW, Wu DC, Lu J, Tymianski M, Craig AM, & Wang YT (2007). NMDA receptor subunits have differential roles in mediating excitotoxic neuronal death both in vitro and in vivo. *J Neurosci* **27**, 2846-2857.

Luo J, Wang Y, Chen H, Kintner DB, Cramer SW, Gerdts JK, Chen X, Shull GE, Philipson KD, & Sun D (2007). A concerted role of Na(+)-K(+)-Cl(-) cotransporter and Na(+)/Ca(2+) exchanger in ischemic damage. *J Cereb Blood Flow Metab* 1-10.

Luthi-Carter R, Apostol BL, Dunah AW, DeJohn MM, Farrell LA, Bates GP, Young AB, Standaert DG, Thompson LM, & Cha JH (2003). Complex alteration of NMDA receptors in transgenic Huntington's disease mouse brain: analysis of mRNA and protein expression, plasma membrane association, interacting proteins, and phosphorylation. *Neurobiol Dis* **14**, 624-636.

Luthi-Carter R, Strand A, Peters NL, Solano SM, Hollingsworth ZR, Menon AS, Frey AS, Spektor BS, Penney EB, Schilling G, Ross CA, Borchelt DR, Tapscott SJ, Young AB, Cha JH, & Olson JM (2000). Decreased expression of striatal signaling genes in a mouse model of Huntington's disease. *Hum Mol Genet* **9**, 1259-1271.

MacDermott AB, Mayer ML, Westbrook GL, Smith SJ, & Barker JL (1986). NMDA-receptor activation increases cytoplasmic calcium concentration in cultured spinal cord neurones. *Nature* **321**, 519-522.

MacDonald ME, Ambrose CM, Duyao MP, Myers RH, Lin C, Srinidhi L, Barnes G, Taylor SA, James M, Groot N, MacFarlane H, Jenkins B, Anderson MA, Wexler NS, Gusella JF, Bates GP, Baxendale S, Hummerich H, Kirby S, North M, Youngman S, Mott R, Zehetner G, Sedlacek Z, Poustka A, Frischauf AM, Lehrach H, Buckler AJ, Church D, Doucette-Stamm L, O'Donovan MC, Riba-Ramirez L, Shah M, Stanton VP, Strobel SA, Draths KM, Wales JL, Dervan P, Housman DE, Altherr M, Shiang R, Thompson L, Fielder T, Wasmuth JJ, Tagle D, Valdes J, Elmer L, Allard M, Castilla L, Swaroop M, Blanchard K, Collins FS, Snell R, Holloway T, Gillespie K, Datson N, Shaw D, & Harper PS (1993). A novel gene containing a trinucleotide repeat that is expanded and unstable on Huntington's disease chromosomes. *Cell* **72**, 971-983.

Malouitre S, Dube H, Selwood D, & Crompton M (2010). Mitochondrial targeting of cyclosporin A enables selective inhibition of cyclophilin-D and enhanced cytoprotection after glucose and oxygen deprivation. *Biochem J* **425**, 137-148.

Manev H, Favaron M, Guidotti A, & Costa E (1989). Delayed increase of Ca2+ influx elicited by glutamate: role in neuronal death. *Mol Pharmacol* **36**, 106-112.

Mangiarini L, Sathasivam K, Seller M, Cozens B, Harper A, Hetherington C, Lawton M, Trottier Y, Lehrach H, Davies SW, & Bates GP (1996). Exon 1 of the HD gene with an expanded CAG repeat is sufficient to cause a progressive neurological phenotype in transgenic mice. *Cell* **87**, 493-506.

Mao L & Wang JQ (2001). Upregulation of preprodynorphin and preproenkephalin mRNA expression by selective activation of group I metabotropic glutamate receptors in characterized primary cultures of rat striatal neurons. *Brain Res Mol Brain Res* **86**, 125-137.

Martinez-Vicente M, Talloczy Z, Wong E, Tang G, Koga H, Kaushik S, de VR, Arias E, Harris S, Sulzer D, & Cuervo AM (2010). Cargo recognition failure is responsible for inefficient autophagy in Huntington's disease. *Nat Neurosci* **13**, 567-576.

Masu M, Nakajima Y, Moriyoshi K, Ishii T, Akazawa C, & Nakanashi S (1993). Molecular characterization of NMDA and metabotropic glutamate receptors. *Ann N Y Acad Sci* **707**, 153-164.

Mattson MP (2003). Excitotoxic and excitoprotective mechanisms: abundant targets for the prevention and treatment of neurodegenerative disorders. *Neuromolecular Med* **3**, 65-94.

McBain CJ & Mayer ML (1994). N-methyl-D-aspartic acid receptor structure and function. *Physiol Rev* **74**, 723-760.

McBride JL, Ramaswamy S, Gasmi M, Bartus RT, Herzog CD, Brandon EP, Zhou L, Pitzer MR, Berry-Kravis EM, & Kordower JH (2006). Viral delivery of glial cell line-derived neurotrophic factor improves behavior and protects striatal neurons in a mouse model of Huntington's disease. *Proc Natl Acad Sci U S A* **103**, 9345-9350.

McCormack JG, Halestrap AP, & Denton RM (1990). Role of calcium ions in regulation of mammalian intramitochondrial metabolism. *Physiol Rev* **70**, 391-425.

McEntee WJ & Crook TH (1993). Glutamate: its role in learning, memory, and the aging brain. *Psychopharmacology (Berl)* **111**, 391-401.

McGeer EG & McGeer PL (1976). Duplication of biochemical changes of Huntington's chorea by intrastriatal injections of glutamic and kainic acids. *Nature* **263**, 517-519.

Mechmann S & Pott L (1986). Identification of Na-Ca exchange current in single cardiac myocytes. *Nature* **319**, 597-599.

Milakovic T, Quintanilla RA, & Johnson GV (2006). Mutant huntingtin expression induces mitochondrial calcium handling defects in clonal striatal cells: functional consequences. *J Biol Chem* **281**, 34785-34795.

Milnerwood AJ, Gladding CM, Pouladi MA, Kaufman AM, Hines RM, Boyd JD, Ko RW, Vasuta OC, Graham RK, Hayden MR, Murphy TH, & Raymond LA (2010). Early increase in extrasynaptic NMDA receptor signaling and expression contributes to phenotype onset in Huntington's disease mice. *Neuron* **65**, 178-190.

Minelli A, Castaldo P, Gobbi P, Salucci S, Magi S, & Amoroso S (2007). Cellular and subcellular localization of Na+-Ca2+ exchanger protein isoforms, NCX1, NCX2, and NCX3 in cerebral cortex and hippocampus of adult rat. *Cell Calcium* **41**, 221-234.

Miyawaki A, Llopis J, Heim R, McCaffery JM, Adams JA, Ikura M, & Tsien RY (1997). Fluorescent indicators for Ca2+ based on green fluorescent proteins and calmodulin. *Nature* **388**, 882-887.

Monyer H, Burnashev N, Laurie DJ, Sakmann B, & Seeburg PH (1994). Developmental and regional expression in the rat brain and functional properties of four NMDA receptors. *Neuron* **12**, 529-540.

Morris RG, Anderson E, Lynch GS, & Baudry M (1986). Selective impairment of learning and blockade of long-term potentiation by an N-methyl-D-aspartate receptor antagonist, AP5. *Nature* **319**, 774-776.

Myers RH (2004). Huntington's disease genetics. *NeuroRx* **1**, 255-262.

Nance MA & Myers RH (2001). Juvenile onset Huntington's disease--clinical and research perspectives. *Ment Retard Dev Disabil Res Rev* **7**, 153-157.

Nicholls DG (1986). Intracellular calcium homeostasis. *Br Med Bull* **42**, 353-358.

Nicholls DG (2004). Mitochondrial dysfunction and glutamate excitotoxicity studied in primary neuronal cultures. *Curr Mol Med* **4**, 149-177.

Nicholls DG & Budd SL (1998). Mitochondria and neuronal glutamate excitotoxicity. *Biochim Biophys Acta* **1366**, 97-112.

Nixon RA (2003). The calpains in aging and aging-related diseases. *Ageing Res Rev* **2**, 407-418.

Novgorodov SA, Gudz TI, Milgrom YM, & Brierley GP (1992). The permeability transition in heart mitochondria is regulated synergistically by ADP and cyclosporin A. *J Biol Chem* **267**, 16274-16282.

Nowak L, Bregestovski P, Ascher P, Herbet A, & Prochiantz A (1984). Magnesium gates glutamate-activated channels in mouse central neurones. *Nature* **307**, 462-465.

Okubo Y, Sekiya H, Namiki S, Sakamoto H, Iinuma S, Yamasaki M, Watanabe M, Hirose K, & Iino M (2010). Imaging extrasynaptic glutamate dynamics in the brain. *Proc Natl Acad Sci U S A* **107**, 6526-6531.

Oliveira JM, Jekabsons MB, Chen S, Lin A, Rego AC, Goncalves J, Ellerby LM, & Nicholls DG (2007). Mitochondrial dysfunction in Huntington's disease: the bioenergetics of isolated and in situ mitochondria from transgenic mice. *J Neurochem* **101**, 241-249.

Orrenius S, Gogvadze V, & Zhivotovsky B (2015). Calcium and mitochondria in the regulation of cell death. *Biochem Biophys Res Commun* **460**, 72-81.

Panov AV, Burke JR, Strittmatter WJ, & Greenamyre JT (2003). In vitro effects of polyglutamine tracts on Ca2+-dependent depolarization of rat and human mitochondria: relevance to Huntington's disease. *Arch Biochem Biophys* **410**, 1-6.

Panov AV, Gutekunst CA, Leavitt BR, Hayden MR, Burke JR, Strittmatter WJ, & Greenamyre JT (2002). Early mitochondrial calcium defects in Huntington's disease are a direct effect of polyglutamines. *Nat Neurosci* **5**, 731-736.

Paoletti P & Neyton J (2007). NMDA receptor subunits: function and pharmacology. *Curr Opin Pharmacol* **7**, 39-47.

Papa M, Canitano A, Boscia F, Castaldo P, Sellitti S, Porzig H, Taglialatela M, & Annunziato L (2003). Differential expression of the Na+-Ca2+ exchanger transcripts and proteins in rat brain regions. *J Comp Neurol* **461**, 31-48.

Paulson HL & Albin RL (2011). Huntington's Disease Clinical Features and Routes to Therapy. In *Neurobiology of Huntington's Disease Applications to Drug Discovery*, eds. Lo DC & Hughes RE, pp. 1-27. CRC Press, Boca Raton.

Perry GM, Tallaksen-Greene S, Kumar A, Heng MY, Kneynsberg A, van GT, Detloff PJ, Albin RL, & Lesort M (2010). Mitochondrial calcium uptake capacity as a therapeutic target in the R6/2 mouse model of Huntington's disease. *Hum Mol Genet* **19**, 3354-3371.

Piekarz AD, Due MR, Khanna M, Wang B, Ripsch MS, Wang R, Meroueh SO, Vasko MR, White FA, & Khanna R (2012). CRMP-2 peptide mediated decrease of high and low voltage-activated calcium channels, attenuation of nociceptor excitability, and anti-nociception in a model of AIDS therapy-induced painful peripheral neuropathy. *Mol Pain* **8**, 54.

Pignataro G, Cuomo O, Vinciguerra A, Sirabella R, Esposito E, Boscia F, Di RG, & Annunziato L (2013). NCX as a key player in the neuroprotection exerted by ischemic preconditioning and postconditioning. *Adv Exp Med Biol* **961**, 223-240.

Planells-Cases R, Lerma J, & Ferrer-Montiel A (2006). Pharmacological intervention at ionotropic glutamate receptor complexes. *Curr Pharm Des* **12**, 3583-3596.

Pouladi MA, Morton AJ, & Hayden MR (2013). Choosing an animal model for the study of Huntington's disease. *Nat Rev Neurosci* **14**, 708-721.

Quinn CC, Chen E, Kinjo TG, Kelly G, Bell AW, Elliott RC, McPherson PS, & Hockfield S (2003). TUC-4b, a novel TUC family variant, regulates neurite outgrowth and associates with vesicles in the growth cone. *J Neurosci* **23**, 2815-2823.

Quintanilla RA, Jin YN, von BR, & Johnson GV (2013a). Mitochondrial permeability transition pore induces mitochondria injury in Huntington disease. *Mol Neurodegener* **8**, 45.

Quintanilla RA, Jin YN, von BR, & Johnson GV (2013b). Mitochondrial permeability transition pore induces mitochondria injury in Huntington disease. *Mol Neurodegener* **8**, 45.

Ramaswamy S, McBride JL, & Kordower JH (2007). Animal models of Huntington's disease. *ILAR J* **48**, 356-373.

Rasola A & Bernardi P (2011). Mitochondrial permeability transition in Ca(2+)-dependent apoptosis and necrosis. *Cell Calcium* **50**, 222-233.

Reddy PH, Charles V, Williams M, Miller G, Whetsell WO, Jr., & Tagle DA (1999). Transgenic mice expressing mutated full-length HD cDNA: a paradigm for locomotor changes and selective neuronal loss in Huntington's disease. *Philos Trans R Soc Lond B Biol Sci* **354**, 1035-1045.

Reetz K, Romanzetti S, Dogan I, Sass C, Werner CJ, Schiefer J, Schulz JB, & Shah NJ (2012). Increased brain tissue sodium concentration in Huntington's Disease - a sodium imaging study at 4 T. *Neuroimage* **63**, 517-524.

Reiner A, Albin RL, Anderson KD, D'Amato CJ, Penney JB, & Young AB (1988). Differential loss of striatal projection neurons in Huntington disease. *Proc Natl Acad Sci U S A* **85**, 5733-5737.

Ricard D, Rogemond V, Charrier E, Aguera M, Bagnard D, Belin MF, Thomasset N, & Honnorat J (2001). Isolation and expression pattern of human Unc-33-like phosphoprotein 6/collapsin response mediator protein 5 (Ulip6/CRMP5): coexistence with Ulip2/CRMP2 in Sema3a- sensitive oligodendrocytes. *J Neurosci* **21**, 7203-7214.

Rigamonti D, Bauer JH, De-Fraja C, Conti L, Sipione S, Sciorati C, Clementi E, Hackam A, Hayden MR, Li Y, Cooper JK, Ross CA, Govoni S, Vincenz C, & Cattaneo E (2000). Wild-type huntingtin protects from apoptosis upstream of caspase-3. *J Neurosci* **20**, 3705-3713.

Roze E, Bonnet C, Betuing S, & Caboche J (2010). Huntington's disease. *Adv Exp Med Biol* **685**, 45-63.

Sakaue M, Nakamura H, Kaneko I, Kawasaki Y, Arakawa N, Hashimoto H, Koyama Y, Baba A, & Matsuda T (2000). Na(+)-Ca(2+) exchanger isoforms in rat neuronal preparations: different changes in their expression during postnatal development. *Brain Res* **881**, 212-216.

Salinska E, Danysz W, & Lazarewicz JW (2005). The role of excitotoxicity in neurodegeneration. *Folia Neuropathol* **43**, 322-339.

Sattler R & Tymianski M (2000). Molecular mechanisms of calcium-dependent excitotoxicity. *J Mol Med* **78**, 3-13.

Schilling G, Becher MW, Sharp AH, Jinnah HA, Duan K, Kotzuk JA, Slunt HH, Ratovitski T, Cooper JK, Jenkins NA, Copeland NG, Price DL, Ross CA, & Borchelt DR (1999). Intranuclear inclusions and neuritic aggregates in transgenic mice expressing a mutant N-terminal fragment of huntingtin. *Hum Mol Genet* **8**, 397-407.

Schinzel AC, Takeuchi O, Huang Z, Fisher JK, Zhou Z, Rubens J, Hetz C, Danial NN, Moskowitz MA, & Korsmeyer SJ (2005). Cyclophilin D is a component of mitochondrial permeability transition and mediates neuronal cell death after focal cerebral ischemia. *Proc Natl Acad Sci U S A* **102**, 12005-12010.

Schmidt EF & Strittmatter SM (2007). The CRMP family of proteins and their role in Sema3A signaling. *Adv Exp Med Biol* **600**, 1-11.

Secondo A, Staiano RI, Scorziello A, Sirabella R, Boscia F, Adornetto A, Valsecchi V, Molinaro P, Canzoniero LM, Di Renzo G, & Annunziato L (2007). BHK cells transfected with NCX3 are more resistant to hypoxia followed by reoxygenation than those transfected with NCX1 and NCX2: Possible relationship with mitochondrial membrane potential. *Cell Calcium* **42**, 521-535.

Shannon K, Hersch S, Lovecky D, & Tarapata K. Huntington's Disease: A Family Guide. 2009. Huntington's Disease Society of America.
Ref Type: Pamphlet

Shirasaki DI, Greiner ER, Al-Ramahi I, Gray M, Boontheung P, Geschwind DH, Botas J, Coppola G, Horvath S, Loo JA, & Yang XW (2012). Network organization of the huntingtin proteomic interactome in mammalian brain. *Neuron* **75**, 41-57.

Shirendeb U, Reddy AP, Manczak M, Calkins MJ, Mao P, Tagle DA, & Reddy PH (2011). Abnormal mitochondrial dynamics, mitochondrial loss and mutant huntingtin oligomers in Huntington's disease: implications for selective neuronal damage. *Hum Mol Genet*.

Shirendeb UP, Calkins MJ, Manczak M, Anekonda V, Dufour B, McBride JL, Mao P, & Reddy PH (2012). Mutant huntingtin's interaction with mitochondrial protein Drp1 impairs mitochondrial biogenesis and causes defective axonal transport and synaptic degeneration in Huntington's disease. *Hum Mol Genet* **21**, 406-420.

Slee EA, Harte MT, Kluck RM, Wolf BB, Casiano CA, Newmeyer DD, Wang HG, Reed JC, Nicholson DW, Alnemri ES, Green DR, & Martin SJ (1999). Ordering the cytochrome c-initiated caspase cascade: hierarchical activation of caspases-2, -3, -6, -7, -8, and -10 in a caspase-9-dependent manner. *J Cell Biol* **144**, 281-292.

Slow EJ, Graham RK, Osmand AP, Devon RS, Lu G, Deng Y, Pearson J, Vaid K, Bissada N, Wetzel R, Leavitt BR, & Hayden MR (2005). Absence of behavioral abnormalities and neurodegeneration in vivo despite widespread neuronal huntingtin inclusions. *Proc Natl Acad Sci U S A* **102**, 11402-11407.

Slow EJ, van RJ, Rogers D, Coleman SH, Graham RK, Deng Y, Oh R, Bissada N, Hossain SM, Yang YZ, Li XJ, Simpson EM, Gutekunst CA, Leavitt BR, & Hayden MR (2003). Selective striatal neuronal loss in a YAC128 mouse model of Huntington disease. *Hum Mol Genet* **12**, 1555-1567.

Smith DJ, Ng H, Kluck RM, & Nagley P (2008). The mitochondrial gateway to cell death. *IUBMB Life* **60**, 383-389.

Smith GL, Elliott EE, Kettlewell S, Currie S, & Quinn FR (2006). Na(+)/Ca(2+) exchanger expression and function in a rabbit model of myocardial infarction. *J Cardiovasc Electrophysiol* **17 Suppl 1**, S57-S63.

Song W, Chen J, Petrilli A, Liot G, Klinglmayr E, Zhou Y, Poquiz P, Tjong J, Pouladi MA, Hayden MR, Masliah E, Ellisman M, Rouiller I, Schwarzenbacher R, Bossy B, Perkins G, & Bossy-Wetzel E (2011). Mutant huntingtin binds the mitochondrial fission GTPase dynamin-related protein-1 and increases its enzymatic activity. *Nat Med* **17**, 377-382.

Spandou E, Soubasi V, Papoutsopoulou S, Augoustides-Savvopoulou P, Loizidis T, Pazaiti A, Karkavelas G, & Guiba-Tziampiri O (2007). Neuroprotective effect of

long-term MgSO4 administration after cerebral hypoxia-ischemia in newborn rats is related to the severity of brain damage. *Reprod Sci* **14**, 667-677.

Spector AA (1975). Fatty acid binding to plasma albumin. *J Lipid Res* **16**, 165-179.

Stack EC, Kubilus JK, Smith K, Cormier K, Del Signore SJ, Guelin E, Ryu H, Hersch SM, & Ferrante RJ (2005). Chronology of behavioral symptoms and neuropathological sequela in R6/2 Huntington's disease transgenic mice. *J Comp Neurol* **490**, 354-370.

Stanika RI, Pivovarova NB, Brantner CA, Watts CA, Winters CA, & Andrews SB (2009). Coupling diverse routes of calcium entry to mitochondrial dysfunction and glutamate excitotoxicity. *Proc Natl Acad Sci U S A* **106**, 9854-9859.

Steinberg GK, Saleh J, DeLaPaz R, Kunis D, & Zarnegar SR (1989). Pretreatment with the NMDA antagonist dextrorphan reduces cerebral injury following transient focal ischemia in rabbits. *Brain Res* **497**, 382-386.

Sugars KL & Rubinsztein DC (2003). Transcriptional abnormalities in Huntington disease. *Trends Genet* **19**, 233-238.

Sun Y, Savanenin A, Reddy PH, & Liu YF (2001). Polyglutamine-expanded huntingtin promotes sensitization of N-methyl-D-aspartate receptors via post-synaptic density 95. *J Biol Chem* **276**, 24713-24718.

Swayne LA, Chen L, Hameed S, Barr W, Charlesworth E, Colicos MA, Zamponi GW, & Braun JE (2005). Crosstalk between huntingtin and syntaxin 1A regulates N-type calcium channels. *Mol Cell Neurosci* **30**, 339-351.

Tang TS, Slow E, Lupu V, Stavrovskaya IG, Sugimori M, Llinas R, Kristal BS, Hayden MR, & Bezprozvanny I (2005). Disturbed Ca2+ signaling and apoptosis of medium spiny neurons in Huntington's disease. *Proc Natl Acad Sci U S A* **102**, 2602-2607.

Tang TS, Tu H, Chan EY, Maximov A, Wang Z, Wellington CL, Hayden MR, & Bezprozvanny I (2003). Huntingtin and huntingtin-associated protein 1 influence neuronal calcium signaling mediated by inositol-(1,4,5) triphosphate receptor type 1. *Neuron* **39**, 227-239.

Tanveer A, Virji S, Andreeva L, Totty NF, Hsuan JJ, Ward JM, & Crompton M (1996). Involvement of cyclophilin D in the activation of a mitochondrial pore by Ca2+ and oxidant stress. *Eur J Biochem* **238**, 166-172.

Thayer SA & Miller RJ (1990). Regulation of the intracellular free calcium concentration in single rat dorsal root ganglion neurones in vitro. *J Physiol* **425**, 85-115.

Thor H, Hartzell P, & Orrenius S (1984). Potentiation of oxidative cell injury in hepatocytes which have accumulated Ca2+. *J Biol Chem* **259**, 6612-6615.

Thurneysen T, Nicoll DA, Philipson KD, & Porzig H (2002a). Immunohistochemical detection of the sodium-calcium exchanger in rat hippocampus cultures using subtype-specific antibodies. *Ann N Y Acad Sci* **976**, 367-375.

Thurneysen T, Nicoll DA, Philipson KD, & Porzig H (2002b). Sodium/calcium exchanger subtypes NCX1, NCX2 and NCX3 show cell-specific expression in rat hippocampus cultures. *Brain Res Mol Brain Res* **107**, 145-156.

Traynelis SF, Wollmuth LP, McBain CJ, Menniti FS, Vance KM, Ogden KK, Hansen KB, Yuan H, Myers SJ, & Dingledine R (2010). Glutamate Receptor Ion Channels: Structure, Regulation, and Function. *Pharmacol Rev* **62**, 405-496.

Trettel F, Rigamonti D, Hilditch-Maguire P, Wheeler VC, Sharp AH, Persichetti F, Cattaneo E, & MacDonald ME (2000). Dominant phenotypes produced by the HD mutation in STHdh(Q111) striatal cells. *Hum Mol Genet* **9**, 2799-2809.

Trottier Y, Devys D, Imbert G, Saudou F, An I, Lutz Y, Weber C, Agid Y, Hirsch EC, & Mandel JL (1995). Cellular localization of the Huntington's disease protein and discrimination of the normal and mutated form. *Nat Genet* **10**, 104-110.

Trushina E, Dyer RB, Badger JD, Ure D, Eide L, Tran DD, Vrieze BT, Legendre-Guillemin V, McPherson PS, Mandavilli BS, Van HB, Zeitlin S, McNiven M, Aebersold R, Hayden M, Parisi JE, Seeberg E, Dragatsis I, Doyle K, Bender A, Chacko C, & McMurray CT (2004). Mutant huntingtin impairs axonal trafficking in mammalian neurons in vivo and in vitro. *Mol Cell Biol* **24**, 8195-8209.

Tymianski M, Charlton MP, Carlen PL, & Tator CH (1993a). Secondary Ca2+ overload indicates early neuronal injury which precedes staining with viability indicators. *Brain Res* **607**, 319-323.

Tymianski M, Charlton MP, Carlen PL, & Tator CH (1993b). Source specificity of early calcium neurotoxicity in cultured embryonic spinal neurons. *J Neurosci* **13**, 2085-2104.

Velier J, Kim M, Schwarz C, Kim TW, Sapp E, Chase K, Aronin N, & DiFiglia M (1998). Wild-type and mutant huntingtins function in vesicle trafficking in the secretory and endocytic pathways. *Exp Neurol* **152**, 34-40.

von HS, Schmitt I, Nguyen HP, Holzmann C, Schmidt T, Walther T, Bader M, Pabst R, Kobbe P, Krotova J, Stiller D, Kask A, Vaarmann A, Rathke-Hartlieb S, Schulz JB, Grasshoff U, Bauer I, Vieira-Saecker AM, Paul M, Jones L, Lindenberg KS, Landwehrmeyer B, Bauer A, Li XJ, & Riess O (2003). Transgenic rat model of Huntington's disease. *Hum Mol Genet* **12**, 617-624.

Vonsattel JP & DiFiglia M (1998). Huntington disease. *J Neuropathol Exp Neurol* **57**, 369-384.

Vonsattel JP, Myers RH, Stevens TJ, Ferrante RJ, Bird ED, & Richardson EP, Jr. (1985). Neuropathological classification of Huntington's disease. *J Neuropathol Exp Neurol* **44**, 559-577.

Walker FO & Raymond LA (2004). Targeting energy metabolism in Huntington's disease. *Lancet* **364**, 312-313.

Wang GJ & Thayer SA (1996). Sequestration of glutamate-induced Ca2+ loads by mitochondria in cultured rat hippocampal neurons. *J Neurophysiol* **76**, 1611-1621.

Wang LH & Strittmatter SM (1997). Brain CRMP forms heterotetramers similar to liver dihydropyrimidinase. *J Neurochem* **69**, 2261-2269.

Warby SC, Visscher H, Collins JA, Doty CN, Carter C, Butland SL, Hayden AR, Kanazawa I, Ross CJ, & Hayden MR (2011). HTT haplotypes contribute to differences in Huntington disease prevalence between Europe and East Asia. *Eur J Hum Genet* **19**, 561-566.

Waterhouse NJ, Finucane DM, Green DR, Elce JS, Kumar S, Alnemri ES, Litwack G, Khanna K, Lavin MF, & Watters DJ (1998). Calpain activation is upstream of caspases in radiation-induced apoptosis. *Cell Death Differ* **5**, 1051-1061.

Wellington CL, Ellerby LM, Gutekunst CA, Rogers D, Warby S, Graham RK, Loubser O, van Raamsdonk J, Singaraja R, Yang YZ, Gafni J, Bredesen D, Hersch SM, Leavitt BR, Roy S, Nicholson DW, & Hayden MR (2002). Caspase cleavage of mutant huntingtin precedes neurodegeneration in Huntington's disease. *J Neurosci* **22**, 7862-7872.

Wellington CL, Singaraja R, Ellerby L, Savill J, Roy S, Leavitt B, Cattaneo E, Hackam A, Sharp A, Thornberry N, Nicholson DW, Bredesen DE, & Hayden MR (2000). Inhibiting caspase cleavage of huntingtin reduces toxicity and aggregate formation in neuronal and nonneuronal cells. *J Biol Chem* **275**, 19831-19838.

Wheeler VC, Auerbach W, White JK, Srinidhi J, Auerbach A, Ryan A, Duyao MP, Vrbanac V, Weaver M, Gusella JF, Joyner AL, & MacDonald ME (1999). Length-dependent gametic CAG repeat instability in the Huntington's disease knock-in mouse. *Hum Mol Genet* **8**, 115-122.

Wheeler VC, White JK, Gutekunst CA, Vrbanac V, Weaver M, Li XJ, Li SH, Yi H, Vonsattel JP, Gusella JF, Hersch S, Auerbach W, Joyner AL, & MacDonald ME (2000). Long glutamine tracts cause nuclear localization of a novel form of huntingtin in medium spiny striatal neurons in HdhQ92 and HdhQ111 knock-in mice. *Hum Mol Genet* **9**, 503-513.

White RJ & Reynolds IJ (1995). Mitochondria and Na+/Ca2+ exchange buffer glutamate-induced calcium loads in cultured cortical neurons. *J Neurosci* **15**, 1318-1328.

Wieckowski MR, Brdiczka D, & Wojtczak L (2000). Long-chain fatty acids promote opening of the reconstituted mitochondrial permeability transition pore. *FEBS Lett* **484**, 61-64.

Wilson SM, Xiong W, Wang Y, Ping X, Head JD, Brittain JM, Gagare PD, Ramachandran PV, Jin X, & Khanna R (2012). Prevention of posttraumatic axon sprouting by blocking collapsin response mediator protein 2-mediated neurite outgrowth and tubulin polymerization. *Neuroscience* **210**, 451-466.

Yu SP & Choi DW (1997). Na(+)-Ca2+ exchange currents in cortical neurons: concomitant forward and reverse operation and effect of glutamate. *Eur J Neurosci* **9**, 1273-1281.

Yu ZX, Li SH, Evans J, Pillarisetti A, Li H, & Li XJ (2003). Mutant huntingtin causes context-dependent neurodegeneration in mice with Huntington's disease. *J Neurosci* **23**, 2193-2202.

Yu-Taeger L, Petrasch-Parwez E, Osmand AP, Redensek A, Metzger S, Clemens LE, Park L, Howland D, Calaminus C, Gu X, Pichler B, Yang XW, Riess O, & Nguyen HP (2012). A novel BACHD transgenic rat exhibits characteristic neuropathological features of Huntington disease. *J Neurosci* **32**, 15426-15438.

Zeron MM, Hansson O, Chen N, Wellington CL, Leavitt BR, Brundin P, Hayden MR, & Raymond LA (2002). Increased sensitivity to N-methyl-D-aspartate receptor-mediated excitotoxicity in a mouse model of Huntington's disease. *Neuron* **33**, 849-860.

Zhang H, Li Q, Graham RK, Slow E, Hayden MR, & Bezprozvanny I (2008). Full length mutant huntingtin is required for altered Ca2+ signaling and apoptosis of striatal neurons in the YAC mouse model of Huntington's disease. *Neurobiol Dis* **31**, 80-88.

Zhou M & Baudry M (2006). Developmental changes in NMDA neurotoxicity reflect developmental changes in subunit composition of NMDA receptors. *J Neurosci* **26**, 2956-2963.

Zoratti M & Szabo I (1995). The mitochondrial permeability transition. *Biochim Biophys Acta* **1241**, 139-176.

Zuccato C & Cattaneo E (2007). Role of brain-derived neurotrophic factor in Huntington's disease. *Prog Neurobiol* **81**, 294-330.

Zuccato C & Cattaneo E (2009). Brain-derived neurotrophic factor in neurodegenerative diseases. *Nat Rev Neurol* **5**, 311-322.

Zuccato C, Ciammola A, Rigamonti D, Leavitt BR, Goffredo D, Conti L, MacDonald ME, Friedlander RM, Silani V, Hayden MR, Timmusk T, Sipione S, & Cattaneo E (2001). Loss of huntingtin-mediated BDNF gene transcription in Huntington's disease. *Science* **293**, 493-498.

Zuccato C, Valenza M, & Cattaneo E (2010). Molecular mechanisms and potential therapeutical targets in Huntington's disease. *Physiol Rev* **90**, 905-981.

CURRICULUM VITAE

Jessica J. Pellman

Education

Aug 2009 – Aug 2016
Ph.D. in Toxicology
Department of Pharmacology and Toxicology
Indiana University, Indianapolis, IN

Aug 2005 – May 2009
B.S. in Pharmaceutical Sciences with College and Departmental Honors
Major: Pharmacology and Toxicology, Minor: Chemistry
The University of Toledo College of Pharmacy, Toledo, OH

Experience

Aug 2012 – July 2015
Graduate Research with Dr. Nickolay Brustovetsky
Regulation of neuronal calcium homeostasis in Huntington's Disease
Department of Pharmacology and Toxicology
Indiana University School of Medicine
Indianapolis, IN

Jan – Mar 2010, May 2010 – July 2012
Laboratory Rotation, Graduate Research
with Drs. Gerry Oxford and Joyce Hurley
TRP channel toxicology
Department of Pharmacology and Toxicology
Indiana University School of Medicine
Indianapolis, IN

March 2010 – May 2010
Laboratory Rotation with Dr. Zachary Rodd
Ethanol self-administration in alcohol-preferring rats
Department of Psychiatry
Indiana University School of Medicine
Indianapolis, IN

Oct 2009 – Dec 2009
Laboratory Rotation with Dr. William Sullivan Jr.
DNA damage repair in *Toxoplasma gondii*
Department of Pharmacology and Toxicology
Indiana University School of Medicine
Indianapolis, IN

May 2009 – July 2009
Toxicology Intern
Drinking Water Treatment Unit Certification
NSF International
Ann Arbor, MI

Jan 2007 – May 2009
Undergraduate Research with Dr. William S. Messer Jr.
Honors thesis: Pharmacology of novel muscarinic antagonists *in vitro*
Department of Pharmacology and Toxicology
The University of Toledo College of Pharmacy
Toledo, OH

Publications

Hamilton J, **Pellman JJ**, Brustovetsky T, Harris RA, Brustovetsky N. (2016) Oxidative metabolism and Ca^{2+} handling in isolated brain mitochondria and striatal neurons from R6/2 mice, a model of Huntington's disease. Hum Mol Genet. (ePub ahead of Print).

Pellman JJ, Hamilton J, Brustovetsky T, Brustovetsky N. (2015) Ca^{2+} handling in isolated brain mitochondria and cultured neurons derived from the YAC128 mouse model of Huntington's Disease. J Neurochem. 134(4):652-67.

Hamilton J, **Pellman JJ**, Brustovetsky T, Harris RA, Brustovetsky N. (2015) Oxidative metabolism in YAC128 mouse model of Huntington's Disease. Hum Mol Genet. 24(17):4862-78.

Kunkler PE, Zhang LJ, **Pellman JJ**, Oxford GS, Hurley JH. (2015). Sensitization of the trigeminovascular system after environmental irritant exposure. Cephalalgia. 35(13):1192-201.

Brustovetsky T, **Pellman JJ**, Yang XF, Khanna R, Brustovetsky N. (2014). Collapsin response mediator protein 2 (CRMP2) interacts with N-methyl-D-aspartate (NMDA) receptor and Na^{+}/Ca^{2+} exchanger and regulates their functional activity. J. Biol. Chem. 289(11):7470-7482.

Kunkler PE, Ballard CJ, **Pellman JJ**, Zhang LJ, Oxford GS, Hurley JH (2014). Intraganglionic signaling as a novel nasal-meningeal pathway for TRPA1-dependent trigeminovascular activation by inhaled environmental irritants. PLoS One. 9(7): e103086.

Wilson SM, Schmutzler BS, Brittain JM, Dustrude ET, Ripsch MS, **Pellman JJ**, Yeum T-S, Hurley JH, Hingtgen CM, White FA, Khanna R. (2012). Inhibition of transmitter release and attenuation of anti-retroviral-associated and tibial nerve injury-related painful peripheral neuropathy by novel synthetic Ca^{2+} channel peptides. J Biol Chem. 287(42):35065-35077.

Maheshwari A, Rao P, Larke L, **Pellman JJ**, Harmeyer B, Messer W. Development of M_1 muscarinic receptor agonists for the treatment of cognitive deficits. (Submitted).

Presentations and Accepted Abstracts

Hamilton J, **Pellman JJ**, Brustovetsky T, Brustovetsky N. Respiratory activity and calcium uptake capacity in brain mitochondria from R6/2 mice, a model of Huntington's disease. Accepted Abstract. 2015 Neuroscience Meeting. Chicago, IL: Society for Neuroscience, 2015.

Pellman JJ, Brustovetsky T, Brustovetsky N. Calcium uptake capacity and induction of the permeability transition pore in brain mitochondria from YAC128 mice. Presentation No.795.21. 2014 Neuroscience Meeting, Washington, DC; Society for Neuroscience, 2014.

Pellman JJ, Hamilton J, Brustovetsky T, Brustovetsky N. Calcium uptake capacity and induction of the permeability transition pore in brain mitochondria from YAC128 mice. 2014 Gil Symposium, Bloomington, IN, 2014

Pellman JJ, Hamilton J, Brustovetsky T, Brustovetsky N. Calcium uptake capacity and induction of the permeability transition pore in brain mitochondria from YAC128 mice. Indianpolis Chapter of the Society for Neuroscience, Indianapolis, IN, 2014.

Brustovetsky T, **Pellman JJ**, Khanna R, Brustovetsky N. CBD3 peptide, a fragment of CRMP2, protects against glutamate-induced Ca dysregulation by attenuating both NMDAR and Na/Ca exchanger activities. Nanosymposium, **Presenting Author**. Program No. 601.11. 2013 Neuroscience Meeting, San Diego, CA; Society for Neuroscience, 2013.

Pellman JJ, Brustovetsky T, Yang X-F, Khanna R, Brustovetsky N. Collapsin response mediator protein 2 interacts with NMDA receptor and Na^{+}/Ca^{2+} exchanger and regulates their functional activity. Indianpolis Chapter of the Society for Neuroscience, Indianapolis, IN, 2013.

Pellman JJ, Brustovetsky T, Yang X-F, Khanna R, Brustovetsky N. Collapsin response mediator protein 2 interacts with NMDA receptor and Na^{+}/Ca^{2+} exchanger and regulates their functional activity. 2013 Gill Symposium, Bloomington, IN, 2013.

Pellman JJ, Kunkler PE, Hurley JH, Oxford GS. Function and expression of TRPA1 channels in response to environmental irritant exposure *in vitro*. Accepted Abstract. Program No. 784.04. 2012 Neuroscience Meeting Planner. New Orleans, LA: Society for Neuroscience, 2012.

Pellman JJ, Kunkler PE, Hurley JH, Oxford GS. Function and expression of TRPA1 channels in response to environmental irritant exposure *in vitro*. Poster Presentation. 51st Society of Toxicology Annual Meeting, San Francisco, CA, 2012.

Pellman JJ, Messer W. Development of M_5 muscarinic acetylcholine receptor antagonists. 23rd National Conference on Undergraduate Research, La Crosse, WI, 2009.

Jennings JJ, Messer W. Development of M_5 muscarinic acetylcholine receptor antagonists. 22nd National Conference on Undergraduate Research. Salisbury, MD, 2008.

Awards

IUSM Graduate Student Travel Grant
Indiana University School of Medicine, *2015*
Paradise Travel Award, Department of Pharmacology and Toxicology
Indiana University School of Medicine, *2013*
Graduate Student Travel Award
Society of Toxicology, *2012*
College Honors
The University of Toledo College of Pharmacy, *2009*
Departmental Honors, Department of Pharmacology and Toxicology,
The University of Toledo College of Pharmacy, *2009*
Undergraduate Summer Research Award
The University of Toledo College of Pharmacy, *2007*
Levis Leadership UT, Fellow and Facilitator
The University of Toledo, *2005-09*

Professional Organizations

Society of Toxicology, *July 2011-Present*
Specialty Sections: Neurotoxicology, Women in Toxicology
Ohio Valley Society of Toxicology, *Aug 2011-Present*
Society for Neuroscience, *April 2012-Present*
American Association for the Advancement of Science, *Mar 2012-Present*

Leadership and Service

Central Indiana Science Outreach (CINSO)
Board and Founding Member, *Sept 2014-Present*
Indiana State Museum 1816 Advisory
Board Member, *Feb 2015-Present*
Pharmacology and Toxicology
Student Journal Club Coordinator, *Aug 2012-Aug 2014*
Trained two Ph.D. rotation students and one M.S. student
Fall 2012, Winter 2013, Spring 2014
Indiana BioMedical Gateway Program
Recruitment of new graduate students, *Jan 2010-Feb 2013*